Characterization of Brackish Groundwater Resources in Victoria County

Prepared for:

Victoria County Groundwater Conservation District

Prepared by:

INTERA Incorporated
9600 Great Hills Trail
Suite 300W
Austin, TX 78759
512.425.2000

December 2018

This page intentionally left blank.

Characterization of Brackish Groundwater Resources in Victoria County

Prepared By

Steve C. Young, Ph.D., P.G., P.E.

Ross Kushnereit

This page intentionally left blank.

TABLE OF CONTENTS

LIST OF FIGURES

LIST OF TABLES

Acronyms and Abbreviations

°F	degrees Fahrenheit
%	percent
ft	feet
ft^2/day	square feet per day
ac-ft	acre-feet
BRACS	Brackish Resources Aquifer Characterization System
GAM	groundwater availability model
GHBC	General Head Boundary Condition
gpm/ft	gallons per minute per foot
LCRB	Lower Colorado River Basin
mg/L	milligrams per liter
msl	mean sea level
PWS	public water supply
SP	spontaneous potential
TAC	Texas Administrative Code
TCEQ	Texas Commission on Environmental Quality
TDS	Total Dissolved Solids
TWDB	Texas Water Development Board
USGS	United States Geological Survey
VCGCD	Victoria County Groundwater Conservation District
VCGFM	Victoria County Groundwater Flow Model

This page intentionally left blank.

1.0 INTRODUCTION

This report documents the work INTERA performed to improve the characterization of brackish groundwater resources and support the development of rules for managing brackish groundwater resources in Victoria County Groundwater Conservation District (VCGCD). The objectives of the report are to:

- Improve the characterization of brackish groundwater in Victoria County,
- Develop and apply a methodology for predicting impacts to groundwater resources caused by pumping brackish groundwater, and
- Investigate management goals and criteria that are suitable for VCGCD to use for developing rules to regulate the development of brackish groundwater.

Part of the study's scope of work is the construction of a groundwater flow model. The model includes an area that extends approximately 50 miles around Victoria County. To support the model's development, aquifer information was assembled across the entire model domain. Throughout the report, there are references to the study area. The study area and the model domain refer to the same area.

Section 2 describes the stratigraphy, lithology, and water quality of the Gulf Coast Aquifer System. The majority of the aquifer characterization is based on the interpretation of geophysical logs performed as part of studies funded by the Texas Water Development Board. Section 2 includes sand percent maps and profiles of Total Dissolved Solids (TDS) concentrations for formations comprising the Gulf Coast Aquifer System. Section 3 characterizes the hydraulic properties of the Gulf Coast Aquifer System. The majority of the aquifer hydraulic properties are based on the analysis of aquifer pumping tests and specific capacity tests. The methodologies used to generate transmissive and storage properties for the aquifer formations is based on the methodologies used o as part of studies funded by the Texas Water Development Board. Section 3 includes maps of transmissivity values for formations comprising the Gulf Coast Aquifer System . Section 4 describes the development and application of a groundwater flow model for Victoria County called the Victoria County Groundwater Flow Model (VCGFM). The VCGFM is a three-dimensional MODFLOW-based groundwater flow model that covers 495 square miles and includes portions of 14 counties. The VCGFM includes fifteen model layers to represent nine of the formations that comprise the Gulf Coast Aquifer System. The VCGFM is used to simulate drawdown from pumping salinity saline water from five locations.

This page intentionally left blank.

2.0 CHARACTERIZATION OF THE GULF COAST AQUIFER SYSTEM STRATIGRAPHY, LITHOLOGY, AND WATER QUALITY

This section describes the stratigraphy, lithology, and water quality of the Gulf Coast Aquifer System in the vicinity of VCGCD. The majority of the data analyses involved the interpretation of geophysical logs. The analyses build on and augment Gulf Coast Aquifer studies funded by the Texas Water Development Board (TWDB).

2.1 Stratigraphy

The stratigraphy of the Gulf Coast Aquifer System is based on Young and others (2010, 2012a) and is comprised of, from shallowest to deepest, the Chicot Aquifer, the Evangeline Aquifer, the Burkeville Confining Unit, and the Jasper Aquifer, with parts of the Catahoula Formation acting as the Catahoula Confining System. **Table 2-1** lists the formations associated with the Chicot, Evangeline, and Jasper aquifers. The information from Young and others (2010, 2012a) is well suited for this study because the TWDB performed these studies to support updates to the groundwater availability models (GAMs) for the Gulf Coast Aquifer System.

Table 2-1 Simplified Stratigraphic and Hydrogeologic Chart of the Gulf Coast Aquifer System (Young and others, 2010)

Era	Epoch		Est. Age (M.Y.)	Formation	Hydrogeologic Unit
Cenozoic	Pleistocene		0.7	Beaumont	CHICOT AQUIFER
			1.6	Lissie	
	Pliocene		3.8	Willis	
	Miocene	Late	11.2	Upper Goliad	EVANGELINE AQUIFER
			14.5	Lower Goliad	
		Middle	17.8	Upper Lagarto	
				Middle Lagarto	BURKEVILLE
		Early		Lower Lagarto	JASPER AQUIFER
			24.2	Oakville	
	Oligocene		32	Frio	CATAHOULA
			34	Vicksburg	

The physical and hydraulic properties associated with the formations in Table 2-1 are largely determined by their depositional environment, which can be mapped using depositional facies. Depositional facies account for changes in the environmental factors that affect the composition of a deposit. These environmental factors include, but are not limited to: climate, ocean level, sediment sources, and chemistry. As these factors change over time, the composition of the deposits change, and cycles of repeating sequences of sand and clay occur.

This study adopted the depositional facies maps developed by Young and others (2010). These depositional maps are based on the work of Galloway (2000) that have also been used by Young and Kelley (2006) and Young and others (2010b). These facies can be divided into fluvial facies, coastal facies, and shelf facies. Fluvial facies are associated with deposition in rivers and on the floodplains of rivers. Coastal facies are associated with depositions in coastal and shoreline environments. Shelf facies are associated with off-shore environments. The depositional facies in this study that will be used in the development of a groundwater model in Section 4 include:

- Floodplain clays deposited during flooding of coastal streams and, less frequently, major rivers;
- Fluvial channel sands deposited within or immediately adjacent to coastal streams or major rivers;
- Coastal or deltaic bayfill clays, silts, and, rarely, sands deposited behind barrier islands, away from channels on alluvial aprons, or between deltaic distributary channels;
- Lower coastal plain fluvial or coastal sands deposited on alluvial aprons fed by streamplain systems or on delta plains of major extrabasinal rivers;
- Delta front sands, most likely deposited as narrow strike-elongated bodies of a wave-dominated delta;
- Coastal sands deposited as barrier bars, strandplains, or delta fronts where local fluvial input is minor and sand is transported and deposited primarily by along-shore currents; and
- Shallow marine shelf clays and minor silts and sands deposited seaward of the highstand shoreline, which may include interbedded muddy floodplain, bayfill, or lagoonal lowstand deposits.

The depositional facies described above have different range of hydrological flow characteristics as a consequence of varying grain size, sorting, mineralogy, sedimentary features, and the degree to which contrasting lithologies are intimately interbedded. Deposition facies map for each formation in Table 2-1 are provide by Young and others (2010). **Figure 2-1** shows the depositional map for the Lissie formation developed by Young and others (2010).

2.2 Lithology

The technical approach used to characterize the lithology of the hydrogeologic units listed in Table 2-1 is described by TWDB study performed by Young and others (2016). Young and others (2016) interpreted 609 geophysical logs (**Figure 2-2**) to construct continuous profiles of sand and clay sequences. For this study, lithologic profiles developed from the interpretation of 251 geophysical logs shown in **Figure 2-3**. Out of the 251 geophysical logs, 97 logs are from the TWDB brackish study of the Gulf Coast Aquifer System (Young and others, 2016) and 154 logs from this study.

The geophysical logs were interpreted using the same methods as used by Young and others (2016). Sands were identified on geophysical logs bases on the analysis of a shallow resistivity curve and a spontaneous potential (SP) curve. The geophysical log analyses were performed using PETRA. PETRA is a commercial software designed to allow geologists to visualize an enlarged image of the geophysical log and mark the top and bottom elevation of sand layers with a click of a mouse.

Figures 2-4 and **2-5** show maps of percent sands for the formations that comprise the Chicot, Evangeline, and Jasper aquifers. Each map shows the location of the geophysical logs used to develop

estimates of sand percentage. The number of log locations are the fewest at the shallowest formations because many of the logs start their coverage several hundred feet below ground surface. A review of the figures will show that the density of data points is significantly better for the Evangeline Aquifer.

2.3 Water Quality

A measure of the overall quality of groundwater is salinity. A common measurement of groundwater salinity is the concentration of Total Dissolved Solids (TDS), which is typically reported in units of milligrams per liter (mg/L). The primary sources of groundwater to the Gulf Coast Aquifer System consist of relatively fresher meteoric water derived from precipitation recharging the aquifers since their deposition. As groundwater moves through the subsurface, it becomes mineralized, and its salinity increases as the groundwater interacts with the aquifer materials. Among the sources of groundwater salinity in the Texas Gulf Coast Aquifer System are saline connate water trapped in the sediments at the time of deposition, dissolution of salt domes, the upwelling of brine from geothermal zones along growth faults, natural deposits of evaporate minerals, salt water intrusion, sea salt spray, and oil and gas development (Young and others, 2013).

2.3.1 Salinity Classification by TDS Concentrations

For this study, groundwater water quality is classified using the criteria presented in **Table 2-2**. The four criteria were developed by the United States Geological Survey (USGS) (Winslow and Kister, 1956). A complete description of the various groundwater quality classification schemes based upon TDS concentration exists in the USGS Professional Paper 1833 (Stanton and others, 2017).

Table 2-2 Groundwater salinity classification based on the criteria established by Winslow and Kister (1956)

Salinity Classification	TDS Concentration Range (mg/L)
Fresh	Less than 1,000
Slightly Saline*	1,000 to 3,000
Moderately Saline*	3,000 to 10,000
Very Saline	10,000 to 35,000

*Brackish water includes slightly saline and very saline water.

For this study, the definition of TDS is consistent with the Texas Administrative Code (TAC) and the definition provided by the TWDB website. The TAC Title 30 (Environmental Quality), Part 1 (Texas Commission on Environmental Quality [TCEQ]) and Chapter 307 (Texas Surface Water Quality Standards) Rule 307.3 (ii) (C) (74) defines TDS as "The amount of material (inorganic salts and small amounts of organic material) dissolved in water and commonly expressed as a concentration in terms of milligrams per liter. The term is equivalent to the term filterable residue, as used in 40 Code of Federal Regulations Part 136 and in previous editions of the publication entitled, *Standard Methods for the Examination of Water and Wastewater"* (TAC, 2016).

The TWDB website describing the groundwater database provides the following definition for dissolved solids:

> **"Dissolved Solids:** (sum of constituents) This is calculated based on the values, in mg/L, of the major anions and cations, silica, and 0.4917 of the bicarbonate. Nothing is added into the 'TDS' from the infrequent table. However, some high values that might be considered as contributing to the TDS, while not included in the TWDB's formula, are Fe, Br, B, Ba, and Zn. If a sample is missing one or more major anions or cations so that the analysis is unbalanced, a TDS determined by residue can be entered into the dissolved solids field. However, if all constituents are present, the TDS is calculated and replaces anything else in the field" (TWDB, 2016)

2.3.2 Estimate TDS Concentration from Electrical Resistivity in the Study Area

The method selected for estimating TDS concentrations from electrical resistivity data for the study area are the same methods used by Young and others (2016) for the Texas Gulf Coast Aquifer System. The development and application of these methods have been accepted by the TWDB Brackish Resources Aquifer Characterization System (BRACS) personnel and have been demonstrated to produce reasonable and defensible results. The purpose of this section is to explain the underlying assumptions and data associated with both the Mean R_o and R_{wa} Minimum methods.

2.3.2.1 Mean R_o Method

The Mean R_o method is used in this study to estimate TDS concentrations that are less than 5,000 mg/L. The Mean R_o method involves correlating deep formation resistivity (long normal or deep induction) of sand with a TDS concentration of groundwater samples from the same zone. The correlation between deep formation resistivity and TDS concentration requires that a geophysical log be paired to a water well with a measured TDS concentration. Young and others (2016) required that the horizontal distance between a paired geophysical log and the water well be less than one mile. The R_o-TDS graphs for the Chicot, Evangeline, and Jasper aquifers developed by Young and others (2016) are shown in **Figures 2-9**, **2-10**, and **2-11**, respectively. In Figures 2-9 through 2-11, there is a scatter of data points about the best fit line used to represent the relationship between resistivity and TDS concentrations. The scatter in the data exists partly because the R_o method does not explicitly account for differences in chemical composition of the TDS concentration, effects of mud filtrate, resolution of the logging tool, variations in the sands, and the possible inclusion of clays in the sand layer. As explained by Young and others (2016), the relationships in the R_o-TDS graphs can be used to estimate TDS concentrations after adjustments are made for environmental factors such as groundwater temperature and ionic composition of the groundwater.

2.3.2.2 R_{wa} Minimum Method

The R_{wa} method is used in this study to estimate TDS concentrations greater than 5,000 mg/L. The development of the R_{wa} Minimum Method follows the formulas provided by Estepp (1988) and Meyer and others (2014). The R_{wa} Minimum method to predict TDS concentrations is implemented using **Equation 2-1**.

$$R_{we77} = \Phi^m \times R_{o77} \quad \text{(Equation 2-1)}$$

where

R_{we77} = resistivity of water equivalent (ohm-meters) at 77 degrees Fahrenheit (°F)
Φ = porosity
m = the cementation exponent
R_{o77} = the formation resistivity of a 100% water saturated formation (ohm-meters) at 77 °F

After applying Equation 2-1, **Equation 2-2** is used to convert resistivity to specific conductance, and then we applied **Equation 2-3** to convert specific conductance to TDS.

$$C_{w77} = 10{,}000 / R_{we77} \quad \text{(Equation 2-2)}$$

$$TDS = ct * C_{w77} \quad \text{(Equation 2-3)}$$

where

C_{w77} = specific conductance (µmhos/cm at 77 °F)
ct = specific conductivity-total dissolved solids concentration conversion factor
TDS = TDS concentrations (mg/L) that is measured using the filterable residue approach

The application of Equations 2-1, through 2-3 requires that three variables be defined. These variables are porosity or Φ, the cementation exponent, *m*, and ct, the conversion factor from specific conductivity to TDS. The value for porosity is defined using **Equation 2-4**, which is developed based on field data by Young and others (2016). Equation 2-4 defined porosity as a parameter that is depth dependent. The values for ct and *m* are set as constants at 0.57 and 1.3, respectively. These values for ct and *m* are values used by Young and others (2016).

$$\Phi_S = 36.6 - 0.001 * d \quad \text{(Equation 2-4)}$$

where

Φ_S = porosity of sand

d = depth of burial

A summary of the relationship between resistivity, porosity, and the estimated TDS is presented **Table 2-3** for TDS values between 10,000 and 35,000 mg/L.

Table 2-3 Formation resistivity cutoff values for the R_{wa} Minimum Method that produces measured TDS concentration values of 10,000 and 35,000 mg/L using a ct conversion factor of 0.57 and a porosity range from 0.36 to 0.27

Porosity	Formation Resistivity (at 77°F)	Measured TDS Concentrations (mg/L)
0.36	2.15	10,000
	0.71	35,000
0.33	2.40	10,000
	0.80	35,000
0.3	2.70	10,000
	0.91	35,000
0.27	3.10	10,000
	1.04	35,000

2.3.3 Cross-Sections Comprised of Geophysical Logs Showing Lithology and TDS Concentrations

Figure 2-12 shows the locations of eight cross-sections that were developed by using information developed from the analysis of geophysical logs. The cross-sections include five dip sections (Sections 1, 1a, 2, 2a, and 3) and three strike sections (A, B, and C). **Figures 2-13** through **2-17** show the five dip sections. **Figures 2-18** through **2-20** show the three strike sections.

For each log on each cross-section, the deep resistivity curve is plotted on the right-hand side, and the SP is plotted on the left-hand side. Where sands have been identified on the geophysical log, the interval between the deep resistivity and the SP curve is colored to indicate the salinity of the groundwater. The salinity zones are listed in the legend in the lower left corner of every plot. Intervals between the sand beds are colored black and represent clays. On top of the geophysical logs is the API identification number for the log. The dash lines between the geophysical logs are markers showing the boundaries between the formations.

2.3.4 Maps of Salinity Zones

Figures 2-21 through **2-25** are maps showing the base of five salinity zones. The base surfaces were determined by marking the base of the respective salinity zones on each geophysica log and contouring the elevations. The geophysical logs that were used to develop the contours are shown in Figure 2-3. The methods and assumptions used to construct the surfaces are discussed by Young and others (2016).

Figure 2-21 shows the contours of the elevation for the base of of fresh groundwater, which has TDS concentrations of 1,000 mg/L or less. In Victoria County, the the base of ranges from depths between 800 and 1,400 feet (ft). The deepest location of fresh water is near the boundary with Calhoun County. Figure 2-22 shows the contours of elevation for the base of groundwater with a TDS concentration less than 2,000 mg/L. In Victoria County, the base of this salinity zone ranges between depths of 1,400 and 1,700 ft. The general pattern of the contours are similar to the shape of the contours for the base of fresh water.

Figure 2-23 shows contours of elevation for the base of groundwater with a TDS concentration less than 3,000 mg/L. In Victoria County, the base of this salinity zone ranges between depths of 1,500 and 2,000 ft. The depth to the base of a TDS concentration of 3,000 mg/L increases toward the coast, with the deepest portion of slightly saline groundwater occurring near the bounty between Calhoun and Victoria counties. Figure 2-24 shows contours of elevation for the base of groundwater with a TDS concentration less than 5,000 mg/L. In Victoria County, the elevation of the base of groundwater with TDS concentration of 5,000 mg/L range between 1,800 and about 2,100 ft. In Victoria County, the location of the deepest groundwater with 5,000 mg/L occurs long the county boundary with Regufio County and Calhoun counties.

Figure 2-25 shows contours of elevation for the base of groundwater with a TDS concentration less than 10,000 mg/L. In Victoria County, the base of this salinity zone ranges between depths of 2,200 and 2,500 ft. The depth to the base of a TDS concentration of 10,000 mg/L increase toward the coast with the deepest penetration occuring near the border with Calhoun County.

2.3.5 Cross-sections Showing Wells, Formations, and Salinity Zones

Figure 2-26 shows the location of four transects used to develop cross-sections showing wells, formations, the base of salinity zones. The cross-sections are labeled from east to west as Cross-sections A, B, C, and D. The well locations shown in Figure 2-26 were extracted for a recent version of the VCGCD well database. Each of the four cross-sections will show the depth of the wells that fall within the pink-colored buffer zones associated with each cross-section. Each of the buffer zones extends approximately 5 miles from each of the four transects.

Figure 2-27 shows Cross-section A, which is the most eastern cross-section. The majority of the wells terminated above the base of the Lissie Formation. All of the wells terminate above the base of the fresh water. Fewer than ten wells terminate in the Evangeline Aquifer. The Upper Goliad Formation is the thickest formation with a maximum thickness of about 700 ft. For much of the cross-section the elevation of the base fresh groundwater is below an elevation of -700 ft mean sea level (msl), and the elevation of the base slightly saline ground water is below an elevation of -1,500 ft msl

Figure 2-28 shows Cross-section B. The majority of the wells terminated above the base of the Willis Formation. All of the wells except for one terminate above the base of the fresh water. Fewer than fifteen wells terminate in the Evangeline Aquifer. The Upper Goliad Formation is the thickest formation, with a maximum thickness of about 850 ft. Along most of the down dip direction, the base of the fresh, slightly saline, and moderately saline groundwater zones lowers about 300 feet elevation. The greatest depths reached by the base of fresh, slightly saline, and moderately saline groundwater in Victoria County is approximately -1,400, -1,900, and -2,400 ft msl, respectively.

Figure 2-29 shows Cross-section C. The majority of the wells terminated above the base of the Upper Goliad Formation. All of the wells terminate above the base of the fresh water. The three deepest wells terminate in the Lower Goliad Formation. The Upper Goliad Formation is the thickest formation, with a maximum thickness of about 850 ft. Along most of the down dip direction, the base of the fresh, slightly saline, and moderately saline groundwater zones lowers about 600 feet elevation. The greatest depths reached by the base of fresh, slightly saline, and moderately saline groundwater in Victoria County is approximately -1,300, -2,000, and -2,500 ft msl, respectively.

Figure 2-30 shows Cross-section D, which is the most western cross-section The majority of the wells terminated above the base of the Upper Goliad formation. All of the wells terminate above the base of the fresh water. The three deepest wells terminate in the Lower Goliad Formation. The Upper Goliad Formation is the thickest formation, with a maximum thickness of about 900 ft. Along most of the down dip direction, the base of the fresh, slightly saline, and moderately saline groundwater zones lowers about 500 feet elevation. The greatest depths reached by the base of fresh, slightly saline, and moderately saline groundwater in Victoria County is approximately -1,200, -1,700, and -2,200 ft msl, respectively.

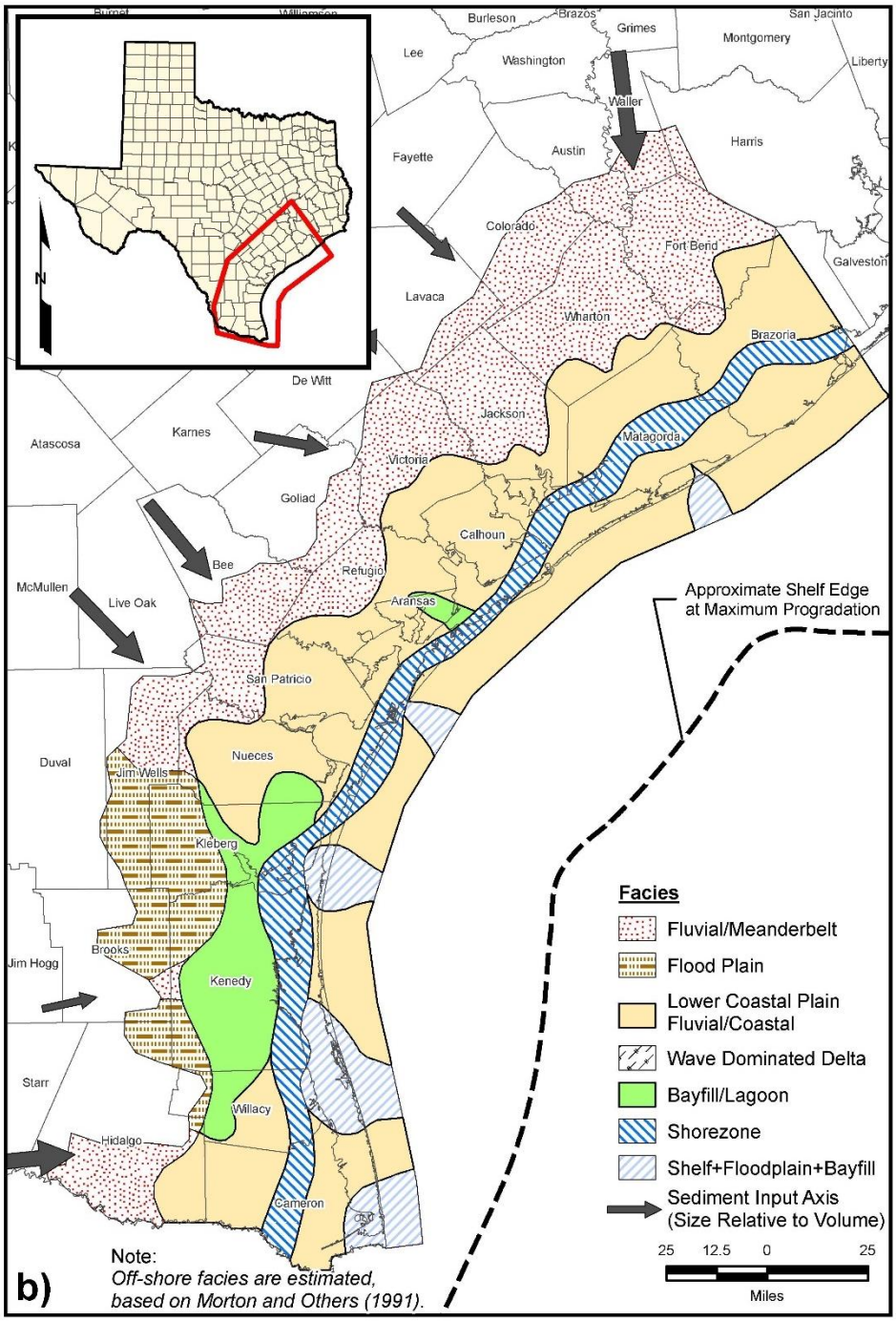

Figure 2-1 Depositional facies map for the Lissie Formation in the southern region of the Texas Gulf Coast Aquifer System (from Young and others, 2010)

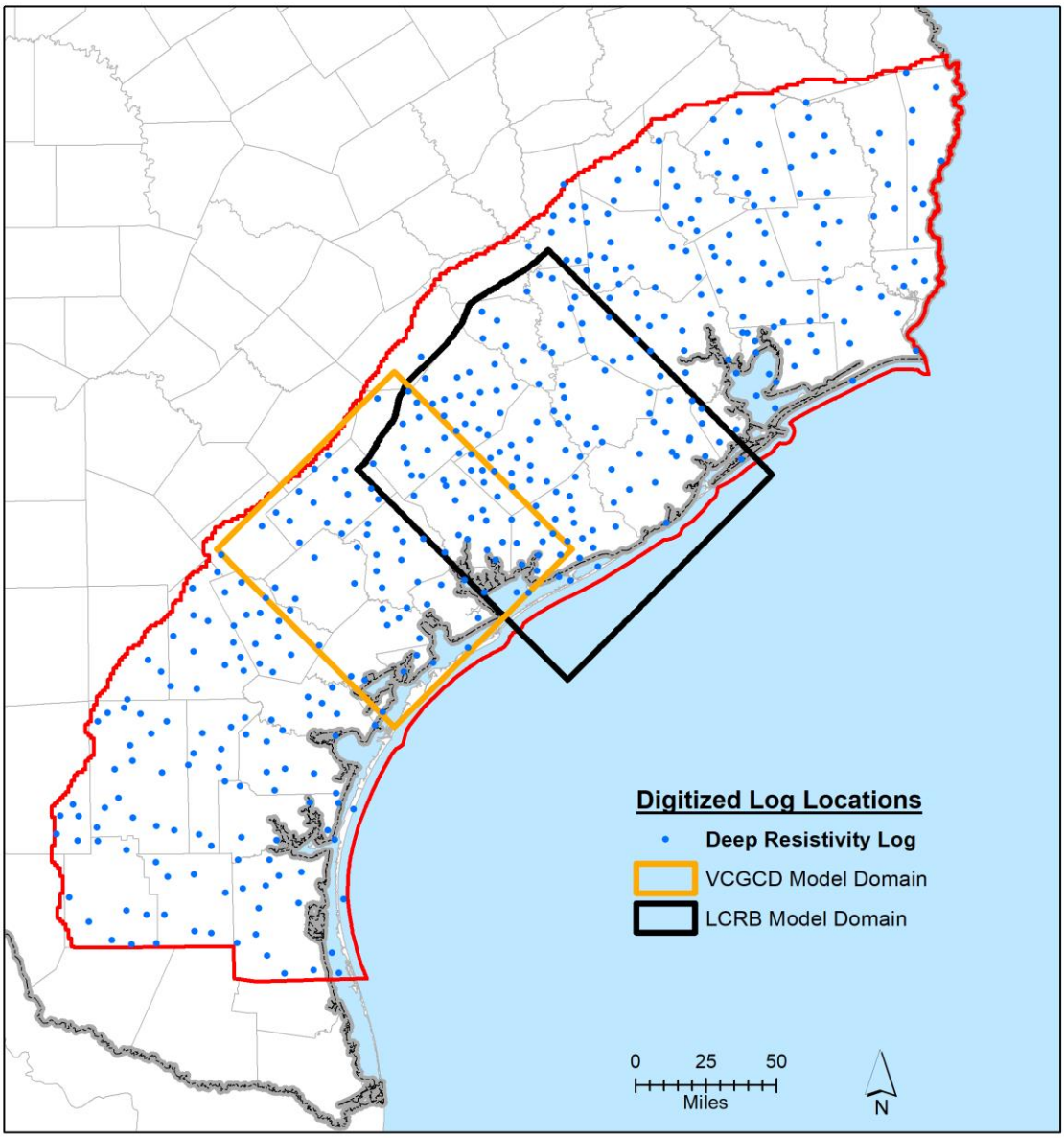

Figure 2-2 Locations of the (1) geophysical logs interpreted by Young and others (2016) to characterize the lithology of the Gulf Coast Aquifer System, (2) domain for the groundwater model developed as as part of this study, and (3) domain for the Lower Colorado River Basin groundwater flow model

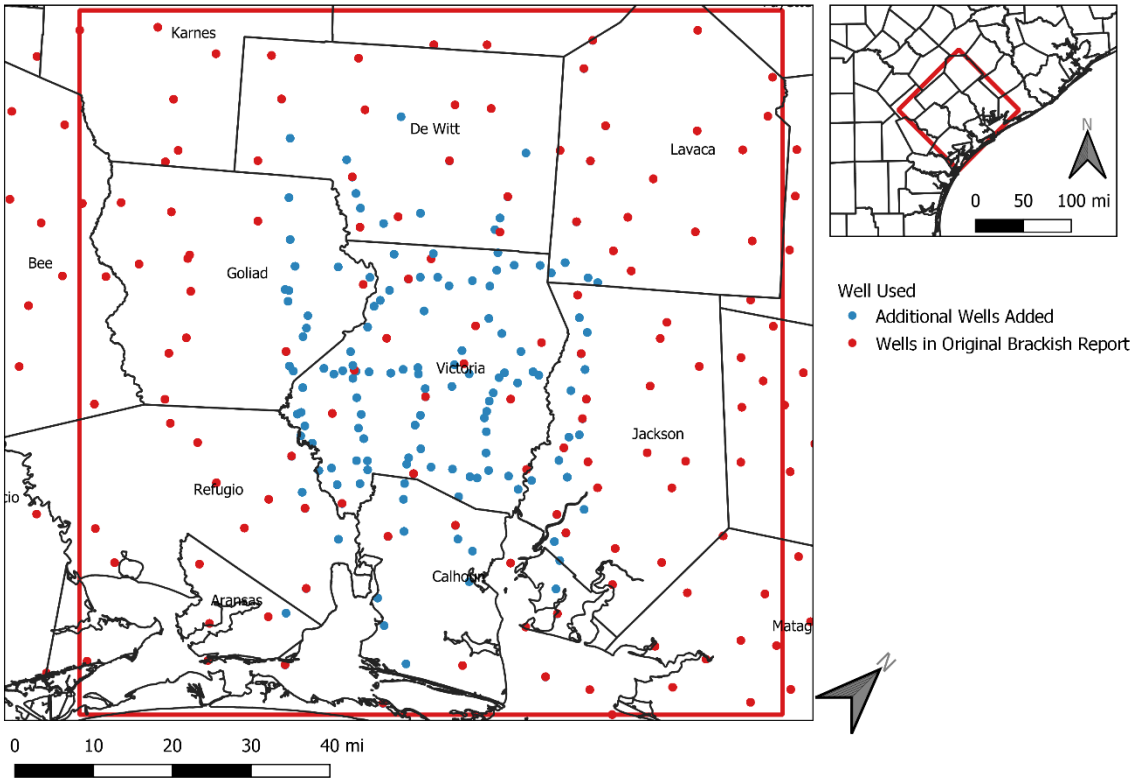

Figure 2-3 Location of geophysical logs interpreted by Young and others (2016) to characterize the lithology of the Gulf Coast Aquifer System

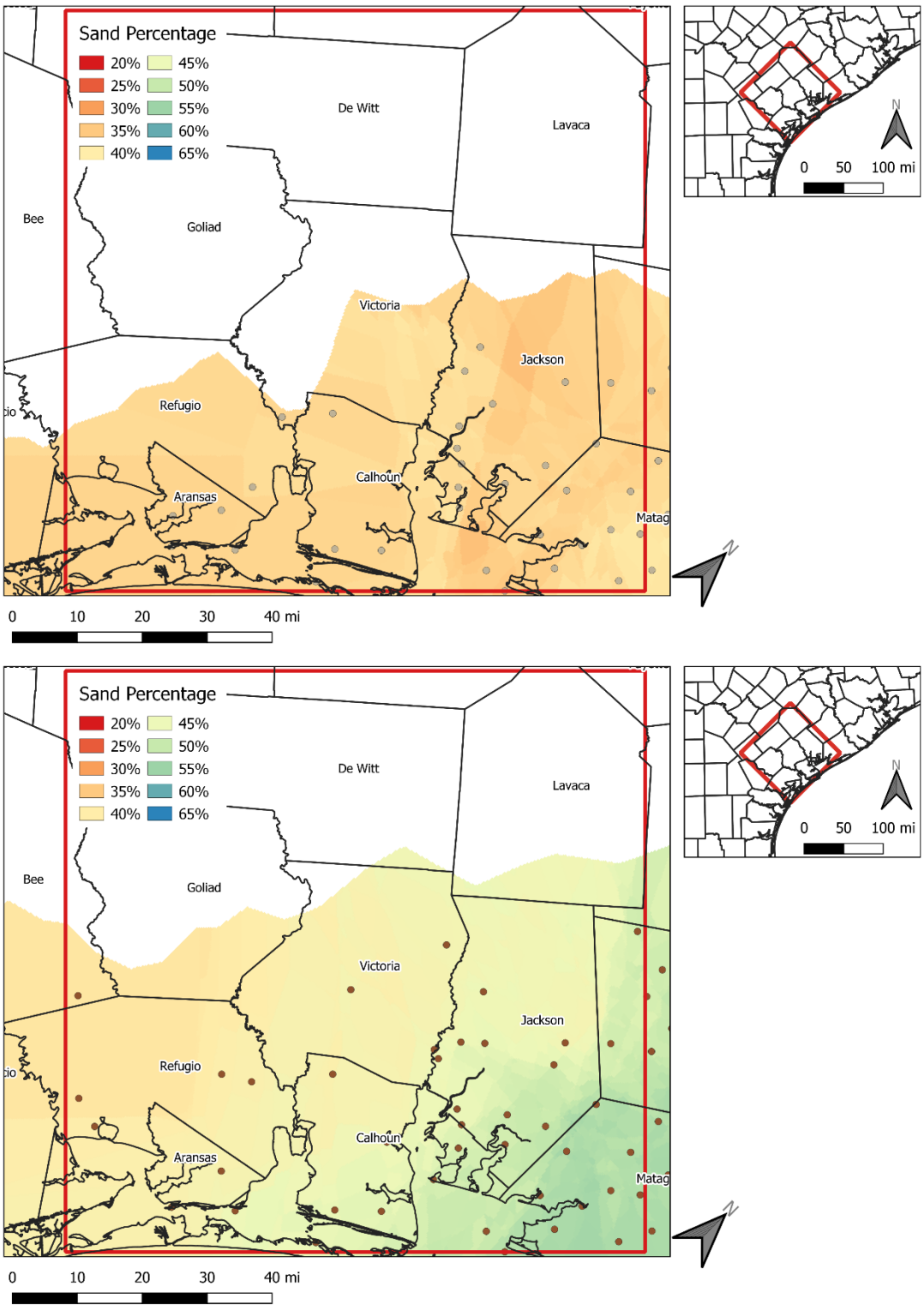

Figure 2-4 Sand percent map for the Beaumont (top) and Lissie (bottom) formations based on the interpolation of geophysical logs by Young and others (2010) and this study

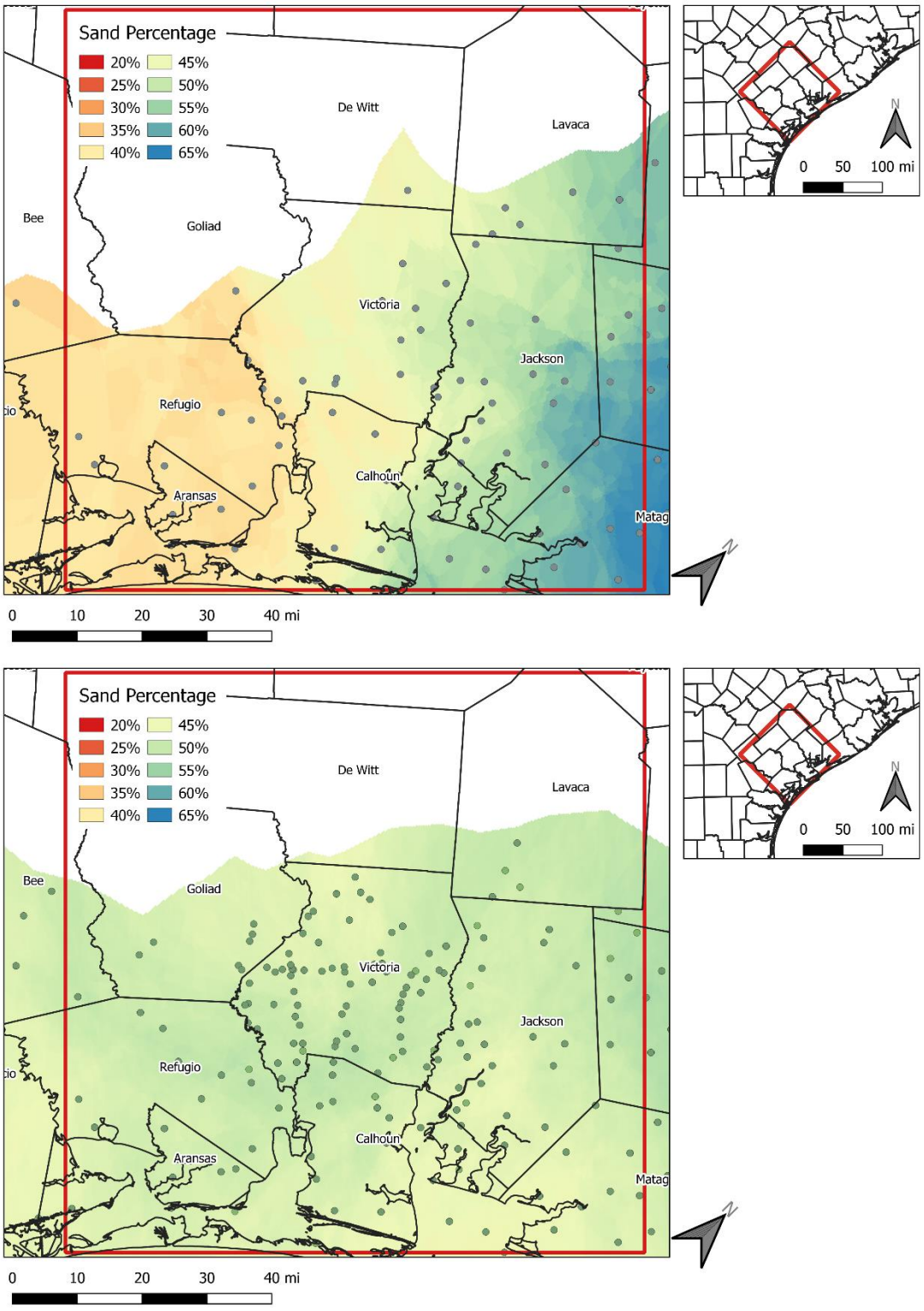

Figure 2-5 Sand percent map for the Willis (top) and Upper Goliad (bottom) formations based on the interpolation of geophysical logs by Young and others (2010) and this study

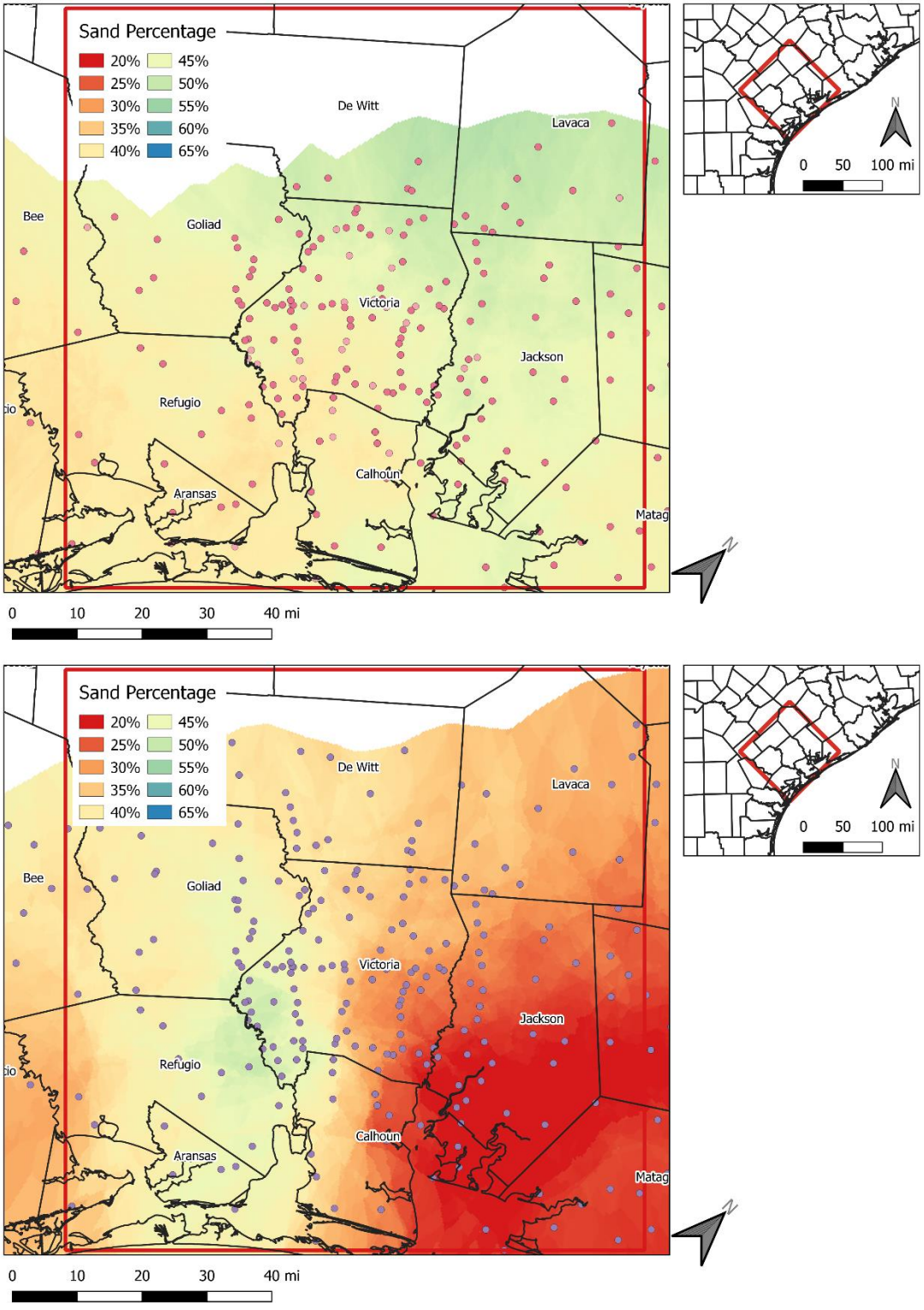

Figure 2-6 Sand percent map for the Lower Goliad (top) and Upper Lagarto (bottom) formations based on the interpolation of geophysical logs by Young and others (2010) and this study

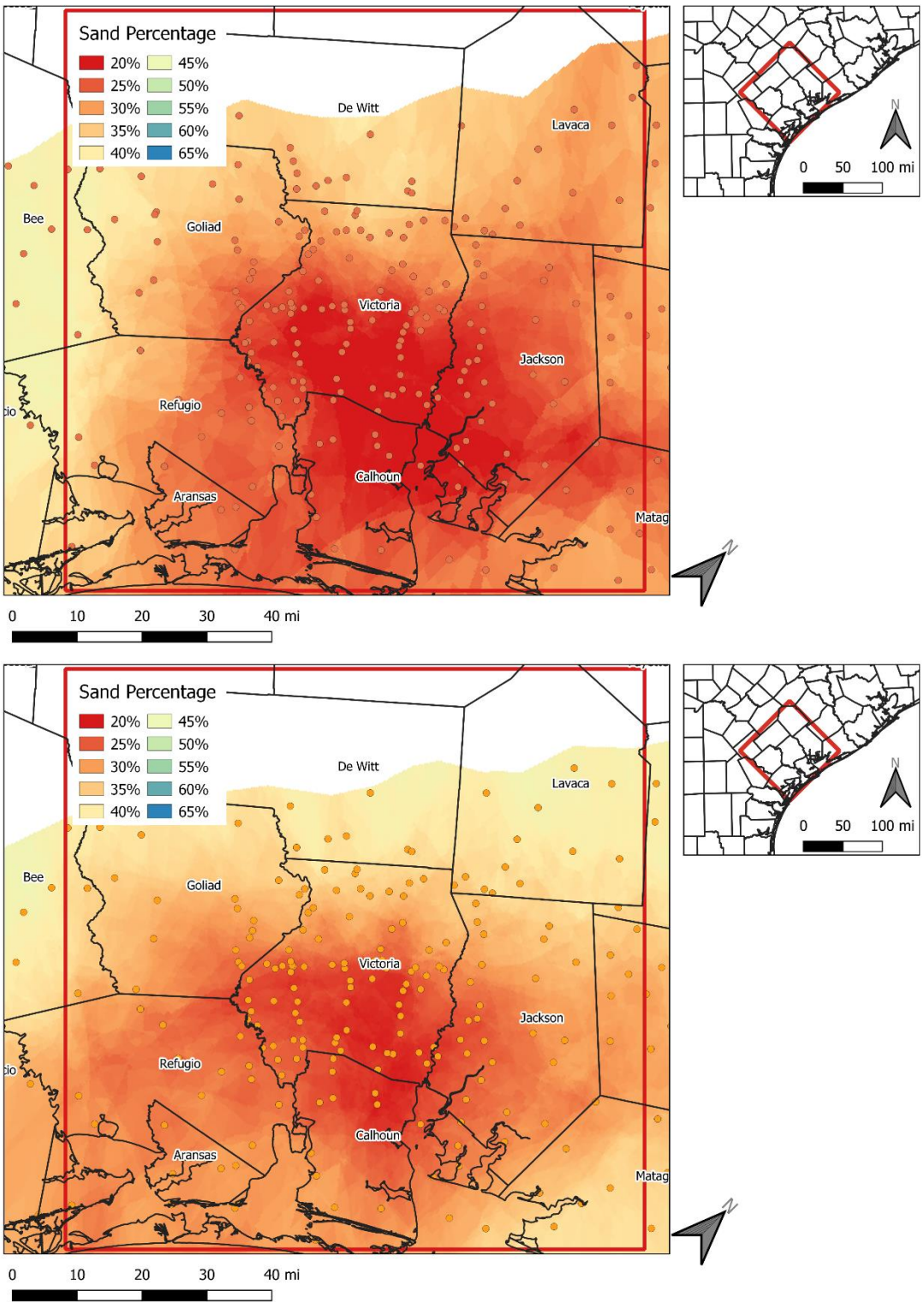

Figure 2-7 Sand percent map for the Middle Lagarto (top) and Lower Lagarto (bottom) formations based on the interpolation of geophysical logs by Young and others (2010) and this study

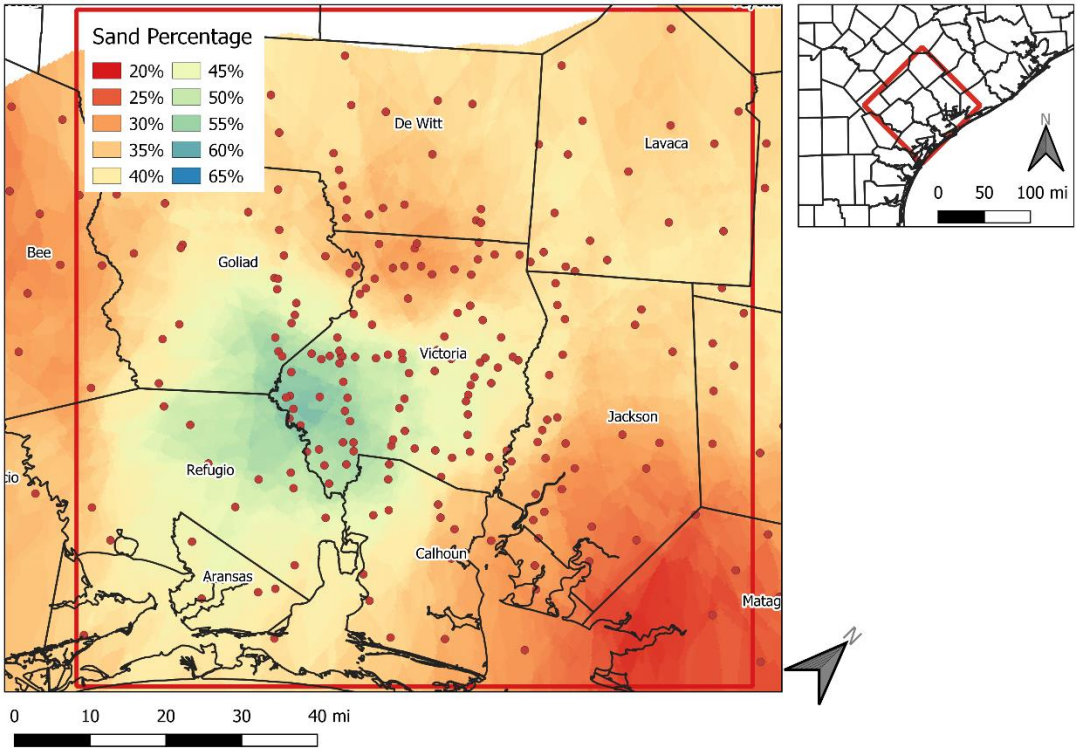

Figure 2-8 Sand percent map for the Oakville Formation (top) based on the interpolation of geophysical logs by Young and others (2010) and this study

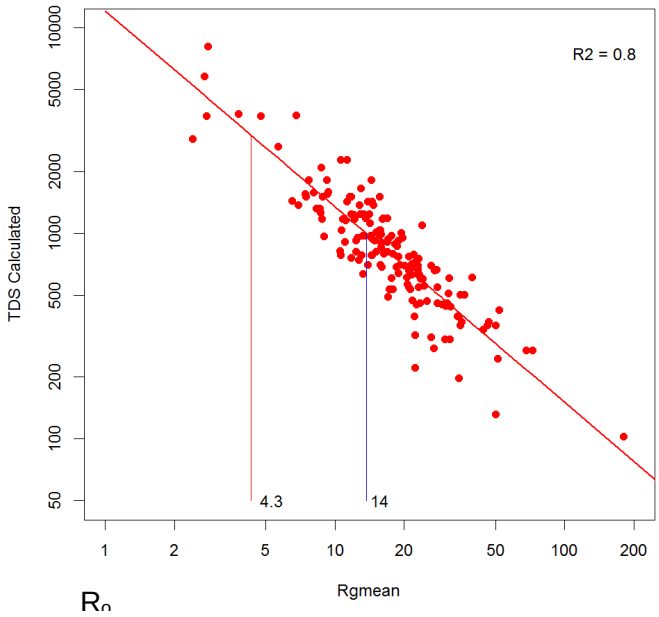

Figure 2-9 R_o-TDS graph for the Chicot Aquifer Group (including the Beaumont, Lissie, and Willis formations) based on 164 well-log pairs. Vertical lines show the formation resistivity values for a 1,000 mg/L (blue) and 3,000 mg/L (red) TDS concentration (from Young and others, 2016).

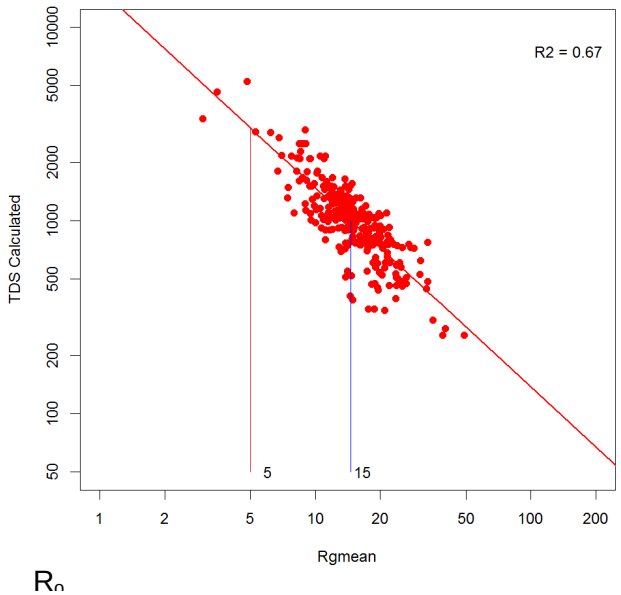

Figure 2-10 R_o-TDS graph for the Evangline Aquifer Group (including the Upper Goliad, Lower Goliad, Upper Lagarto, and Middle Lagarto formations) based on 305 well-log pairs. Vertical lines show the formation resistivity values for a 1,000 mg/L (blue) and 3,000 mg/L (red) TDS concentration (from Young and others, 2016).

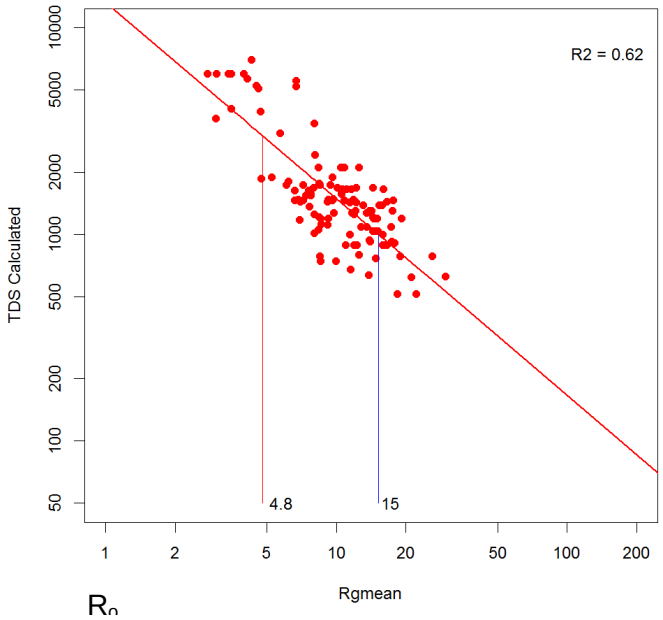

Figure 2-11 R_o-TDS graph for the Jasper/Catahoula Aquifer Group (including the Lower Lagarto, Oakville, and Catahoula formations) based on 117 well-log pairs. Vertical lines show the formation resistivity values for a 1,000 mg/L (blue) and 3,000 mg/L (red) TDS concentration (from Young and others, 2016).

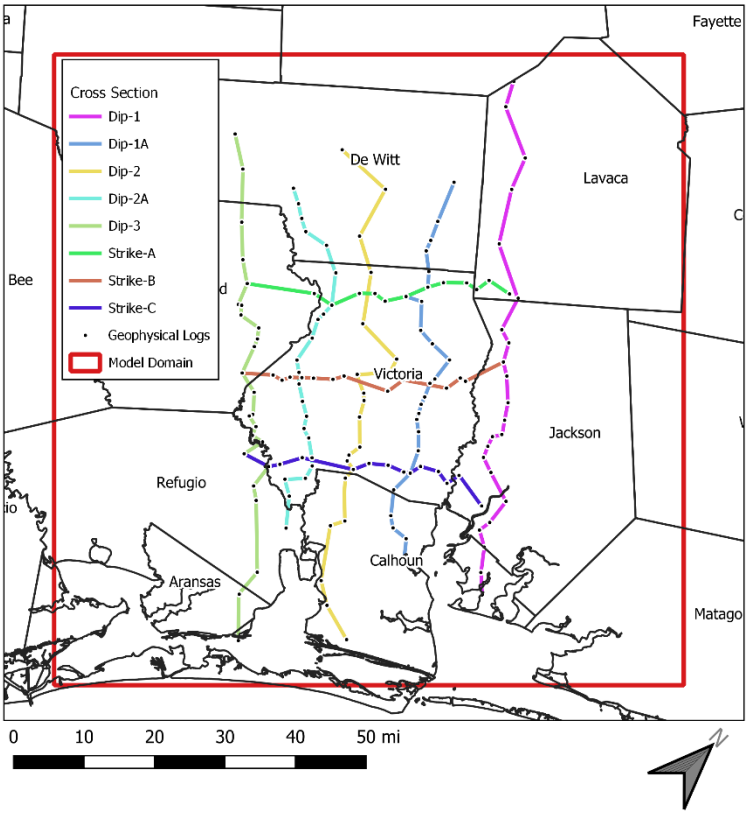

Figure 2-12 Location of five dip cross-sections and three strike cross sections that were constructed using geophysical log information to show vertical profiles of sand and clay sequences and TDS concentrations for groundwater contained in the sand layers.

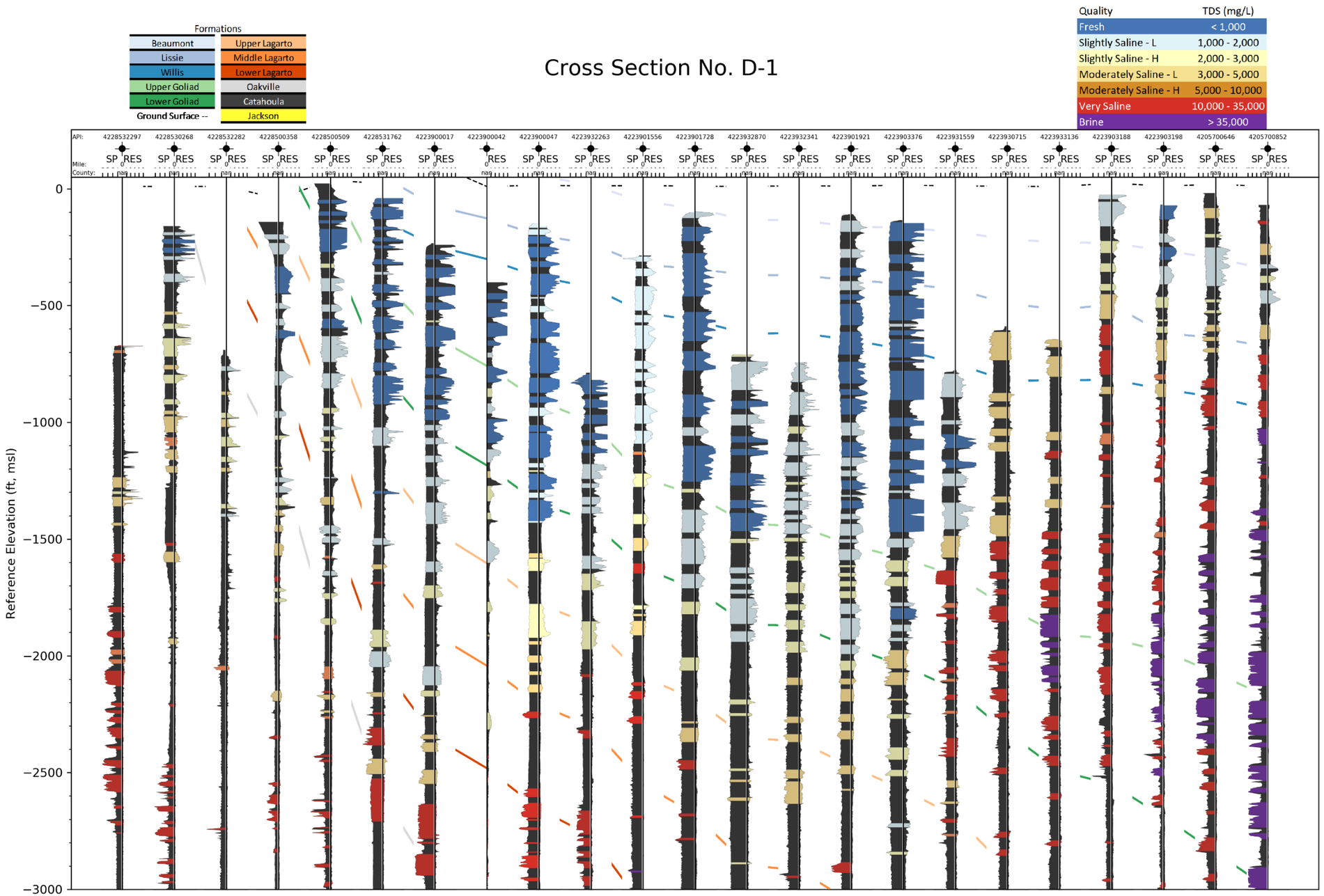

Figure 2-13 Dip cross-section number 1 (see Figure 2-9) showing formation boundaries and the water quality classification of groundwater in the sand beds identified in 23 logs

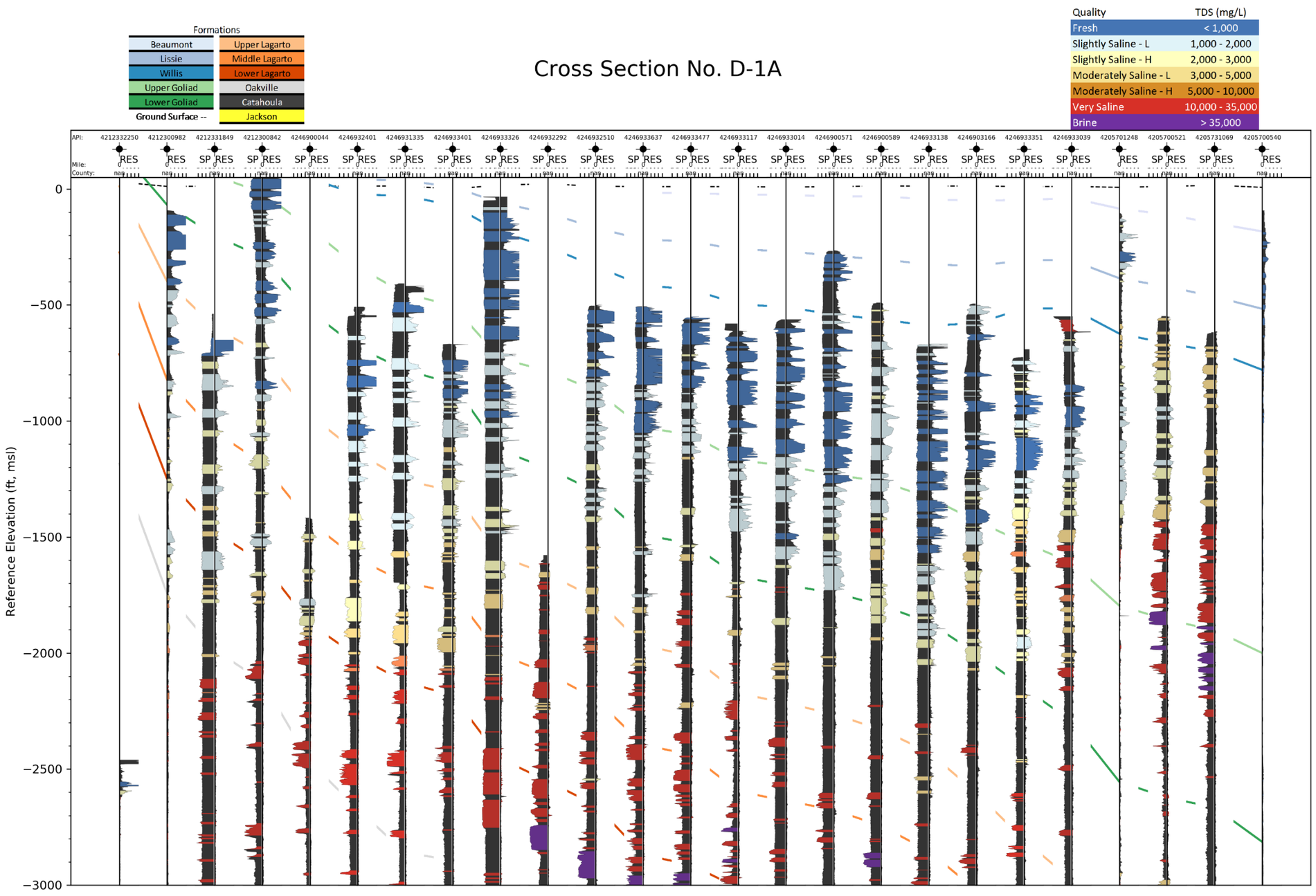

Figure 2-14 Dip cross-section number 1a (see Figure 2-9) showing formation boundaries and the water quality classification of groundwater in the sand beds identified in 25 logs

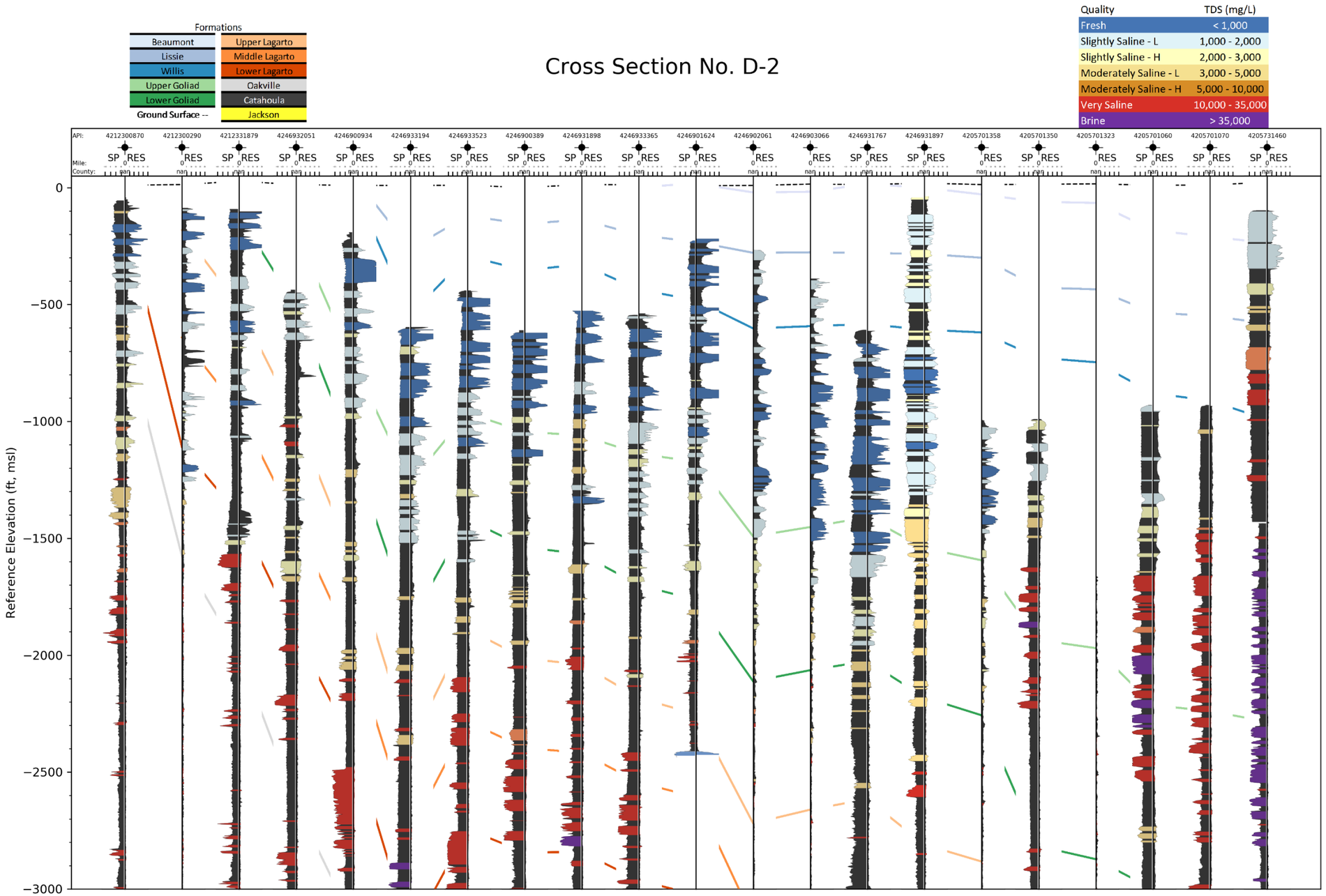

Figure 2-15 Dip cross-section number 2 (see Figure 2-9) showing formation boundaries and the water quality classification of groundwater in the sand beds identified in 21 logs

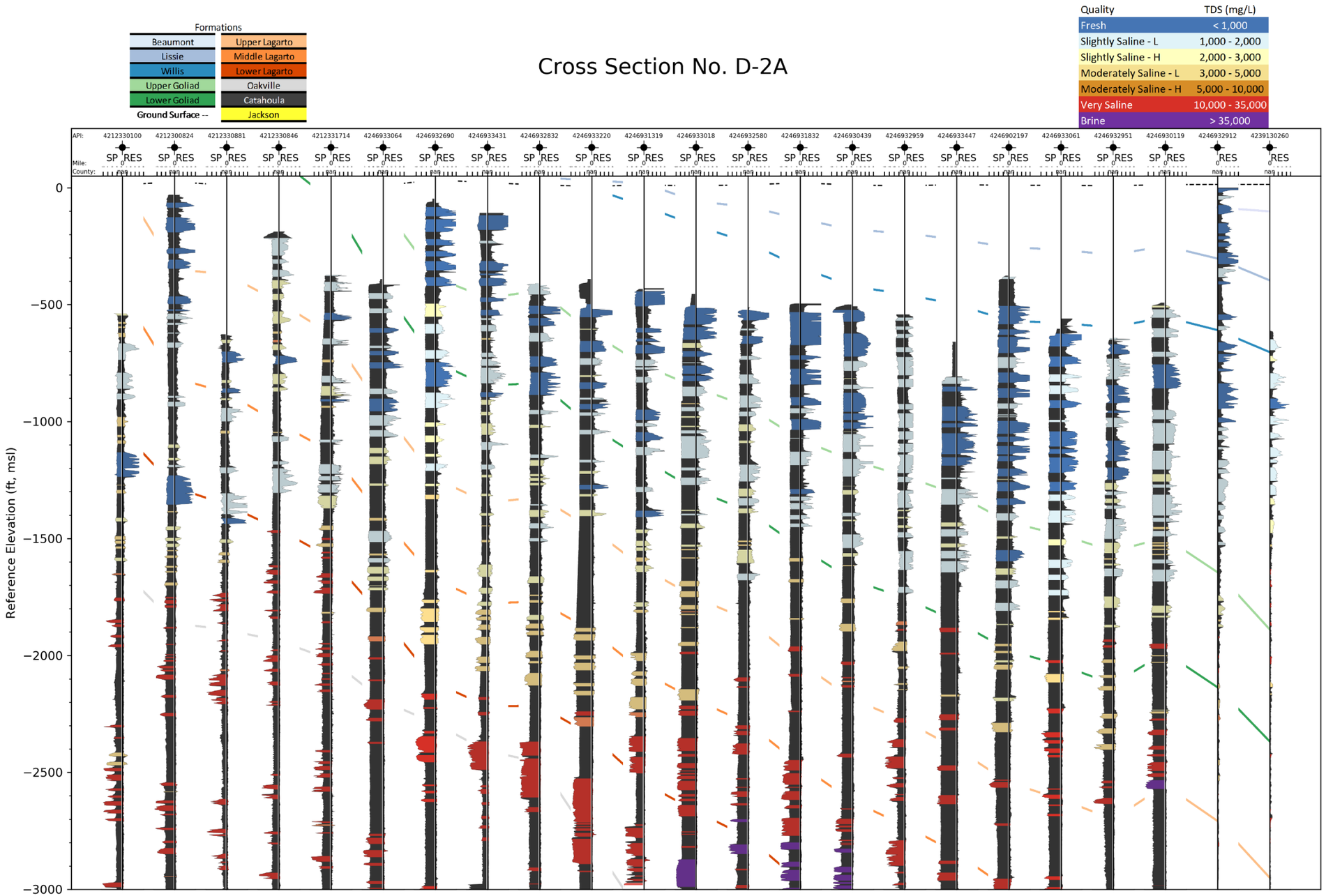

Figure 2-16 Dip cross-section number 2a (see Figure 2-9) showing formation boundaries and the water quality classification of groundwater in the sand beds identified in 23 logs

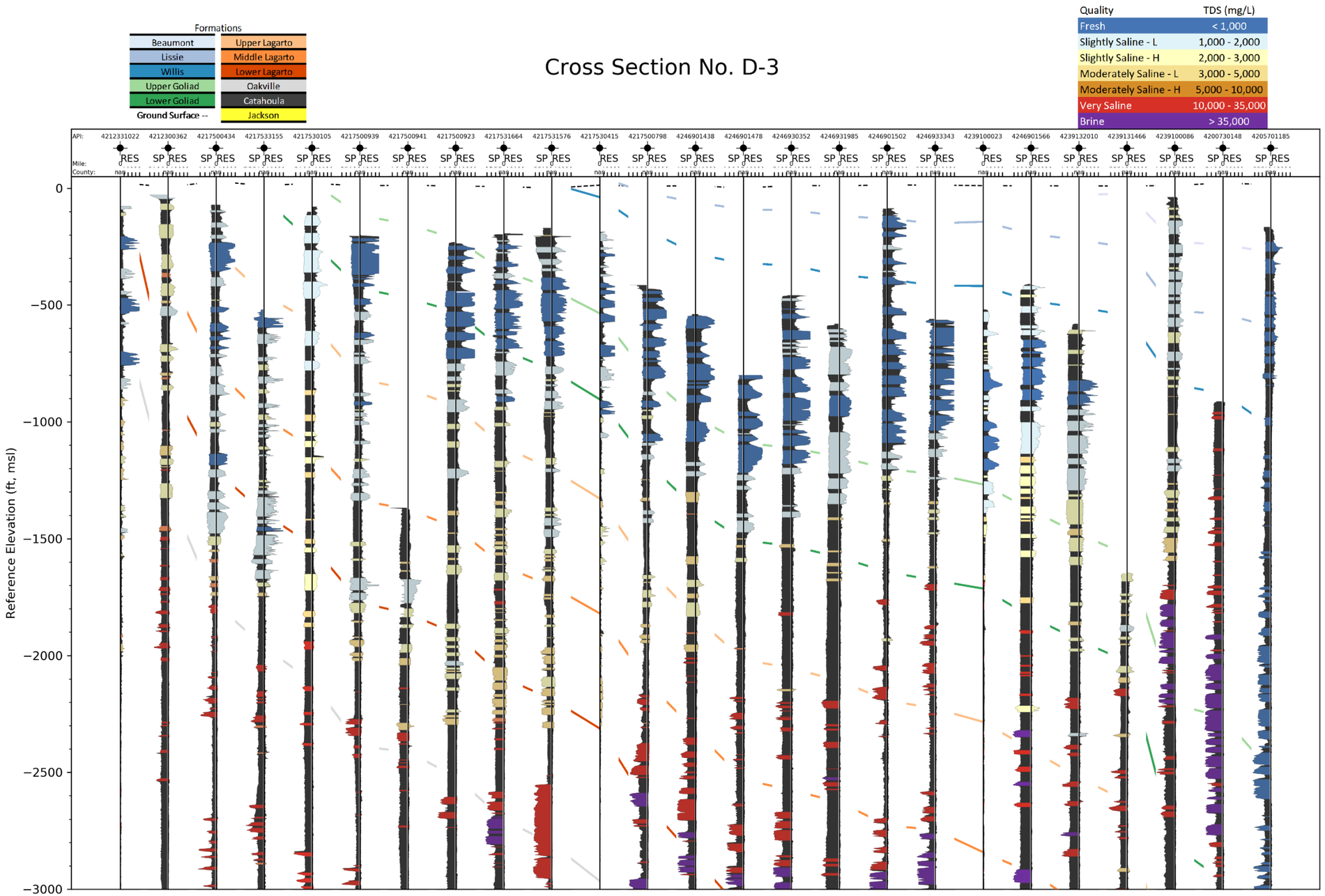

Figure 2-17 Dip cross-section number 3 (see Figure 2-9) showing formation boundaries and the water quality classification of groundwater in the sand beds identified in 25 logs

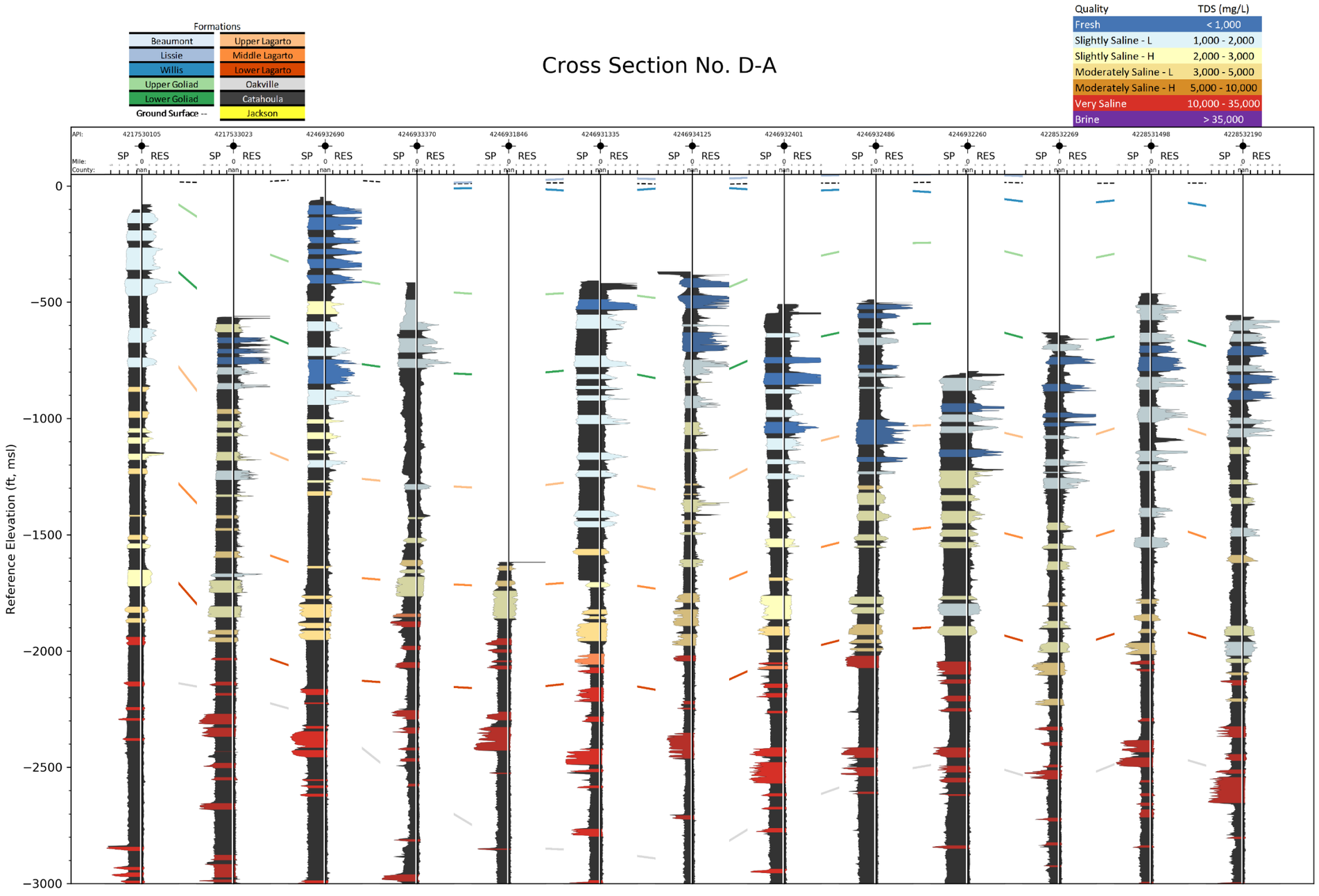

Figure 2-18 Strike cross-section number A (see Figure 2-9) showing formation boundaries and the water quality classification of groundwater in the sand beds identified in 13 logs

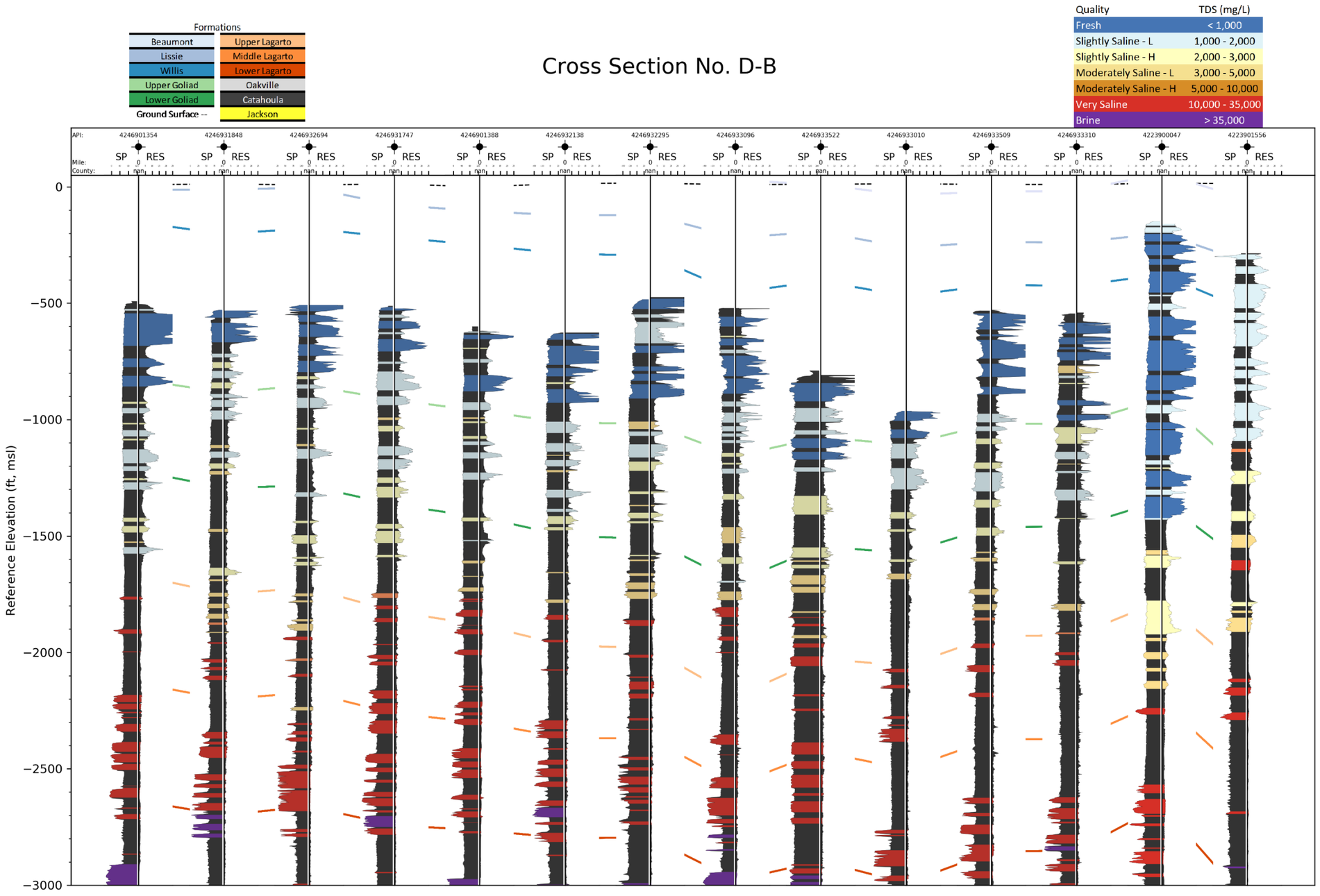

Figure 2-19 Strike cross-section number B (see Figure 2-9) showing formation boundaries and the water quality classification of groundwater in the sand beds identified in 14 logs

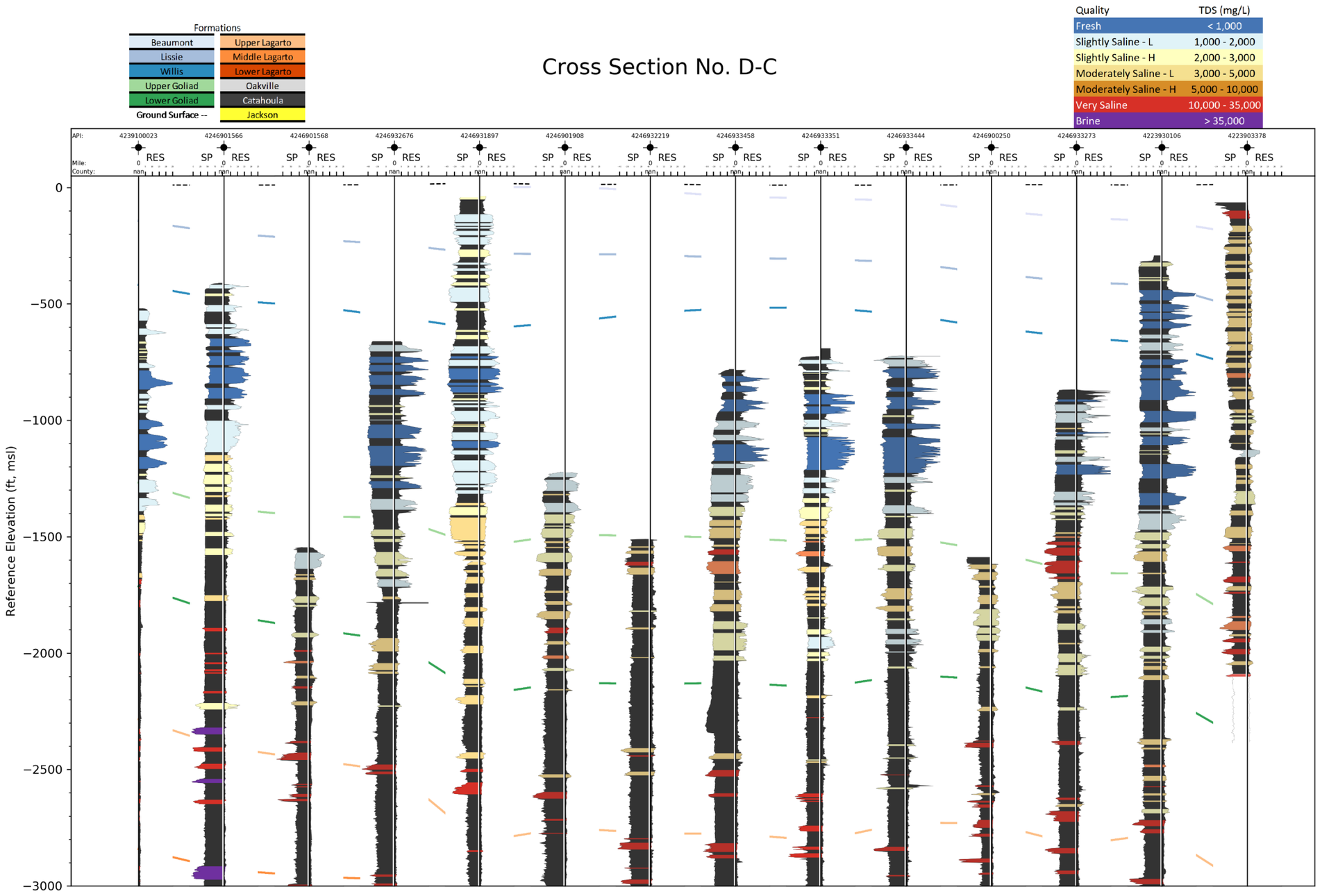

Figure 2-20 Strike cross-section number C (see Figure 2-9) showing formation boundaries and the water quality classification of groundwater in the sand beds identified in 14 logs

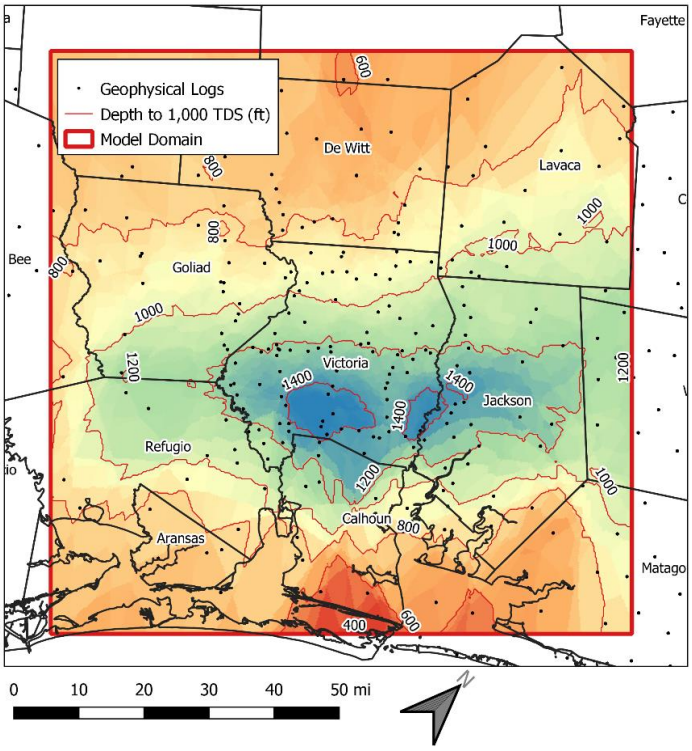

Figure 2-21 Depth to the base of groundwater with a TDS concentration of 1,000 mg/L based on interpretation of geophysical logs

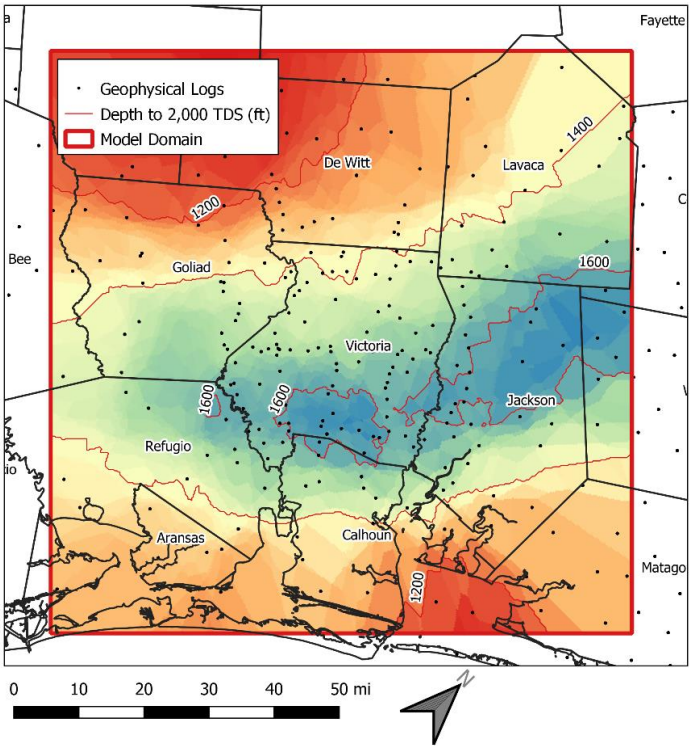

Figure 2-22 Depth to the base of groundwater with a TDS concentration of 2,000 mg/L based on interpretation of geophysical logs

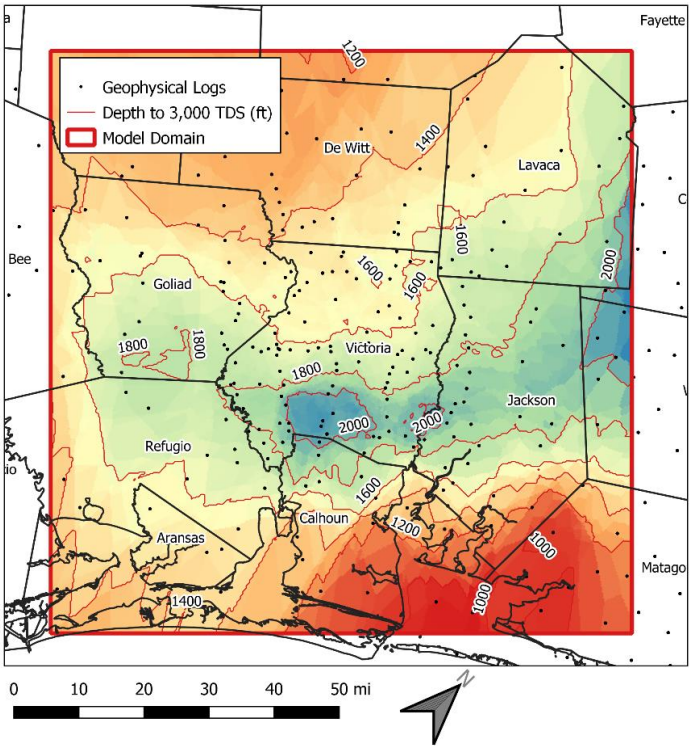

Figure 2-23 Depth to the base of groundwater with a TDS concentration of 3,000 mg/L based on interpretation of geophysical logs

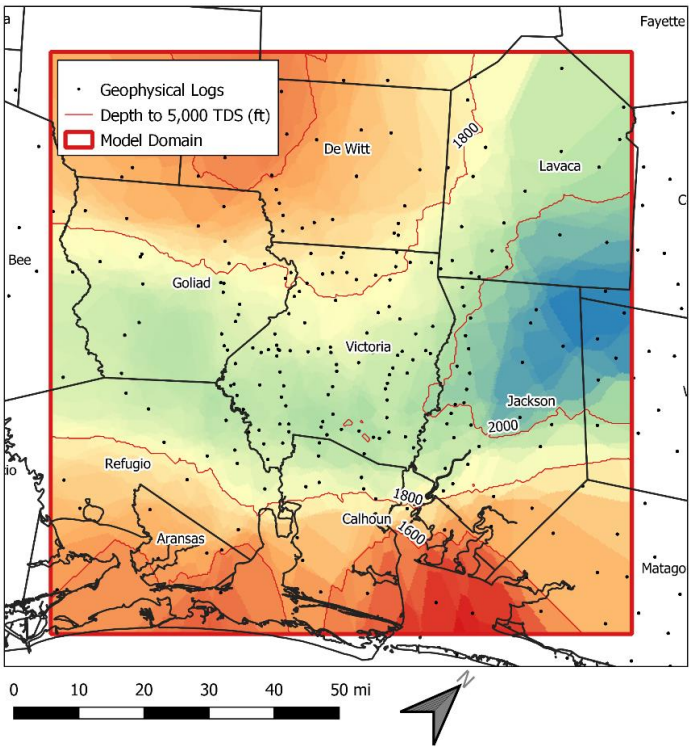

Figure 2-24 Depth to the base of groundwater with a TDS concentration of 5,000 mg/L based on interpretation of geophysical logs

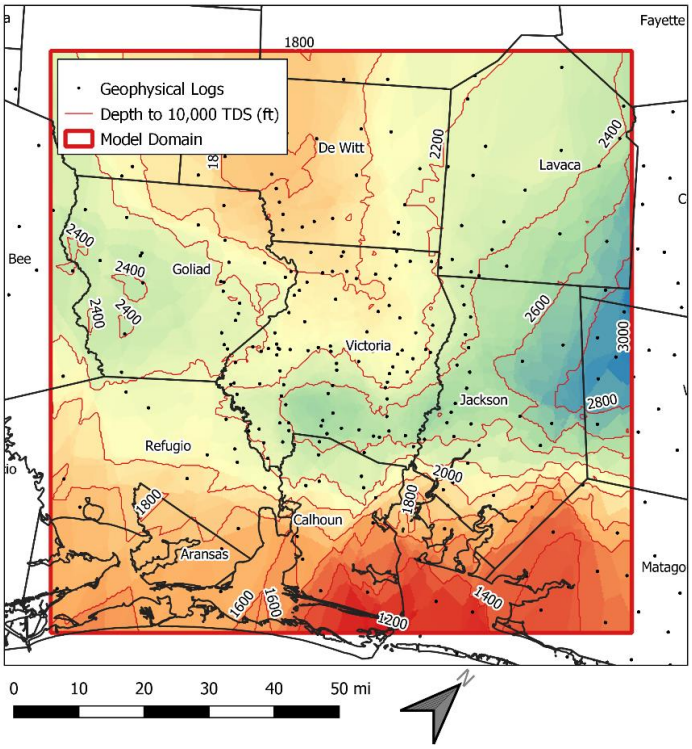

Figure 2-25 Depth to the base of groundwater with a TDS concentration of 10,000 mg/L based on interpretation of geophysical logs

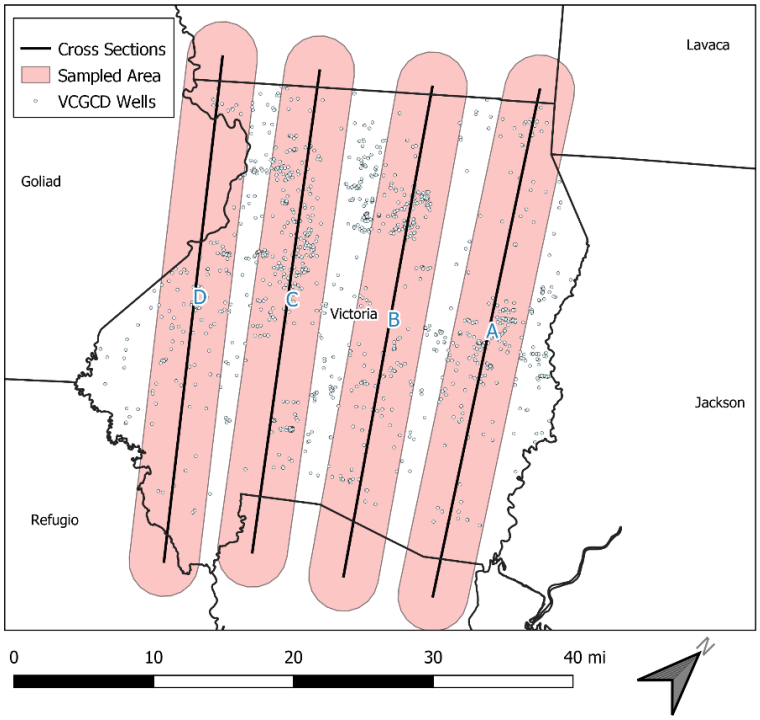

Figure 2-26 Location of four transects used to create vertical cross-sections A, B, C, and D that show bottom boundary of formations and groundwater with different TDS concentrations

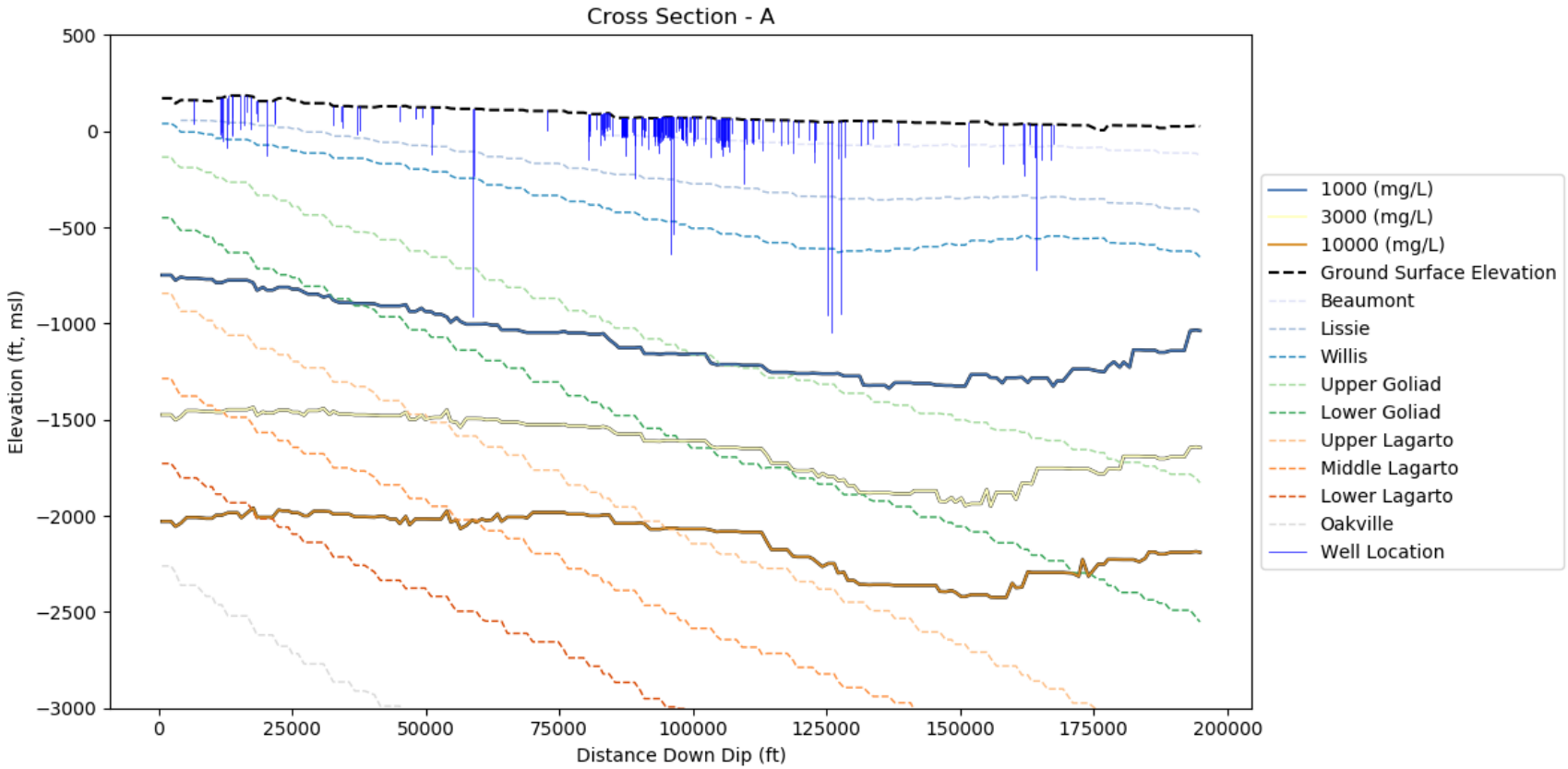

Figure 2-27 Cross-section A showing the base geological formation, salinity zones, and groundwater wells from the VCGCD database

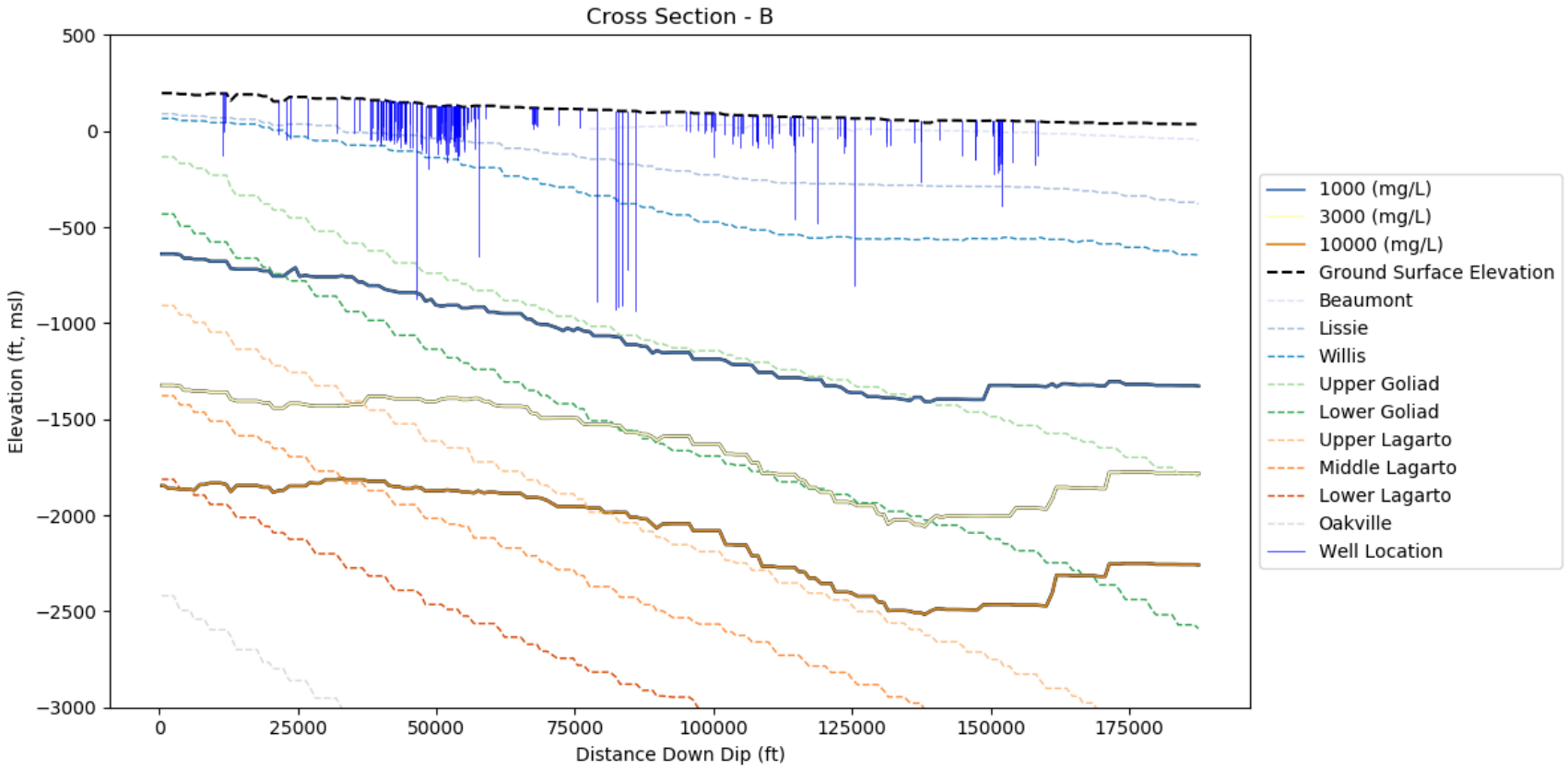

Figure 2-28 Cross-section B showing the base geological formation, salinity zones, and groundwater wells from the VCGCD database

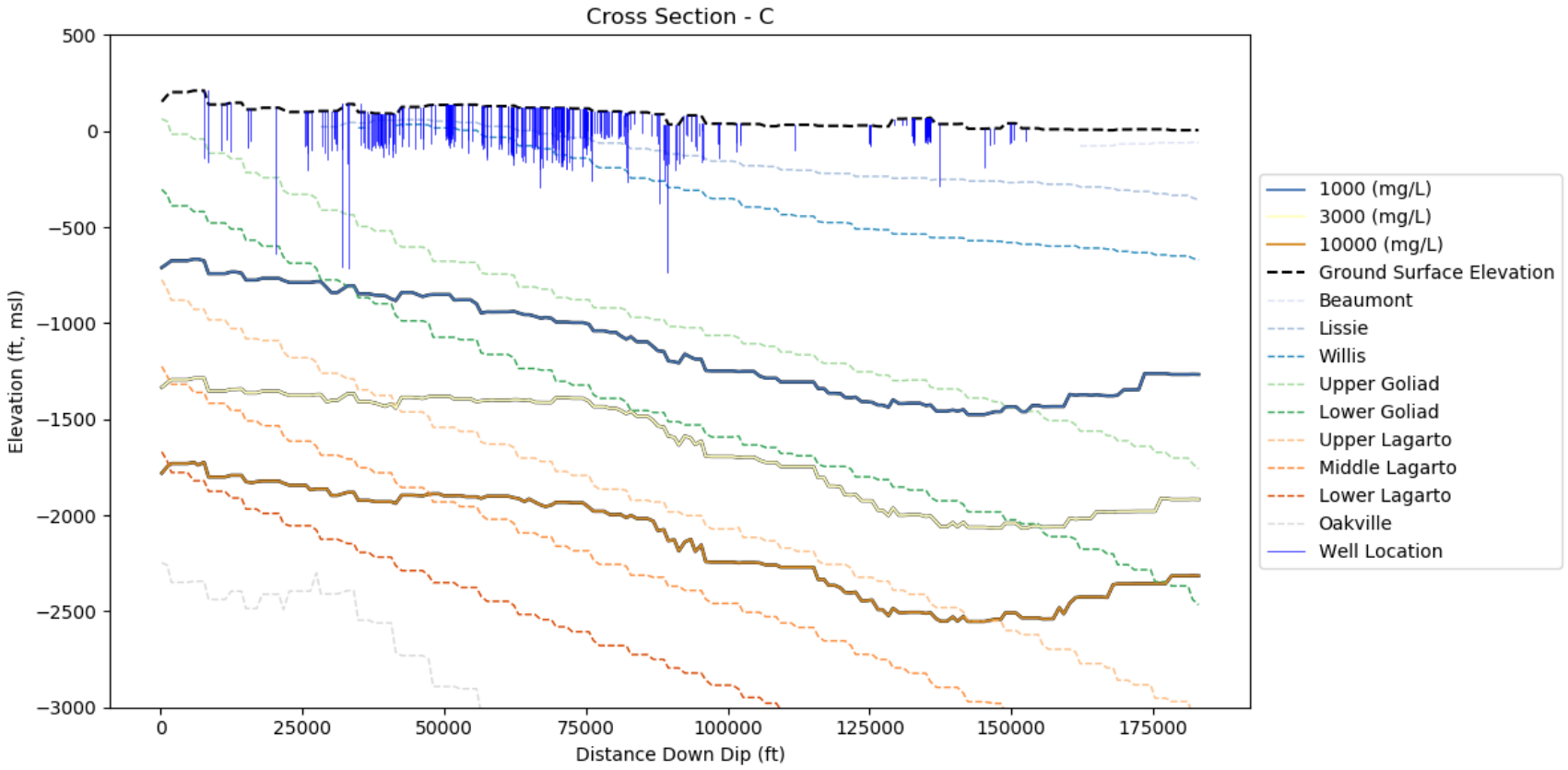

Figure 2-29 Cross-section C showing the base geological formation, salinity zones, and groundwater wells from the VCGCD database

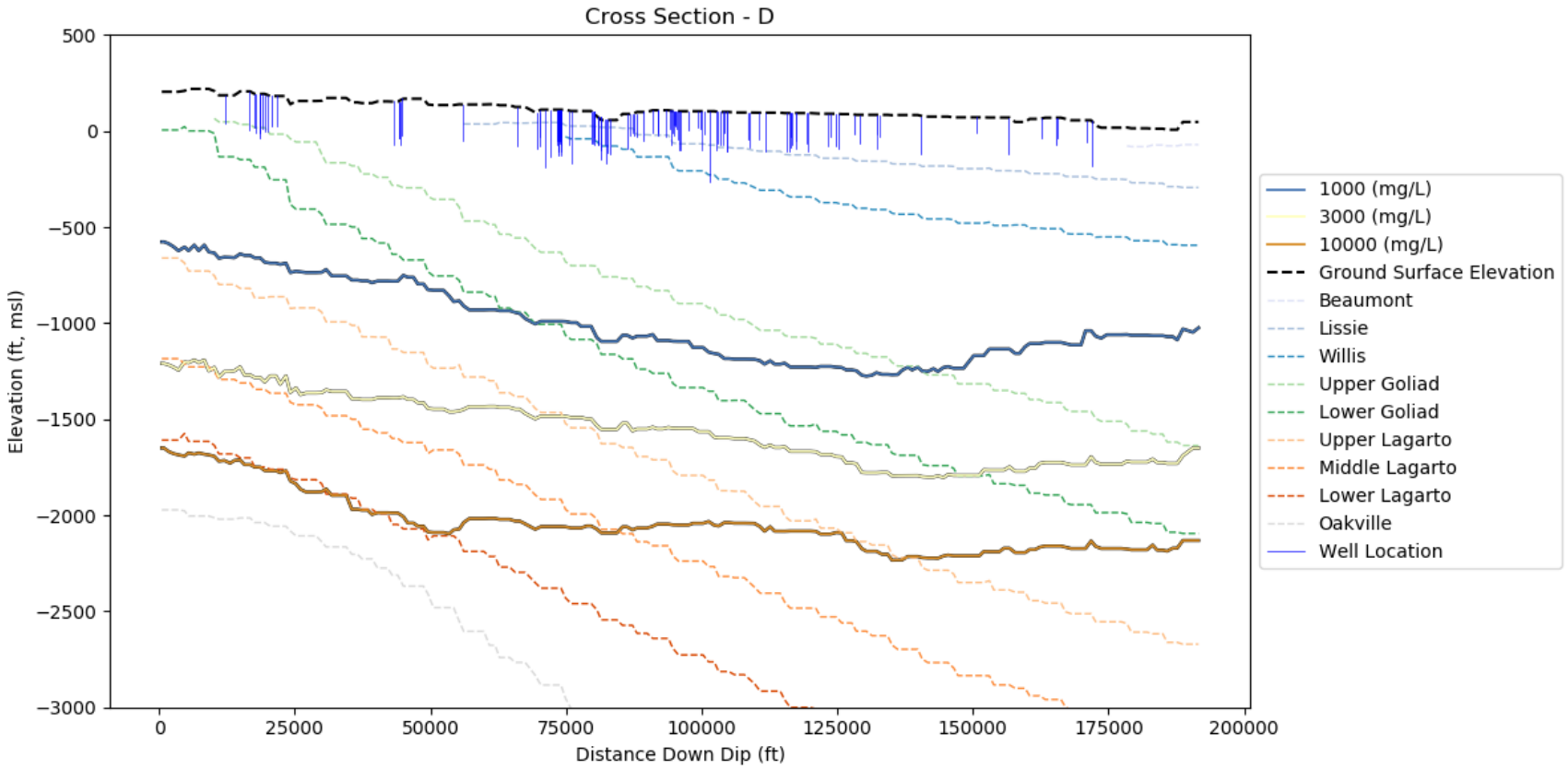

Figure 2-30 Cross-section D showing the base geological formation, salinity zones, and groundwater wells from the VCGCD database

3.0 CHARACTERIZATION OF THE HYDRAULIC PROPERITES OF THE GULF COAST AQUIFER SYSTEM

This section describes the methodologies that will be used to characterize the hydraulic conductivity, porosity, and storage properties of the Gulf Coast Aquifer System in the vicinity of Victoria County.

3.1 Hydraulic Conductivity

Hydraulic conductivity, symbolically represented as K, is an aquifer property that describes the ease with which a fluid (usually water) can move through pore spaces or fractures. Hydraulic conductivity depends on the physical properties of the aquifer deposits, the degree of saturation, and on the density and viscosity of the fluid. Hydraulic conductivity has units with dimensions of length per time (e.g., meters per second or feet per day).

Estimates of hydraulic conductivity are better derived using aquifer pumping tests data obtained from measured responses in the field that span several miles than measurements on cores that are only a few inches thick or wide. The most cost-effective method to determine the transmissivity of an aquifer is to perform hydraulic aquifer tests. Aquifer hydraulic test involve pumping the aquifer and measuring drawdown in the well.

As part of this study, aquifer hydraulic tests were assembled from driller logs from wells that were drilled after 2001 and contained in the TWDB's driller log database and from aquifer tests available from the TCEQ's Public Water Supply (PWS) database. For both sets hydraulic tests, transmissivity values were calculated from the well data, and hydraulic conductivity was calculated from the transmissivity values. The method of Myers (1969) was used to calculate the hydraulic conductivity values by dividing the transmissivity values by the well screen length.

3.1.1 Specific Capacity Tests

The most widely performed hydraulic tests to estimate aquifer productivity and transmissivity are specific capacity tests. Specific capacity tests involve pumping a well and measuring the pumping rate and drawdown in the well. Once the data are obtained, specific capacity is calculated by dividing the total pumping rate by the drawdown (**Equation 3-1**).

$$SC = Q/s \qquad \text{(Equation 3-1)}$$

Where

SC = specific capacity (volume of water per time/per length)
Q = discharge (volume of water per time)
s = drawdown (length)

Specific capacity is generally reported as gallons per minute per foot (gpm/ft). If the well is pumped at a rate of 100 gpm, and the measured drawdown is 10 ft, then the specific capacity is calculated as 10 gpm/ft. A specific capacity of 10 gpm/ft indicates that, for every foot of drawdown available in a well, the well will produce 10 gpm. So, if the well is to be pumped at a constant rate of 50 gpm, then the

drawdown near the well should be about 5 ft. Specific capacity tests are often performed at a newly installed well to estimate the production capacity of the well.

Several studies have developed relationships between specific capacity and transmissivity for aquifers in Texas (Mace, 2001; Kelley and others, 2004; Young and others, 2009; Prudic, 1991). Mace (2001) provides a thorough discussion of the assumptions and different methods for estimating aquifer transmissivity from a specific capacity value. Among the factors that affect how to determine transmissivity values from specific capacity values are unconfined conditions, well construction, well development, the amount a well screen interval intersects the aquifer thicknesses, the degree to which drilling has disturbed the native aquifer material near the well screen, and measurement error.

Most specific capacity tests performed in the Texas Gulf Coast Aquifer were performed by drillers at the time of the well construction. Such tests are often performed quickly, under non-ideal conditions and without proper quality control. Moreover, a driller is performing the test to demonstrate the productive capacity of the well rather than to determine the transmissivity of the aquifer.

For this study, transmissivity values were determined from specific capacity values using **Equation 3-2**. Equation 3-2 was developed by Prudic (1991) using data from more than 2,500 aquifer pumping tests from the Gulf Coast Aquifer System for which transmissivity values had been calculated. The majority of these aquifer pumping tests were performed in Texas, Louisiana, and Mississippi. In Equation 3-2, specific capacity has the units of square feet per day (ft^2/day). To convert specific capacity from units of gpm/ft to units of ft^2/day requires multiplying by a factor of 192.5 ft^3/(gpm*day).

$$T = 3.89 * SC^{0.896} \qquad \text{(Equation 3-2)}$$

Where

T = transmissivity (ft^2/day)

SC = specific capacity (ft^2/day)

Approximately 6,300 specific capacity tests were calculated from driller logs and used in Equation 3-2 to calculate transmissivity values. **Table 3-1** shows the distribution of the specific capacity tests by formations. **Figures 3-1** through **3-9** show the well location where transmissivity values have been calculated from the specific capacity values for the 13 formations listed in Table 2-1. For each formation, hydraulic conductivity values were calculated by dividing the transmissivity values by the screen lengths and then grouped by depositional setting using the maps of depositional settings developed by Young and others (2010). The hydraulic conductivity values associated for each formation were partitioned into one of two groups. One group included all depositional facies associated with coastal depositional settings. The other group included all depositional facies associated with fluvial depositional settings. This grouping is similar to that used by Young and others (2016), who demonstrated that the relationship between sand percent and hydraulic conductivity was dependent on depositional settings. As a general rule, for the same sand percent the hydraulic conductivity will be higher for deposits created by from fluvial deposition than from a coastal deposition.

Table 3-1 Distribution of specific capacity tests by formation in the study area

Formation	Number of Specific Capacity Tests
Beaumont	710
Lissie	722
Willis	449
Lower Goliad	503
Upper Goliad	476
Upper Lagarto	581
Middle Lagarto	587
Lower Lagarto	763
Oakville	1539
Total	6330

To estimate an average hydraulic conductivity for each formation, the hydraulic conductivity values were divided by depositional setting (coastal and fluvial) and by well screen. The hydraulic conductivity values were divided into one of four bins based on well screen length. The bin sizes, based on well screen length, were less than 20 ft, between 20 and 40 ft, between 40 and 100 ft, and between 100 and 400 ft. The grouping by well screen was performed to remove a potential bias that was demonstrated by Young and Kelley (2006) to exist in hydraulic tests in the central Texas Gulf Coast Aquifer System.

As discussed by Young and Kelley (2006), this bias occurs for two reasons. The first reason is that short well screens typically are screened across a zone of relatively high permeability because drillers usually preferentially set screens across the first set of sand beds that will meet the well productivity desired by the well owner. The second reason is that the pumping of a short well screen in a thick aquifer will create a converging flow to the well and cause the transmissivity calculated from traditional methods to be reflective of an aquifer interval longer than that of the well screen. The inverse relationship between the magnitude of hydraulic conductivity and well screen length has been shown to exist in the Central Gulf Coast Aquifer System (Young and Kelley, 2006; Young and others, 2009), in the Northern Trinity Aquifer (Kelley and others, 2014), and in the Yegua-Jackson Aquifer (Deeds and others, 2010).

Figures 3-10 through **3-12** show the sensitivity of average hydraulic conductivity as a function of screen length for formations in the Chicot Aquifer, Evangeline/Burkeville Confining Unit, and the Jasper Aquifer. Results for a formation-depositional setting group are only shown where at least three of the four bins have five or more hydraulic conductivity values. In the three figures, the calculated averages for well screen groups with less than five hydraulic conductivity values are not posted. For each well screen group, with five or more hydraulic conductivity values, the geometric and arithmetic averages of hydraulic conductivity are provided. Out of the 14 plots of hydraulic conductivity versus screen size, 13 confirm the expected result of decreasing hydraulic conductivity values with increasing screen size for both the arithmetic and geometric mean.

For well groups with more than ten hydraulic conductivity values, hydraulic conductivity averages for the largest well screen bin (100 to 400 ft) were compared to hydraulic conductivity values obtained from similar analysis performed to support the development of the Lower Colorado River Basin (LCRB) model (Young and others, 2009). (Figure 2-2 shows that there is considerable overlap in the domain covered this study area and the study area for the LCRB model.) Because the LCRB model included only model layers for the Beaumont, Lissie, Willis, Upper Goliad, and Lower Goliad formations, only five of the nine

well screen groupings could be compared. Based on similar results for these five groups from this study and the LCRB model study (Young and others, 2016), the results from Young and others (2016) were adopted for this study and interpolated to provide a relationship between sand percent and-hydraulic conductivity for the formations older that the Lower Goliad Formation.

The sand percent and hydraulic conductivity relationship for the formations older than the Lower Goliad Formation were scaled to relationship for the Lower Goliad Formation based on the ratio of the average hydraulic conductivity values for the well screen bin for well screens between 100 and 400 feet. This comparison indicated that the Upper Lagarto, Middle Lagarto, Lower Lagarto, and Oakville formations should be scaled 65, 40, 40, and 55 percent (%), respectively. These ratios were used to develop the hydraulic conductivity values in **Table 3-2** for these four formations.

Table 3-2 shows the breakpoints used to estimate hydraulic conductivity from sand percentage based on a fluvial or a coastal deposition setting. The interpolation of the hydraulic conductivity and sand percent is based on minimum and maximum values and values for the 25th, 50th, and 75th percentiles. Interpolation between the five breakpoints is linear. For example, to calculate values for the 37.5th percentile for fluvial deposits in the Beaumont formation, one would take the midpoint between the 25th and the 50th percentiles, which is the 37.5 percentile, and calculate a sand porosity of 57.5% and a formation hydraulic conductivities of 16.5 ft/day.

Table 3-2 Breakpoints used to calculate hydraulic conductivity as a function of sand percent by formation and depositional environment.

Formation	Depositional Environment	Percentile									
		Minimum		25th		50th		75th		maximum	
		K (ft/day)	Sand Percent (%)	K (ft/day)	Sand Percent (%)	K (ft/day)	Sand Percent (%)	K (ft/day)	Sand Percent (%)	K (ft/day)	Sand Percent (%)
Beaumont	Fluvial	5	1	13	33	20	49	28	58	30	76
	Coastal	5	1	8	36	10	46	13	55	15	70
Lissie	Fluvial	10	1	24	59	33	70	51	83	75	95
	Coastal	7	1	11	52	12	60	20	66	30	88
Willis	Fluvial	5	1	14	55	20	66	30	77	50	96
	Coastal	5	1	8	44	13	58	24	69	35	94
Upper Goliad	Fluvial	5	1	8	42	13	56	20	66	35	84
	Coastal	5	1	9	45	13	55	16	62	20	99
Lower Goliad	Fluvial	5	1	7	41	11	53	17	59	25	82
	Coastal	5	1	8	36	10	45	13	55	15	93
Upper Lagarto	Fluvial	3.25	1	5	41	7	53	11	59	16	82
	Coastal	3.25	1	5	36	7	45	8	55	10	93
Middle Lagarto	Fluvial	2	1	3	41	4	53	7	59	10	82
	Coastal	2	1	3	36	4	45	5	55	6	93
Lower Lagarto	Fluvial	2	1	3	41	4	53	7	59	10	82
	Coastal	2	1	3	36	4	45	5	55	6	93
Oakville	Fluvial	2.5	1	3.5	41	5.5	53	8.5	59	12.5	82
	Coastal	2.5	1	4	36	5	45	6.5	55	7.5	93

3.1.2 Aquifer Pumping Tests

One of the largest sets of existing aquifer pumping test data in the state is managed by the TCEQ PWS program. TCEQ has amassed numerous aquifer pumping tests because a long-term pumping test of about 36 hours is required by TCEQ to demonstrate the production capacity of a PWS well. In 2012a, INTERA reviewed these files for five counties in the study area. From these analysis, INTERA (Young, 2012 b, c, d, e, f, g, h, i) calculated 44 transmissivity values based on a Cooper-Jacob straight-line (Cooper and Jacob, 1946) analysis of the time drawdown data. **Figure 3-13** shows the location of these tests. Out of these tests, only the Upper Goliad Formation has ten or more tests with well screen lengths greater than 100 ft. **Table 3-3** lists the transmissivity values calculated for ten wells with well screen intervals greater than 250 ft that primarily intersect the Upper Goliad Formation. The hydraulic conductivity values in Table 3-3 were calculated using the method used by Myers (1969). The average and geometric mean of the hydraulic conductivity values are 11.2 and 10.8 ft/day, respectively. Across these ten well screen locations, the estimated average sand percent is about 54%. These two sets of values compare favorably to the tabulated values for the 50th percentile in Table 3-2 for coastal deposits comprising the Upper Goliad Formation, which is a sand percentage of 55% and an average hydraulic conductivity of 13 ft/day.

Table 3-3 Aquifer Tests in wells with screen intervals greater than 250 feet that primarily intersect coastal deposits comprising the Upper Goliad Formation

Public Well ID	Total Length of Well Screen (ft)	Transmissivity (ft^2/day)	Average Hydraulic Conductivity (ft/day)
G2350002D	368	4,437	12
G2350014B	450	6,337	14
G2350002A	558	6,018	11
G2350002B	585	6,461	11
G2350002I	588	7,480	13
G2350002J	590	10,088	17
G2350002G	614	5,468	9
G2350002F	616	6,712	11
G2350002M	640	3,786	6
G2350002H	644	5,601	9

3.2 Porosity

Porosity is the volume of the void space of a geologic material divided by the total volume of the material. A fully-saturated soil or geologic unit is one where all porosity of the material is filled with water. Because of the different minerals and particles that comprise sands and clays, the two lithologies have different porosities and the two lithologies have different compressibility properties with increase geostatic pressure.

Estimates for clay porosity are based on laboratory measurements of porosity and compressibility reported by the USGS for three study areas near Houston, Texas (Gabrysch and Bonnet; 1974, 1976a, 1976b). Kelley and others (2018) used consolidometer test data from these USGS study to develop **Equation 3-3** to express porosity a depth of burial for clay. An presumption with the application of Equation 3-3 is that above a depth of 100 ft, the clay porosity is 50%.

$$n = 1.4485D^{-0.233} \quad \text{(Equation 3-3)}$$

Where:

D = for depth below ground surface greater than 100 ft

n = porosity

Estimates for sand porosity are based on analysis of neutron-density logs from 34 geophysical logs located through the Gulf Coast Aquifer System. At each log, 10 to 20 porosity measurements were made at depths ranging from the surface to almost 8,000 ft, although most measurements were less than 5,000 ft deep. The data show a decrease in porosity with depth that is expressed by **Equation 3-4**, which is identical to Equation 2-4. Equation 3-4 is similar and agrees with several previous studies. Equation 3-4 indicates that porosity decreases about one percent every 1,000 feet of depth. Wallace and others (1972) report a decrease of 0.95 and 0.85% in porosity every 1,000 ft in the for the Rio Grande and Houston embayments, respectively. Loucks and others (1984) report a range of 1.28 to 2.05% decrease in porosity for every 1,000 ft of depth for the southern, central, and northern portion of the Frio Formation in the Texas Gulf Coast Aquifer System.

$$\Phi = 36.64 - 0.001 * d \quad \text{(Equation 3-4)}$$

Where:

Φ = porosity

d = depth (feet)

Table 3-4 tabulates the change in porosity with depth for clays and sands based on Equations 3-2 and 3-4, respectively. **Figure 3-15** illustrates graphically porosity changes with depth. At ground surface, sand and clay have porosities of about 37% and 50%, respectively. At a depth of 385, the sand and clay have the same porosity of 36.2%. For depths greater than 385 ft, sand has a greater porosity than clay. At a depth of 6,000 ft, the porosity of sand and clay are 36.2 and 34.5%, respectively.

Table 3-4 Estimated porosity values for sand, clay, and a deposit consisting of equal mixture of sand and clay as a function of depth

Depth (ft)	Porosity		
	Sand Porosity (%)	Clay Porosity (%)	Porosity_50_Sand% (%)
100	37	50	43
200	36	42	39
400	36	36	36
800	36	31	33
1,200	35	28	32
1,600	35	26	31
2,000	35	25	30
2,500	34	23	29
3,000	34	22	28
3,500	33	22	27
4,000	33	21	27
4,500	32	20	26
5,000	32	20	26
5,500	31	19	25
6,000	31	19	25

3.3 Specific Storage

Specific storage represents how changes in the hydraulic pressure in a formation affects the volume of space occupied by a certain quantity of groundwater under *confined* conditions. Specific storage and aquifer thickness determine aquifer storativity for confined conditions. Specific storage values were developed using the method of Young and others (2009) for calculating specific storage values for evaluating the impacts of pumping brackish groundwater. This methodology is based on the relationship in **Equation 3-5** (Shestakov, 2002) based on geomechanical considerations.

$$Ss = A / [D + z0] \quad \text{(Equation 3-5)}$$

Where

Ss = specific storage (dimensional analysis is per length)
A = calibrated parameter, which is a function of [1/(1+e)]
D = depth (dimensional analysis is length)
z0 = calibrated parameter

The Shestakov model assumes a power-law relationship between porosity and depth, where the decrease is more pronounced at shallower depth than is allowed by a linear relationship between

porosity and depth. The power-law relationship is consistent with the Magara (1978) observation that the rate of porosity decrease is fast at shallow depths and slows down with greater depth of burial. Applications of the Shestakov model for estimating specific storage values include the Northern Trinity and Woodbine GAM (Kelly and others, 2014), the Yegua-Jackson GAM (Deeds and others, 2010), and the LCRB Model (Young and others, 2009; Young and Kelley, 2006).

For this study, **Equation 3-6** is used to estimate specific storage. Equation 3-6 is based on Shestakov's model and was developed for the LCRB model (Young and others, 2009; Young and Kelley, 2006). Equation 3-6 was implemented using the parameters in **Table 3-5**. Figure 3-15 compares the relationship between specific storage and depth predicted by Equation 3-6 and values of specific storage assembled by Young and Kelly (2006) for the LCRB study area.

$$S_s = S_{s_{min}} + \left\{ \frac{A * [SF + CM * (1 - SF)]}{Z0 + [DM * D^{(DE)}]} \right\} \qquad \text{(Equation 3-6)}$$

Where

$S_{s_{min}}$ = minimum value of specific storage
SF = Sand fraction
CM = Clay multiplier
DE = depth exponent
DM = depth multiplier

Table 3-5 Parameters used in Equation 3-6 in the LCRB model (Young and others, 2009) to estimate specific storage

Parameter	Value
Ss_{min}	0.00000001
A1	0.003
CM	2.0
A2	100
DM	10
DE	0.75

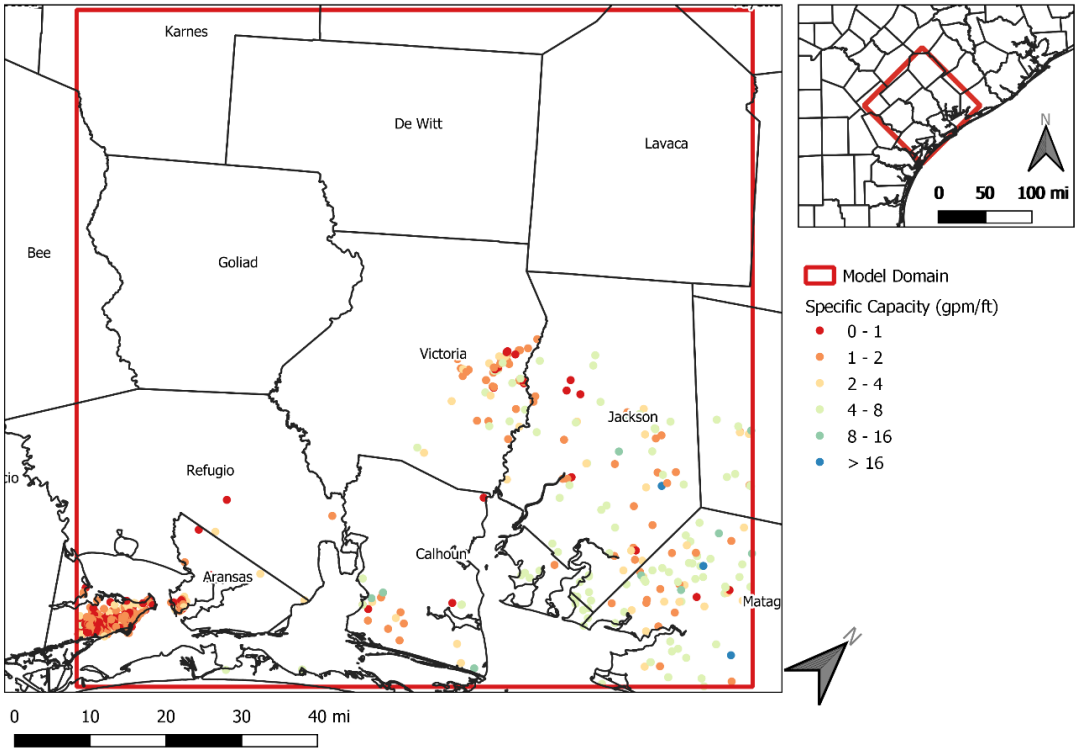

Figure 3-1 Location of specific capacities calculated from driller logs for wells installed in the Beaumont Formation

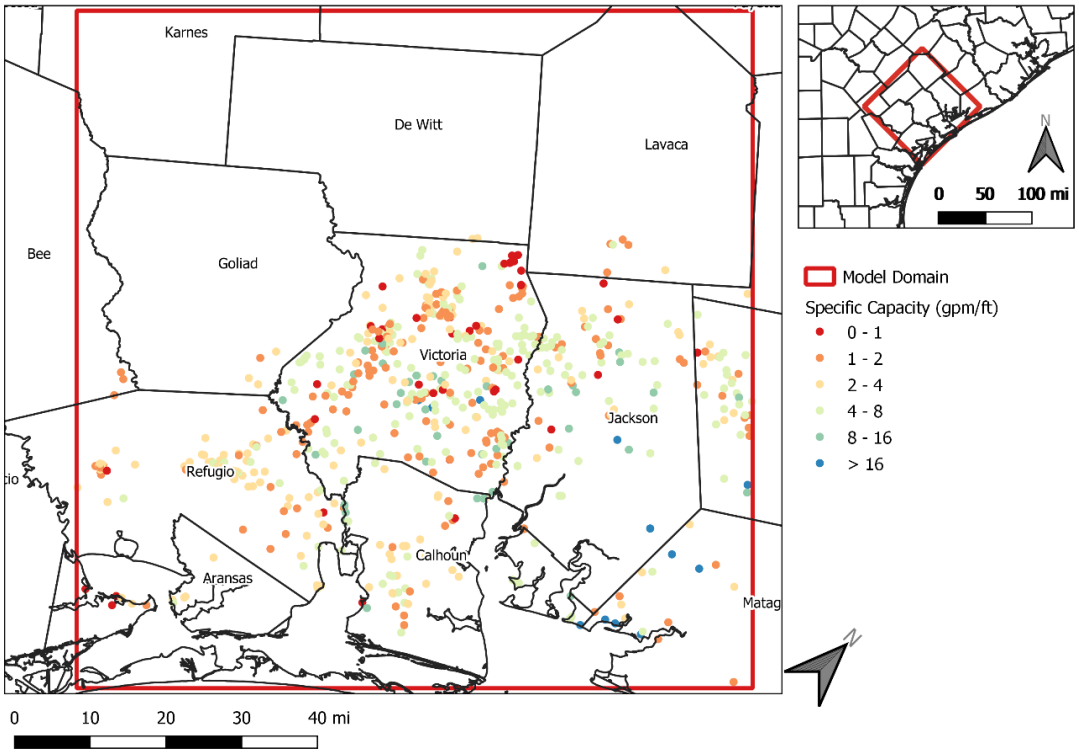

Figure 3-2 Location of specific capacities calculated from driller logs for wells installed in the Lissie Formation

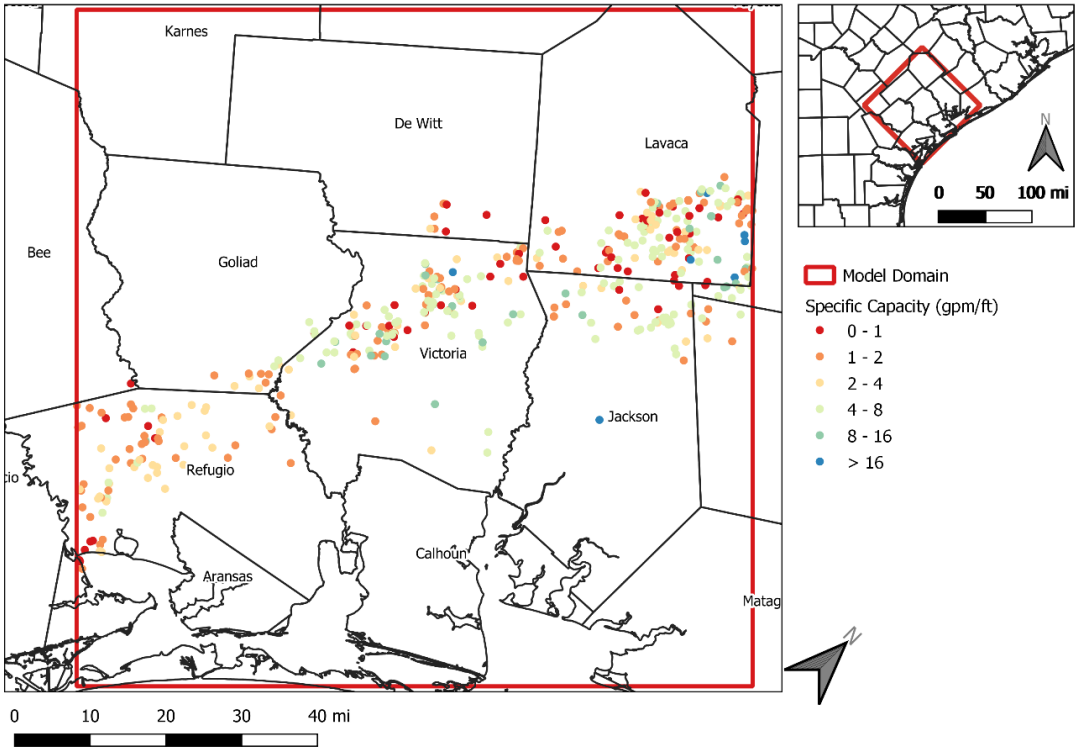

Figure 3-3 Location of specific capacities calculated from driller logs for wells installed in the Willis Formation

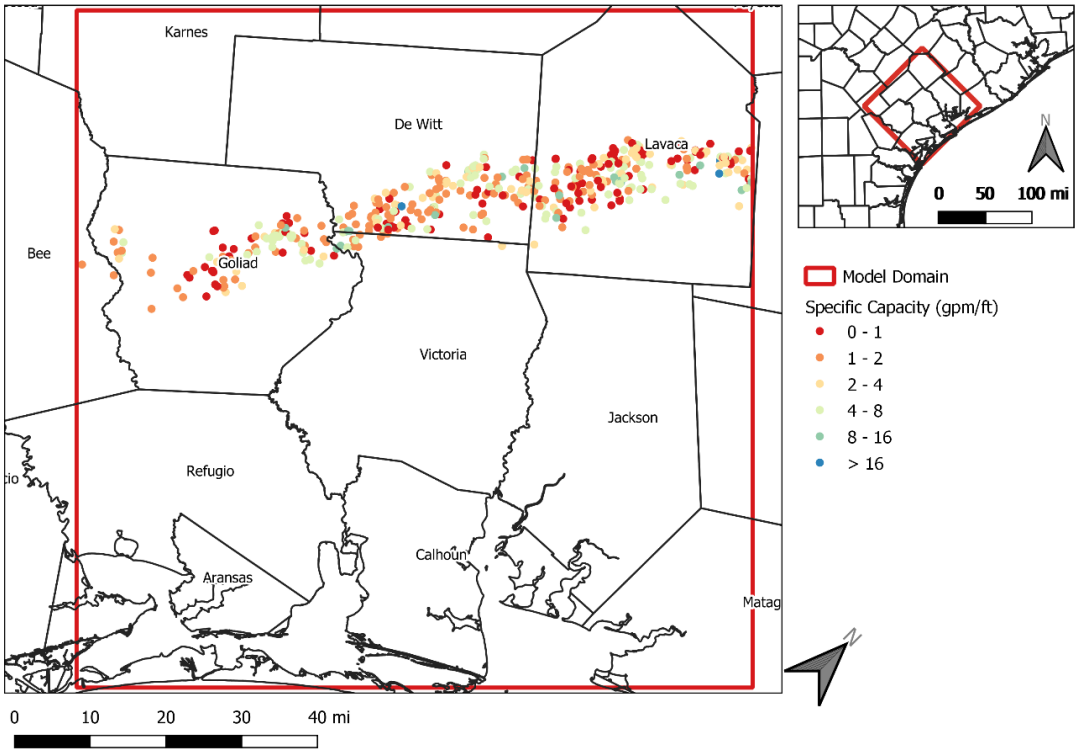

Figure 3-4 Location of specific capacities calculated from driller logs for wells installed in the Upper Goliad Formation

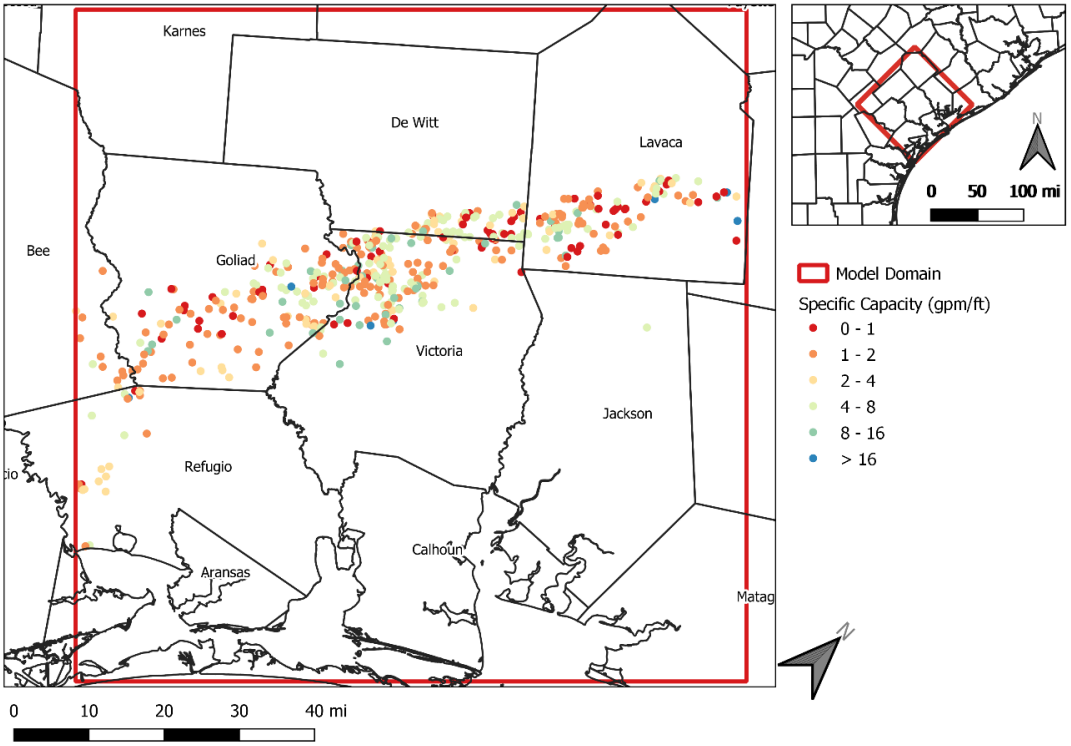

Figure 3-5 Location of specific capacities calculated from driller logs for wells installed in the Lower Goliad Formation

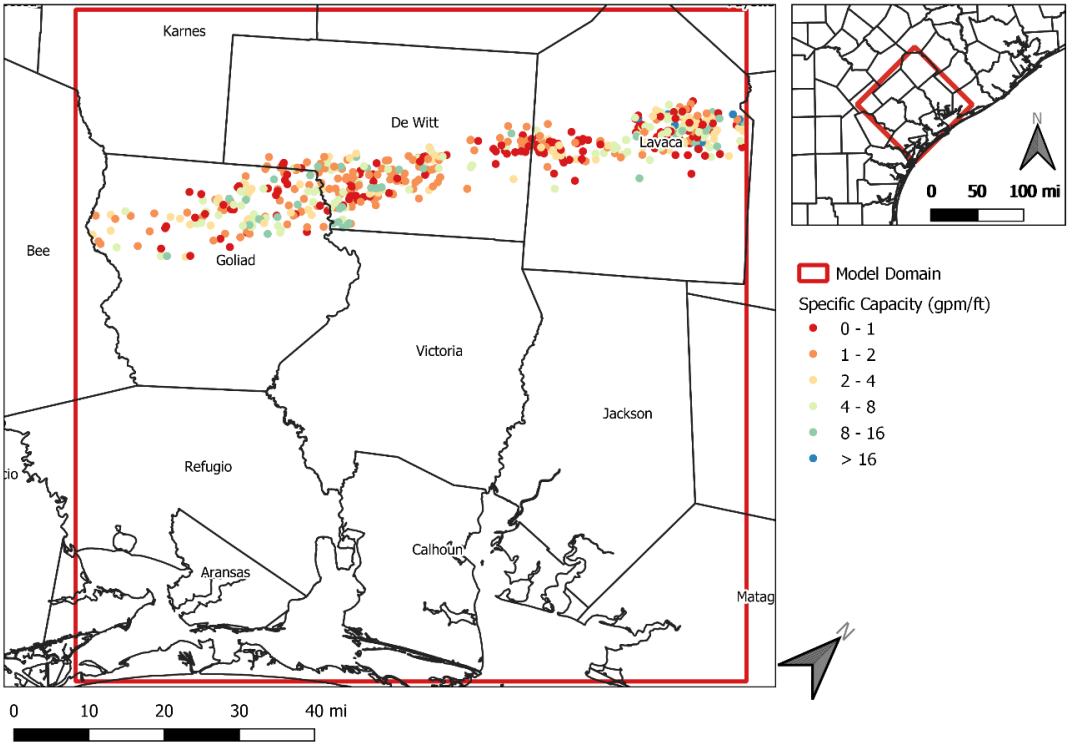

Figure 3-6 Location of specific capacities calculated from driller logs for wells installed in the Upper Lagarto Formation

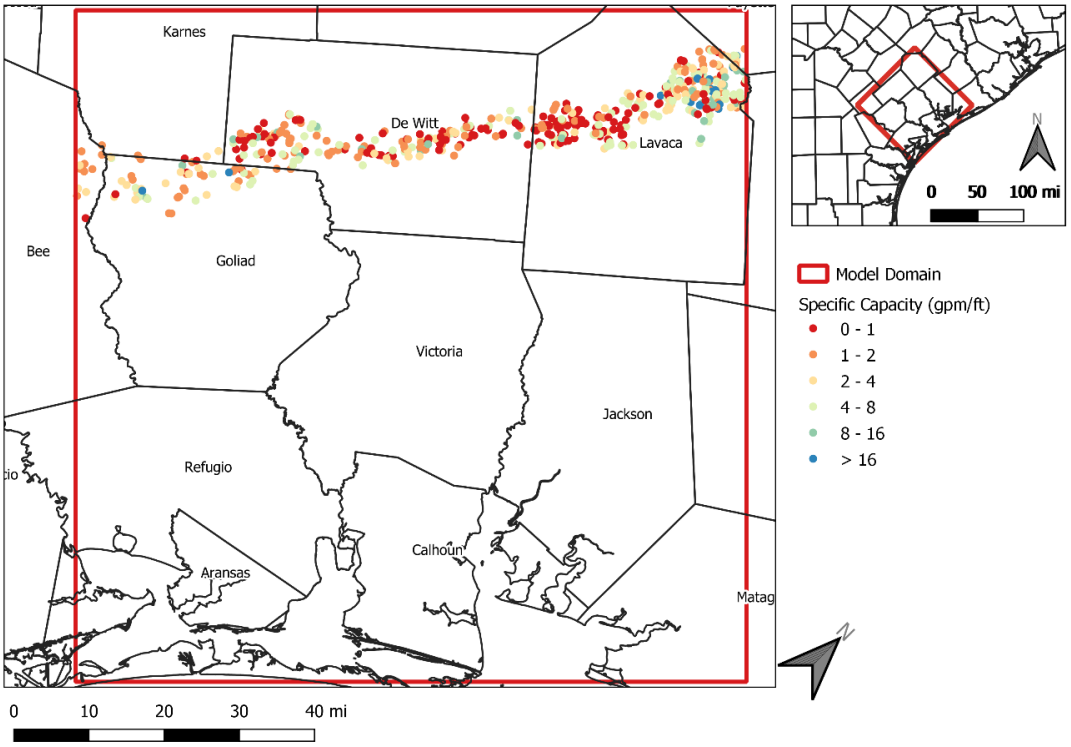

Figure 3-7 Location of specific capacities calculated from driller logs for wells installed in the Middle Lagarto Formation

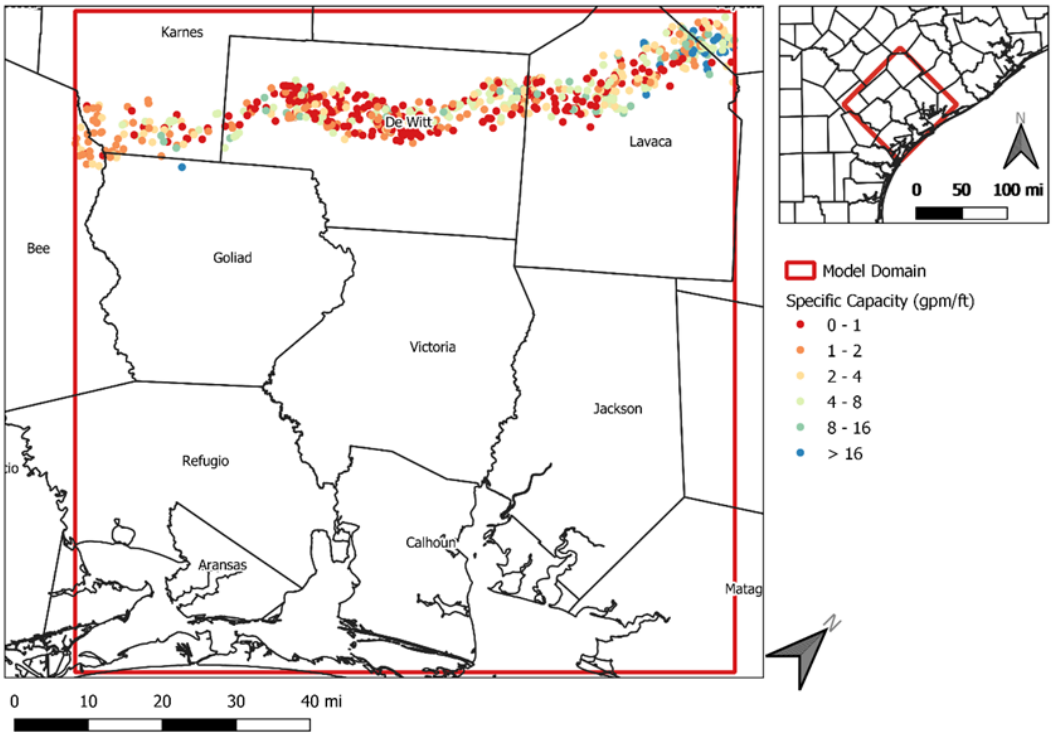

Figure 3-8 Location of specific capacities calculated from driller logs for wells installed in the Lower Lagarto Formation

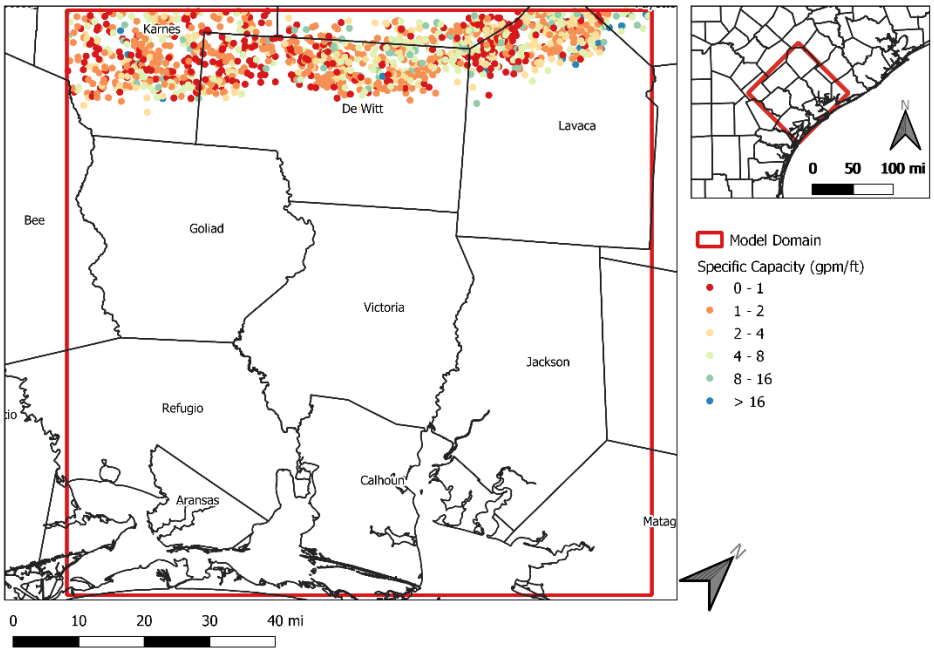

Figure 3-9 Location of specific capacities calculated from driller logs for wells installed in the Oakville Formation

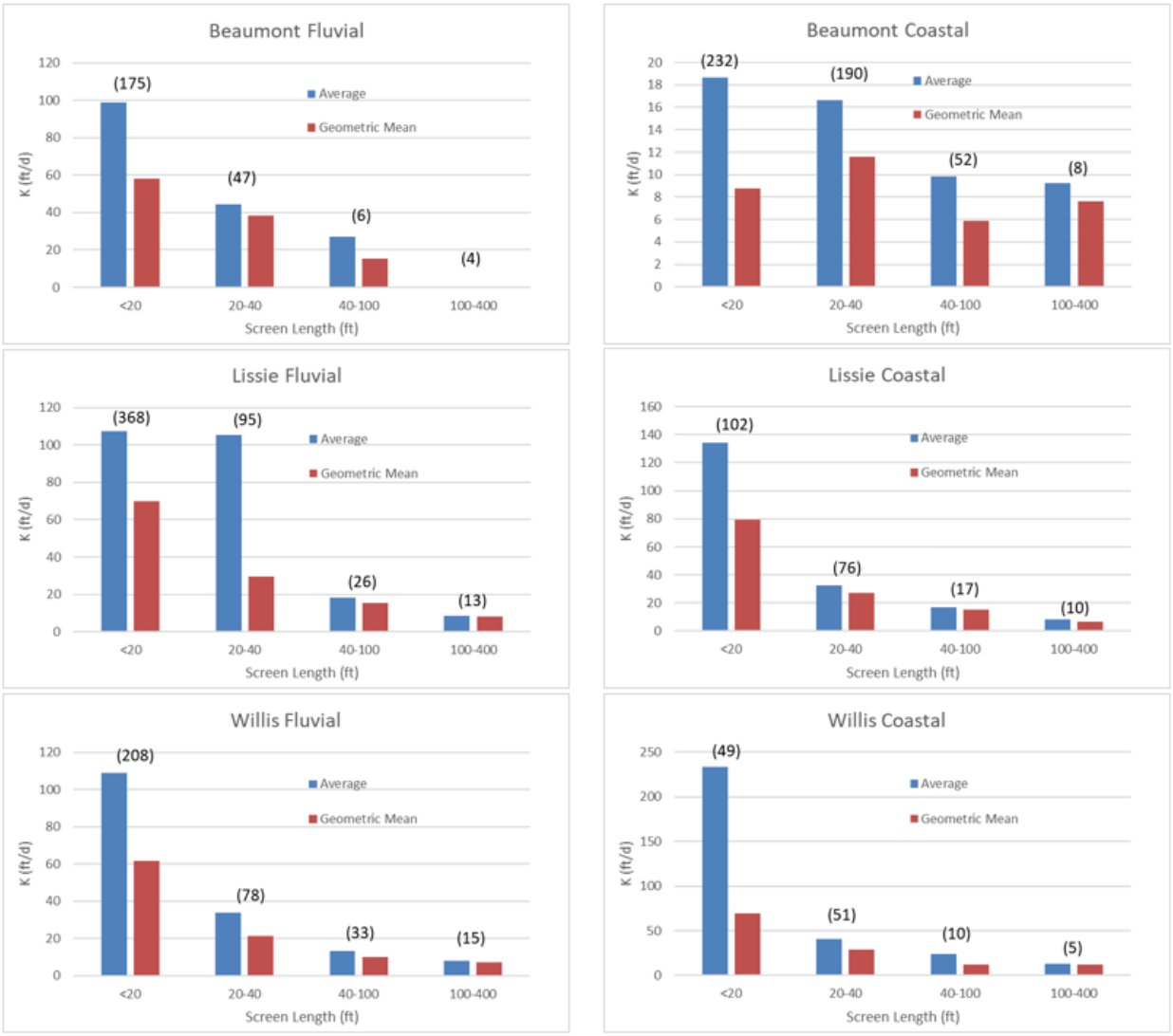

Figure 3-10 Location of aquifer pumping tests performed in Public Supply Wells in the study area

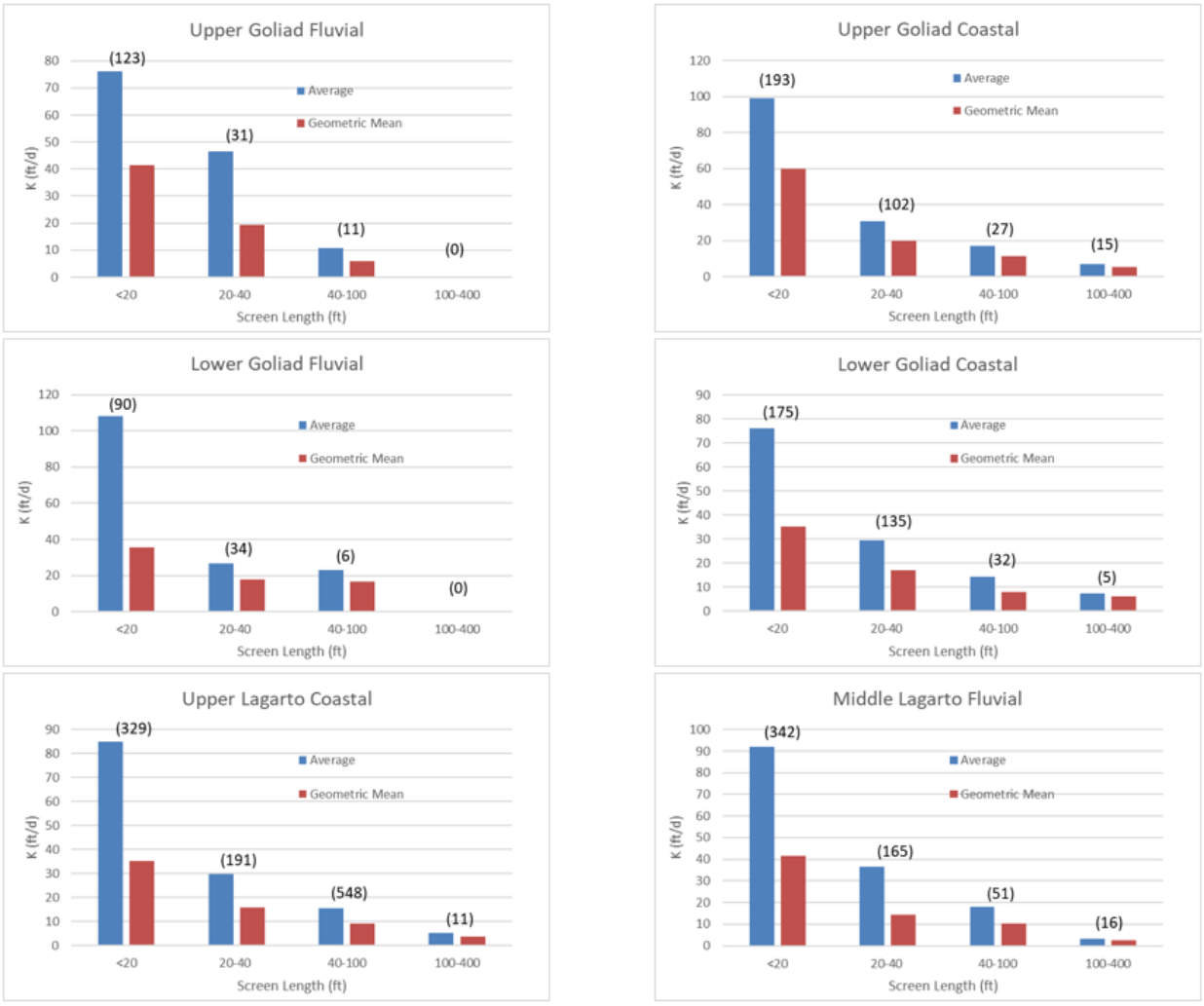

Figure 3-11 Sensitivity of calculated hydraulic conductivity to length of well screen for formations that comprise the Chicot Aquifer in the study area

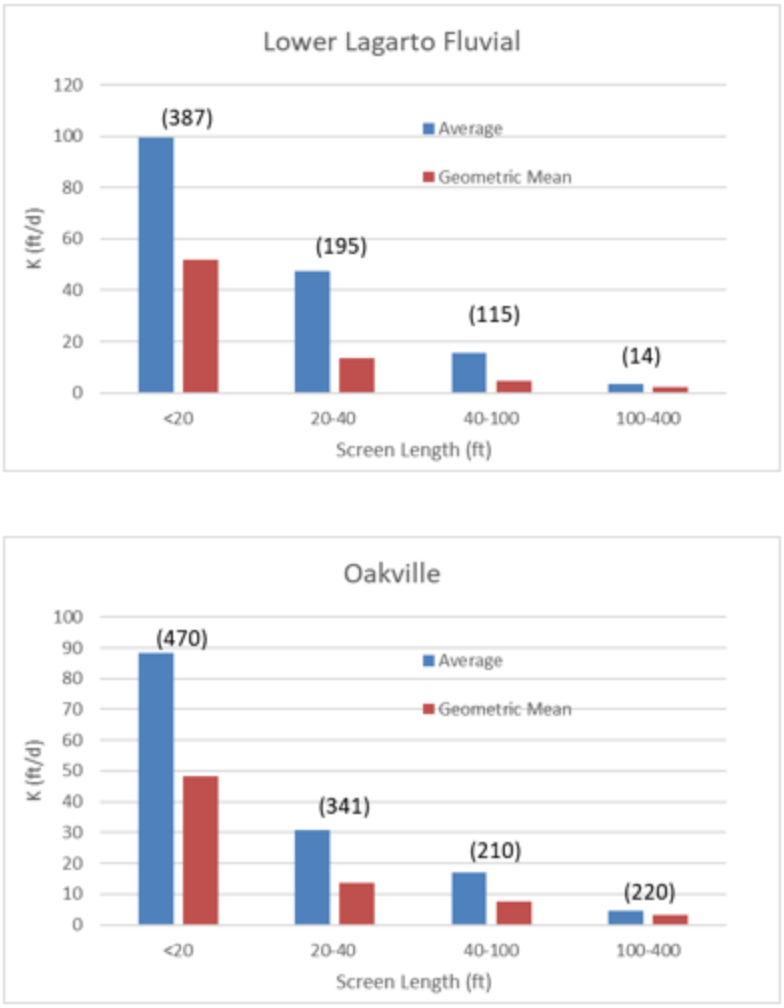

Figure 3-12 Sensitivity of calculated hydraulic conductivity to length of well screen for formations that comprise the Evangeline Aquifer and the Middle Lagarto Formation in the study area

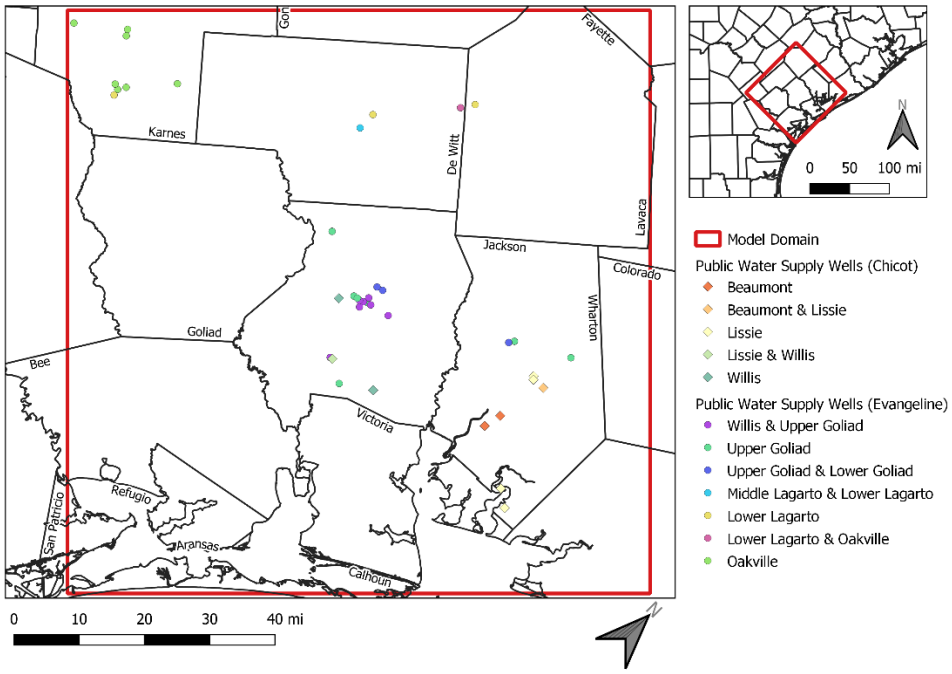

Figure 3-13 Location of aquifer pumping tests performed in Public Supply Wells in the study area

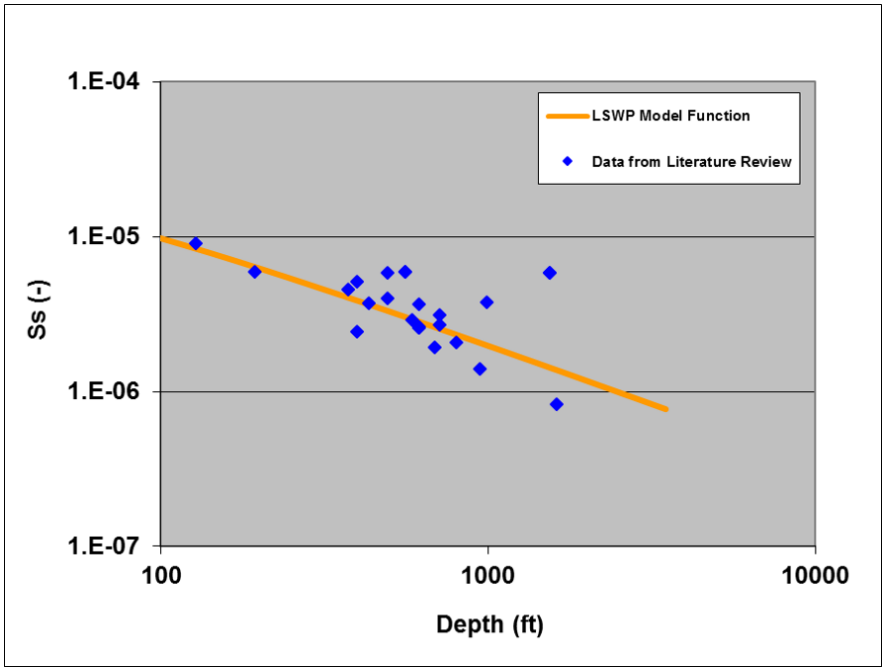

Figure 3-14 Sensitivity of calculated hydraulic conductivity to length of well screen for formations that comprise the Jasper Aquifer in the study area

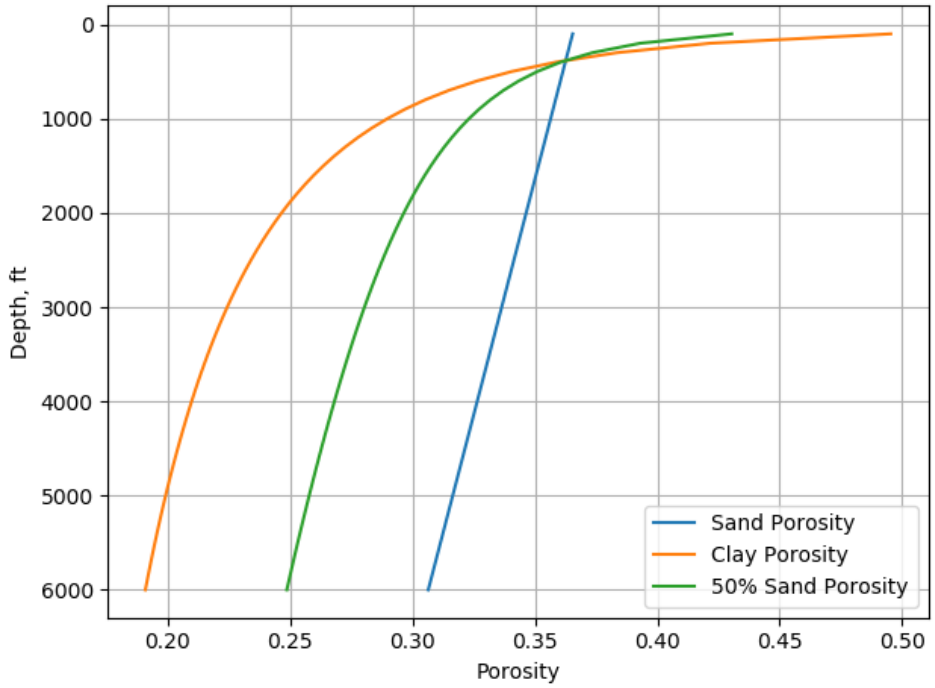

Figure 3-15 Semi-empirical relationship for determing specific storage based on Shetokov (2002) compared to specific storage calculated from aquifer pumping tests (from Young and others, 2016)

4.0 DEVELOPMENT AND APPLICATION OF A GROUNDWATER FLOW MODEL FOR VICTORIA COUNTY

4.1 Construction of Groundwater Flow Model

A three-dimensional groundwater flow model was developed for Victoria County using the MODFLOW-NWT code (Niswonger and others, 2011). The areal extent and horizontal numerical grid for the model is shown in **Figure 4-1**. The model covers an area of 745 square miles and includes a portion of 14 counties. The model domain has been discretized using a numerical grid consisting of 180 rows and ,180 columns. Across most of the model domain, grid cells are represented by 1-mile by 1-mile squares. Toward the middle of the numerical grid, grid cells are represented by 0.25-mile by 0.25-mile squares. The vertical extend of the model extends to a depth of 5425 feet and includes the nine formations listed in Table 2-1 that comprise the Chicot Aquifer, Evangeline Aquifer, Burkeville Confining Unit, and the Jasper Aquifer. These model uses 15 layers to represent these nine formations. For convenience the groundwater flow model is named the Victoria County Groundwater Flow Model (VCGFM).

Figure 4-2 shows the 15 model layers along a northwest-southeast cross-section through the VCGFM grid cells. The model layers were constructed using the formation surfaces provided by Young and others (2010b). Six of the formations are each represented by a single model layer. These formations are the Beaumont, Lissie, Willis, Middle Lagarto, Lower Lagarto, and Oakville. The three formations that comprise the Evangeline Aquifer are represented by multiple model layers. The Upper Goliad, Lower Goliad, and Upper Lagarto formations are represented by four, three, and two model layers, respectively. Additional model layer resolution was used for these three formations for two reasons. One reason is that the majority of the brackish groundwater in Victoria County occurs in the Evangeline Aquifer. The second reason is the formations that comprise the Evangeline Aquifer are significantly thicker than the formations that comprise the Chicot Aquifer. The Evangeline formations were subdivided with the goal to obtain model layers with nearly equal thickness. The vertical positions for subdividing the formations were pick occur a between a sand and clay bed for several geophysical logs located in the middle of Victoria County.

4.2 Hydraulic Properties in the Groundwater Flow Model

This subsection describes the data and methodologies used to determine the hydraulic properties for the groundwater flow model. The hydraulic properties include horizontal hydraulic conductivity, vertical hydraulic conductivity, transmissivity, specific storage, specific yield, and porosity.

4.2.1 Horizontal Hydraulic Conductivity

The horizontal hydraulic conductivity value for each model grid cell was calculated based on a combination of the methodologies used to generate the hydraulic conductivity values for LCRB groundwater flow model (Young and others, 2009) and groundwater flow models used to simulate the pumping of brackish groundwater in the Texas Gulf Coast (Young and others, 2016). Both of these groundwater models calculate hydraulic conductivity values based on the sand percent of the model grid and adjust the hydraulic conductivity value based on the depth the grid block is below ground

surface. For the horizontal hydraulic conductivity values for the VCGCM were calculated using **Equation 4-1**. The depth adjustment for Equation 4-1 is performed in two steps.

$$K_H = K_{LCRA} * A_{depth} \quad \text{(Equation 4-1)}$$

where

- K_H = horizontal hydraulic conductivity of the grid cell based on the sand percent in the grid cell and application relationship between sand percents and hydraulic conductivity expressed by the values in Table 3-2.
- K_{LCRA} = hydraulic conductivity calculated based on sand percent calculated from relationships determined from Table 3-2 used in the development of the LCRB model (Young and Kelley, 2010)
- A_{depth} = adjustments to depth of burial accounts for the change in the viscosity and density of water with temperature increases with depth and reduction in porosity caused by increases in consolidation with depth

Equation 4-1 includes a temperature adjustment because hydraulic conductivity is a function of the density and viscosity of water, which are temperature-dependent, and groundwater temperature varies with depth. Equation 4-2 (Freeze and Cherry, 1979) shows how hydraulic conductivity is dependent on the density and viscosity of water. **Figure 4-3** shows how hydraulic conductivity will increase with increases in temperature from 32 to 180 °F. This increase occurs primarily because the dynamic viscosity of water decreases with increases in temperature. To estimate the change in temperature with depth, we use the same assumptions used by the TWDB report (Young and others, 2016) that model the production of brackish groundwater near Victoria County. For their groundwater model application in Victoria County, Young and others (2016) presume shallow groundwater across the Texas Gulf Coast Aquifer System is 77 °F and a geothermal gradient of about 20 °F per 1,000 ft, or about 100 °F per 5,000 ft. Based on Figure 4-3, the increase in temperature from about 80 to about 180 °F will cause an increase in the hydraulic conductivity of approximately 140%, which translates to approximately 0.028% increase per one foot of depth. This relationship is expressed by Equation 4-2.

$$K = k*\rho*g/\mu \quad \text{(Equation 4-2)}$$

Where:

K = hydraulic conductivity of media (dimensional analysis is length per time)
k = intrinsic permeability of media (dimensional analysis is length squared)
ρ = density of fluid (dimensional analysis is mass per length cubed)
g = gravitational constant (980.6 square centimeters per second)
μ = dynamic viscosity of fluid (dimensional analysis is mass per length times time)

$$A_{temp} = (1 + D*0.00028) \quad \text{(Equation 4-3)}$$

Where:

- A_{temp} = change in hydraulic conductivity as a function of depth because of a change in temperature of the groundwater
- D = intrinsic permeability of media (dimensional analysis is length squared)

Equation 4-1 includes a porosity correction because porosity is depth dependent as discussed in Section 3.3. Several comprehensive reviews of field measurements (Nelson, 1994; Magara, 1978; Loucks

and others, 1986) provide compelling evidence that the permeability of a formation decreases with decreasing formation porosity. Loucks and others (1984) provide a comprehensive summary of laboratory tests on cores from 253 wells located in the Gulf Coast Aquifer System to demonstrate a general relationship between a decrease in permeability and porosity with depth. Among their findings is that the sandstone porosity reduction rate remains relatively constant from a depth of a few hundred feet to over 10,000 feet.

Figure 4-4 shows data compiled by Loucks and others (1984) from the Catahoula Formation (also known as the Frio formation) and other aquifers along the Texas Gulf Coast Aquifer System. Figure 4-4 shows that there is a log-linear relationship between the decrease in porosity and decrease in intrinsic permeability. Intrinsic permeability is plotted instead of hydraulic conductivity because intrinsic permeability is invariant with the properties of the liquid. The data in Figure 4-4 represent approximately a reduction in porosity of 10% correspondence to approximately a 30-fold reduction in permeability. The ratio was used to develop **Equation 4-4**, which was used by Young and others (2016) to account for how a reduction in porosity in the Gulf Coast Aquifer System translates into a reduction hydraulic conductivity. **Equation 4-5** shows that the combined adjustment to hydraulic conductivity for A_{depth}, is the product of $A_{porosity}$ and A_{temp}. **Table 4-1** shows provides several example calculations showing the process involved with determining the horizontal hydraulic conductivity for a grid cell.

$$A_{porosity} = 10^{-0.000148*depth} \quad \text{(Equation 4-4)}$$

$$A_{depth} = A_{porosity} * A_{temp} \quad \text{(Equation 4-5)}$$

Where

$A_{porosity}$ = change in hydraulic conductivity as a function of depth because of a change in porosity caused by increases in the geostatic loading

depth = depth in feet

Table 4-1 Example calculations illustrating adjustments to horizonal hydraulic conductivity values to account for changes in increases in temperature and decreases in porosity with depth

Formation	Depostional Setting	Sand percent	Depth of Burial (ft)	Baseline Hydraulic Conductivity (ft/dy)	Adjustments for Changes with Temperature and Porosity			Final Hydraulic Conductivity (ft/dy)
					A_{temp}	$A_{porosity}$	A_{depth}	
Upper Goliad	Coastal	0.5	100	13	1.028	0.966	0.994	12.9
Upper Goliad	Coastal	0.25	500	8	1.140	0.843	0.961	7.7
Upper Goliad	Coastal	0.75	1000	20	1.280	0.711	0.910	18.2
Upper Goliad	Coastal	0.375	3000	14	1.840	0.360	0.662	9.3

4.2.2 Transmissivity

Transmissivity is calculated by multiplying the saturated thickness of the aquifer by the horizontal hydraulic conductivity (**Equation 4-6**).

$$T = b * K_h \quad \text{(Equation 4-6)}$$

where

T = transmissivity (volume of water per width per time)
b = thickness of the aquifer (length)
K_h = horizontal hydraulic conductivity (volume of water per area per time)

Figures 4-5 through **4-19** show the tranmissivity field for the model layers. Appendix A provide the transmissivity for each of the nine formations that comprise the Gulf Coast Aquifer System. The symbology for the transmissivity values are the same for each figure to help facilitate comparison among different figures. When comparing different figures, one needs to remember that all of the formations that comprise the Evangeline aquifer are represented by two or more layers.

4.2.3 Vertical Hydraulic Conductivity

The physical properties of a deposit that affect the hydraulic properties of a deposit include the size, arrangement, and geometry of the subsurface sediments comprising the deposits as well as the amount of compaction and cementation that the deposit has experienced. Because the arrangement and geometry of the subsurface materials have a directional component, the value of hydraulic conductivity changes with direction. The vertical hydraulic conductivity is measured perpendicular to the direction of horizontal hydraulic conductivity.

In the Gulf Coast Aquifer System, the vertical hydraulic conductivity of groundwater is less than horizontal hydraulic conductivity, meaning that water moves more quickly and easily in the horizontal direction. Vertical anisotropy is usually defined as the ratio of K_h (horizontal hydraulic conductivity) to K_v (vertical hydraulic conductivity), or K_h/K_v. In the Gulf Coast Aquifer System, the vertical hydraulic conductivity of groundwater is less than horizontal hydraulic conductivity, meaning that water moves more quickly and easily in the horizontal direction. Vertical anisotropy is usually defined as the ratio of K_h (horizontal hydraulic conductivity) to K_v (vertical hydraulic conductivity), or K_h/K_v.

At a much larger scale of several miles and greater, vertical anisotropic ratios can be greater than 100:1 (Maidment, 1992), meaning that horizontal hydraulic conductivity can be greater than 100 times vertical hydraulic conductivity. The GAMs for the Gulf Coast Aquifer System (Hutchison and others, 2011; Kasmarek, 2012; and Chowdhury and others, 2004) have K_h/K_v values for Chicot, Evangeline, and Jasper aquifers that are greater than 1,000. At the scale of aquifers and regional groundwater flow, the differences between the horizontal and vertical hydraulic conductivities are largely controlled by the layering of sediments deposited by different depositional environments. For example, if an aquifer is comprised of alternating layers of relatively permeable sands associated with beach deposits and of relatively impermeable clays associated with lagoon deposits, then the vertical anisotropy across the entire aquifer thickness will be greater than 1,000 ft because the effective K_h for the aquifer is primarily controlled by the K_h of the sand layers, but the effective K_v for the aquifer is primarily controlled by the K_v of the clay layers.

The methodology used to determine vertical hydraulic conductivity will the same as the methodology used to determine the vertical hydraulic conductivity for the LCRB model. This methodology calculates calculating vertical hydraulic conductivity using the weighted harmonic average of the vertical hydraulic conductivity for the sand fraction and the clay fraction that comprises the grid cell. The vertical hydraulic conductivity for both lithologies is weighted by their respective thickness. The harmonic average

represents the effective hydraulic conductivity of one-dimensional groundwater flow through a series of material with different hydraulic conductivity values (Freeze and Cherry, 1979). This methodology has been used to develop GAMs (Deeds and others, 2003; Dutton and others, 2003) and other regional models funded by the TWDB in the Gulf Coast (Young and others, 2016) and in the Carrizo-Wilcox (Hamlin and others, 2016). **Equation 4-7** calculates the weighted harmonic average for vertical hydraulic conductivity for a deposit consisting of sand and clay.

$$K_v = B/[(b_s/K_{vs}) + (b_c/K_{vc})] \quad \text{(Equation 4-7)}$$

where:

- B = total aquifer thickness
- b_c = total layer thickness of clay deposits
- b_s = total layer thickness of sand deposits
- K_{vc} = vertical hydraulic conductivity of clay
- K_v = effective vertical hydraulic conductivity of sand and clay deposit
- K_{vs} = vertical hydraulic conductivity of sand

For our study, the vertical hydraulic conductivity for the sand is calculated as one-tenth of the horizontal hydraulic conductivity. Based aquifer parameters used calibrate the LCRB model, the vertical conductivity of the clay is set to 0.009 ft/day (3.2E-06 centimeters per second) at ground surface. The hydraulic conductivity of the clay, however, decreases with depth at a different rate than does the hydraulic conductivity of the sand. Based on work of Neglia (2004) and Kelley and others (2018), the hydraulic conductivity of clay decreases with depth is a linear-log relationship similar to that shown in **Figure 4-20**. Figure 4-20 shows that the hydraulic conductivity of clay decreases by a factor of 10 for every 4,000 ft increase in depth. For our study, we adopt the relationship used by the LCRB model, which is that the hydraulic conductivity of clay reduces 10-fold for every 3,500 ft increase in depth.

4.2.4 Specific Storage, Specific Yield, and Porosity

The specific yield for the aquifers were set to 0.10 based on a review of the specific yield used in the LCRB model and the groundwater availability model for the central Gulf Coast Aquifer System (Chowdhury and others, 2004). The specific storage and porosity values were based on equations that considered difference in sand and clay percentages and the effect of depth of burial. The specific storage values were calculated using Equation 3-6. Porosity values were calculated using Equations 3-3 and 3-4.

To help facilitate the placement of potential brackish well fields, the distribution of six salinity zones are shown by model layer in **Figures 4-21** through **4-35**. These distribution were created by interpolation of the brackish information discussed in Section 2. **Table 4-2** shows the total amount of groundwater contained in each model layer and formation in Victoria County for fresh, slightly saline, moderately saline, and very saline groundwater.

The total amount of groundwater contained in the nine formations is 648 million acre-feet (ac-ft). Out of the 648 million ac-ft, 241 million ac-ft (37%) is fresh water; 95 million ac-ft (15%) is slightly saline; 76 million ac-ft (12%) is moderately saline, and 237 million ac-ft (36%) is very saline groundwater. Out of the 241 million ac-ft that is fresh water, approximately 36% exists in the Chicot Aquifer and 63% exists in the Evangeline Aquifer. Out of the 171 million ac-ft that is brackish water, 78% exists in the Evangeline aquifer. The Upper Goliad formation is the formation that contains the most groundwater. The Upper

Goliad contains 122 million ac-ft (51%) of the fresh water and 26 million ac-ft (15%) of the brackish groundwater.

Table 4-3 shows the total amount of groundwater by depth in Victoria County for fresh, slightly saline, moderately saline groundwater. These volumes are based on the assumption that for the sand percent is 30% for all formations at depths shallower than 1,300 feet, the sand percent 26% for all formations between depths of 1,300 and 1,900 ft and the sand percent is 21% for all formations below a depth of 1900 feet. The tabulated volumes in Table 4-3 show that 95 percent of all fresh water exists above a depth of 1,000 feet, that 93 percent of all slightly saline water exists above a depth of 1,800 feet, and 97% of all moderately saline water exists above a depth of 2,400 feet.

Table 4-2 Groundwater volumes (in 1,000 acre-feet) in Victoria County for fresh, slightly saline, moderately saline, and very saline groundwater by model layer and by formation

Formation	Model Layer	Fresh	Slightly Saline			Moderately Saline			Very Saline	Total
		TDS (mg/L)	TDS (mg/L)		Total	TDS (mg/L)		Total	TDS (mg/L)	
		< 1000	1,000 to 2,000	2,000 to 3,000		3,000 to 5,000	5,000 to 10,000		> 35,000	
Beaumont	1	1	0	0	0	0	0	0	0	8,590
Lissie	2	42,791	0	0	0	0	0	0	0	42,791
Willis	3	36,285	0	0	0	0	0	0	0	36,285
Upper_Goliad	4	33,720	0	0	0	0	0	0	0	33,720
Upper_Goliad	5	33,236	83	0	83	0	0	0	0	33,319
Upper_Goliad	6	30,306	2,407	0	2,407	0	0	0	0	32,713
Upper_Goliad	7	25,007	5,821	974	6,796	160	0	160	0	31,963
Total (UG)	4-7	122,269	8,311	974	9,285	160	0	160	0	131,714
Lower_Goliad	8	14,728	9,709	3,729	13,439	800	106	906	0	29,073
Lower_Goliad	9	7,380	10,749	7,482	18,232	649	1,623	2,272	110	27,994
Lower_Goliad	10	4,319	8,638	9,842	18,480	609	3,562	4,172	481	27,451
Total (LG)	8-10	26,427	29,097	21,053	50,151	2,059	5,291	7,350	591	84,518
Upper_Lagarto	11	3,715	11,676	4,895	16,571	7,541	11,598	19,139	3,159	42,584
Upper_Lagarto	12	591	7,958	2,876	10,834	7,133	13,149	20,282	9,443	41,150
Total (UL)	11-12	4,306	19,634	7,772	27,405	14,674	24,747	39,421	12,601	83,734
Middle_Lagarto	13	0	3,699	4,215	7,914	9,581	10,139	19,721	39,199	66,834
Lower_Lagarto	14	0	0	0	0	1,830	7,738	9,568	65,905	75,473
Oakville	15	0	0	0	0	0	10	10	118,308	118,318
Total		240,669	60,741	34,014	94,755	28,305	47,926	76,231	236,604	648,258

Table 4-3 Groundwater volumes (in 1,000 acre-feet) in Victoria County for slightly saline and moderately saline groundwater by depth

Depth of Burial (ft)	Slightly Saline			Moderately Saline			Total
	TDS (mg/L)		Total	TDS (mg/L)		Total	
	1,000 to 2,000	2,000 to 3,000		3,000 to 5,000	5,000 to 10,000		
800 to 1000	2,825	0	2,825	0	0	0	2,825
1000 to 1200	11,044	0	11,044	0	0	0	11,044
1200 to 1400	24,948	0	24,948	0	0	0	24,948
1400 to 1600	22,136	10,311	32,447	1,918	0	1,918	34,364
1600 to 1800	0	16,514	16,514	17,115	0	17,115	33,629
1800 to 2000	0	6,701	6,701	11,364	14,920	26,284	32,985
2000 to 2200	0	210	210	0	21,024	21,024	21,234
2200 to 2400					8,291	8,291	8,291
2400 to 2600					2,399	2,399	2,399
Total	60,953	33,736	94,689	30,396	46,634	77,031	171,719

4.3 Development of a Steady-state Flow Model

A steady-state model was constructed using a three-stage process. The first stage consisted of establishing the general head boundary conditions (GHBCs) for the numerical grid. The second stage consisted of selecting water levels for calibration targets. The third stage consisted of adjusting the properties of the general head boundary conditions during model calibration in order to obtain an acceptable match between the simulated and observed hydraulic heads. These three processes are described in this subsection.

4.3.1 Selection of Flow Boundary Conditions

The primary object with creating a steady-state flow model is to represent regional groundwater flow through Victoria County. The conceptual framework for the VCGFM is that infiltrating rain water recharges the aquifers at the water table and groundwater leaves the aquifers as discharge to either streams or the ocean. To simplify the regional flow system, there is no groundwater pumping, and the water level is considered to be stable and unchanging with the total recharge rate equals the total discharge rate.

GHBCs were used to simulate both aquifer recharge and discharge. GHBCs simulate the exchange of water with the aquifer through an equation that includes an elevation for a pressure head and a hydraulic conductance term. If the pressure head in aquifer is higher than the pressure head used by the GHBC, then the GHBC serves as point of discharge. If the pressure head in the aquifer is lower than the pressure head used by the GHBC, then the GHBC serves as a point of recharge. The hydraulic conductance term used by the GHBC controls the rate of flow.

To simulate recharge into the groundwater model, GHBCs were located in every grid cell on the top of the model and in an aquifer outcrop. For these GHBCs, the pressure head was set to an elevation close

to land elevation and the hydraulic conductance was initially set to 10 ft^2/day. To simulate discharge out of the groundwater model, GHBs were located along the major rivers, along the ocean boundary, and across the bay. For the GHBCs along that represented the ocean boundary, the elevation for the pressure head boundary set to 0 ft msl, and the hydraulic conductance was set to 1,000 ft^2/day. For the GHBCs that represented the major rivers, the elevation for the pressure head boundary set to -10 feet below ground surface, and the conductance was initially set to 15 ft^2/day. The use of GHBCs to represent recharge into the aquifer and discharge into streams and the ocean is similar to the how the GAM for GMA 14 (Kasmarek, 2012) uses GHBCs to represent recharge into the aquifer and discharge into streams and the ocean. Along the bottom and the sides of the groundwater model, no-flow boundaries were used.

4.3.2 Selection of Water Levels for Calibration Targets

One hundred fifty water levels were selected to serve as calibration targets for the steady-state model. The process to select these water levels consisted of the following steps.

- Search the TWDB groundwater database to locate wells with at least three water level measured since 2010.
- Calculate the average water levels for wells and eliminate wells with only one water level measurement or a standard deviation greater than 5 ft.
- Assign each well to a model layer based on an estimate of ground elevation and either the total well depth or the well screen interval. Plot the average water levels by aquifer and eliminate water levels that appear to be depressed because of nearby pumping

Table 4-4 provides the distribution of the 150 water levels by county and by aquifer. Sixty-two of the water levels were assigned to model layers associated with the Chicot Aquifer, and 88 of the water levels were assigned to model layers associated with the Chicot Aquifer. The two counties with the most calibration targets are Goliad County and Victoria County with 45 and 33 water levels, respectively.

Table 4-4 Distribution of water level calibration targets by county and by aquifer

County	Number Wells Per Aquifer		Total
	Chicot	Evangeline	
Calhoun	5	0	5
DeWitt	1	16	17
Goliad	6	39	45
Jackson	23	1	24
Lavaca	1	18	19
Refugio	5	2	7
Victoria	21	12	33
Total	62	88	150

4.3.3 Calibration of the Victoria County Groundwater Flow Model

The model was calibrated by coupling PEST software (Doherty, 2018) with the MODFLOW model. PEST is the name given to a suite of programs that collectively undertake calibration and uncertainty analysis for

environmental and other numerical models. The modeling approach using PEST primarily involved adjusting the hydraulic conductance associated with the GHBCs used to simulate recharge. During the model calibration process, no changes were made to any of the hydraulic properties that were calculated in Section 2.0. Also, no pumping was simulated as the groundwater system was considered to represent steady-state conditions.

The calibration process allows the PEST software to adjust the conductances of the GHBs to optimize the match between the model and observed water levels. The calibration metrics used to evaluate the model calibration is based on residuals (Anderson and Woessner, 1992). A residual, *r*, is defined as the difference between an observed and a simulated hydraulic head per **Equation 4-8**.

$$r = h_o - h_s \quad \text{(Equation 4-8)}$$

where:

r = residual,
h_o = observed hydraulic head, and
h_s = simulated hydraulic head.

The root mean square error, which is traditionally the basic measure of calibration for hydraulic heads, is defined as the square root of the average square of the residuals and is expressed mathematically by **Equation 4-9**. Although the root mean square error is useful for describing model error on an average basis, it does not provide insight into spatial trends in the distribution of the residuals. Information about spatial trends is provided by the mean error and the mean absolute error. The mean error, which is described in **Equation 4-10**, is the average of the residuals. The absolute mean error, which is described in **Equation 4-11**, is the average of the absolute value of the mean error.

$$Root\ Mean\ Squared\ Error = \sqrt{\frac{1}{n}\sum_{t=1}^{n}(h_o - h_s)_t^2} \quad \text{(Equation 4-9)}$$

$$Mean\ Error = \sqrt{\frac{1}{n}\sum_{t=1}^{n}(h_o - h_s)_t} \quad \text{(Equation 4-10)}$$

$$Absolute\ Mean\ Error = \sqrt{\frac{1}{n}\sum_{t=1}^{n}|h_o - h_s|_t} \quad \text{(Equation 4-10)}$$

where:

n = number of observations

A typical calibration criterion for hydraulic heads is that the root mean square error and the mean absolute error are less than or equal to 10% of the observed hydraulic head range in the hydrogeologic unit being simulated. **Figure 4-36** shows a comparison of simulated head versus observed hydraulic head. The comparison shows very match between the two set of values over the entire range of values, which is from 1.5 to 353 ft. **Table 4-5** presents the calibration statistics for the hydraulic heads. All of the statistics are within the TWDB standards for groundwater availability models. Both the mean absolute error and the root mean error are less than 5% of the range in the observed hydraulic heads. These statistics demonstrated that the model is well calibrated to the observed hydraulic heads.

Table 4-5 Calibration statistics for hydraulic heads

Metric	Value (ft)
Number of Points	150
Maximum Head	353
Minimum Head	1.5
Range in Head	351.5
Mean Error	-3.9
Absolute Mean Error	9.8
Root Mean Square Error	12.3

Figures 4-37 through **4-51** shows contours for the simulated hydraulic heads for each of the 15 model layers. All of the contours shows uniform flow toward the Gulf Coast. In each figure, the residuals generated from the model calibrations are plotted. Most of the residuals for Victoria County are in the Lissie and Upper Goliad formations. **Table 4-6** lists the head, the observed head and the residual for the 150 calibration targets.

Because the VCGFM was created to provide a simplistic representation of the shallow groundwater flow system, it does not explicitly account for evapotranspiration or surface water interaction the recharge rate will be lower than if these processes were incorporated into a shallow groundwater system. In most coastal aquifers, the majority of recharge remain in the shallow groundwater flow system until it exits by evapotranspiration or by leakage to a stream. In the VCGCD, the recharge rate will be lower than the actual recharge because it does not account for evapotranspiration or by leakage to a stream. The average recharge rate for the VCGFM is approximately 0.07 inches/year. This rate was determined by adding the recharge from each of the GHBCs and dividing by the total area of the aquifer outcrops.

Table 4-6 Observed, simulated, and calculated residual for 150 calibration targets

State Well Number	County	GAM Coordinates		Formation	Model Layer	Hydraulic Head		Residual
		Easting (ft)	Westing (ft)			Observed	Simulated	
7946810	Refugio	5781419	18617118	Lissie	2	17.8	45.6	-27.7
7913226	Goliad	5734864	18826985	Upper Lagarto	11	177.5	200.1	-22.7
6660501	Jackson	6018794	18910246	Lissie	2	28.3	51.4	-23.1
6660205	Jackson	6023333	18921014	Lissie	2	32.9	54.6	-21.7
8002701	Victoria	5931901	18839554	Beaumont	1	33.9	52.7	-18.8
8017101	Victoria	5892357	18778758	Upper Goliad	5	24.3	39.5	-15.2
8010401	Victoria	5933874	18817150	Upper Goliad	5	24.8	43.1	-18.3
8003803	Jackson	5977449	18843111	Upper Goliad	5	19.0	37.6	-18.6
7905606	Goliad	5748885	18846532	Upper Lagarto	11	185.2	203.6	-18.5
8011301	Jackson	5999963	18832964	Beaumont	1	3.7	18.8	-15.1
8002804	Victoria	5944471	18844064	Beaumont	1	32.1	49.8	-17.7

State Well Number	County	GAM Coordinates		Formation	Model Layer	Hydraulic Head		Residual
		Easting (ft)	Westing (ft)			Observed	Simulated	
6660401	Jackson	5998226	18904451	Lissie	2	37.2	56.1	-18.9
7907505	Victoria	5820505	18847573	Upper Goliad	5	98.3	112.8	-14.5
6644402	Lavaca	5996118	18999623	Lower Goliad	9	78.1	99.4	-21.3
7937915	Goliad	5757709	18656391	Upper Goliad	5	48.4	70.1	-21.6
7922903	Goliad	5788910	18752809	Lissie	2	93.6	113.4	-19.8
8004403	Jackson	6006900	18864544	Willis	3	19.4	36.5	-17.1
8011201	Jackson	5983003	18832653	Lissie	2	14.4	29.8	-15.4
8011202	Jackson	5981678	18823508	Lissie	2	11.0	27.0	-16.0
7913111	Goliad	5728379	18819250	Upper Lagarto	11	185.6	201.6	-16.0
7922508	Goliad	5777867	18764071	Upper Goliad	5	99.9	121.4	-21.5
7916701	Victoria	5853411	18794908	Upper Goliad	5	55.6	68.5	-12.9
6739507	Lavaca	5813235	19030424	Oakville	15	316.1	338.8	-22.6
8003909	Jackson	5998901	18847401	Beaumont	1	16.3	30.5	-14.2
8017801	Victoria	5906671	18747087	Lissie	2	10.6	20.5	-9.9
8011502	Jackson	5981625	18819358	Lissie	2	10.2	25.6	-15.4
7924102	Victoria	5853904	18772768	Lissie	2	46.6	59.2	-12.6
7923303	Victoria	5835356	18777848	Upper Goliad	5	64.2	77.2	-13.1
7915904	Victoria	5828746	18789311	Upper Goliad	5	72.2	85.0	-12.9
7932802	Refugio	5869034	18706008	Lissie	2	25.6	37.5	-11.9
6660601	Jackson	6027837	18907391	Beaumont	1	32.9	47.7	-14.8
7937918	Goliad	5762826	18658938	Upper Goliad	5	52.1	69.4	-17.3
8017602	Victoria	5909513	18760114	Lissie	2	18.1	27.2	-9.1
7922509	Goliad	5781505	18760821	Upper Goliad	5	99.5	117.8	-18.3
7915305	Victoria	5833239	18825440	Upper Goliad	5	84.2	93.9	-9.8
7906714	DeWitt	5769968	18841063	Upper Lagarto	11	156.8	168.8	-12.1
7905905	Goliad	5758086	18836632	Upper Lagarto	11	169.6	181.5	-11.9
8004504	Jackson	6023005	18866155	Lissie	2	20.6	33.8	-13.2
6641903	Lavaca	5909796	18973924	Lower Goliad	9	120.5	138.4	-17.8
6660701	Jackson	5998928	18895972	Beaumont	1	40.1	52.1	-12.1
6660708	Jackson	5999377	18895784	Beaumont	1	40.2	52.1	-11.9
8005701	Jackson	6039901	18848371	Lissie	2	9.4	22.8	-13.4
7908406	Victoria	5847636	18848982	Upper Goliad	5	89.4	98.4	-9.0

State Well Number	County	GAM Coordinates		Formation	Model Layer	Hydraulic Head		Residual
		Easting (ft)	Westing (ft)			Observed	Simulated	
6649901	Lavaca	5905666	18939291	Upper Goliad	5	105.4	117.8	-12.4
7905903	Goliad	5758980	18836350	Upper Lagarto	11	170.5	181.1	-10.6
8017603	Victoria	5909585	18760723	Lissie	2	20.6	27.2	-6.6
7907703	Victoria	5812855	18844648	Upper Goliad	5	111.6	119.3	-7.7
7908403	Victoria	5848779	18849416	Lissie	2	91.1	98.8	-7.8
6660707	Jackson	5999531	18893663	Beaumont	1	41.4	51.4	-10.0
7906707	DeWitt	5769490	18842468	Upper Lagarto	11	159.0	168.0	-9.0
7924802	Victoria	5864152	18745425	Lissie	2	37.8	45.0	-7.2
7913507	Goliad	5739646	18812226	Upper Lagarto	11	165.4	176.2	-10.8
7914203	Goliad	5784394	18817538	Upper Lagarto	11	124.0	134.2	-10.2
7908404	Victoria	5848863	18849621	Lissie	2	92.5	98.8	-6.3
7907402	DeWitt	5805258	18857305	Lower Goliad	9	125.6	131.3	-5.7
7906101	DeWitt	5763688	18869847	Middle Lagarto	13	192.8	199.2	-6.4
6739603	Lavaca	5833635	19031485	Oakville	15	276.4	293.4	-17.0
7946601	Refugio	5792387	18629012	Upper Goliad	5	35.2	46.1	-10.9
7913304	Goliad	5745428	18827230	Upper Lagarto	11	176.6	183.8	-7.2
6661407	Jackson	6045535	18905724	Lissie	2	33.2	42.1	-9.0
8010502	Victoria	5943860	18806814	Lissie	2	27.8	34.0	-6.2
7906708	DeWitt	5770807	18843106	Upper Lagarto	11	160.3	166.9	-6.6
8019104	Victoria	5972175	18784375	Lissie	2	8.4	16.6	-8.2
8004101	Jackson	6004035	18876902	Lissie	2	36.0	42.8	-6.9
7924702	Victoria	5844556	18752496	Lissie	2	56.4	62.4	-6.0
8033205	Refugio	5903414	18694200	Beaumont	1	8.4	8.6	-0.2
7913611	Goliad	5748612	18812637	Upper Lagarto	11	161.0	168.7	-7.6
7923601	Victoria	5834062	18762440	Lissie	2	67.4	73.6	-6.2
7913405	Goliad	5729819	18806740	Upper Lagarto	11	182.1	187.6	-5.6
7906706	Goliad	5764634	18833854	Upper Lagarto	11	167.6	172.6	-5.0
7922206	Goliad	5781273	18774066	Upper Goliad	5	111.0	120.3	-9.2
8018103	Victoria	5934174	18775579	Lissie	2	23.9	27.4	-3.5
8033203	Refugio	5903504	18694202	Lissie	2	10.8	11.5	-0.7
8017502	Victoria	5898363	18763672	Upper Goliad	5	31.9	32.3	-0.4
8017501	Victoria	5900382	18765222	Upper Goliad	5	32.0	32.4	-0.4

State Well Number	County	GAM Coordinates		Formation	Model Layer	Hydraulic Head		Residual
		Easting (ft)	Westing (ft)			Observed	Simulated	
8027601	Calhoun	5999861	18720143	Lissie	2	-6.7	1.5	-8.1
7905904	Goliad	5759230	18837064	Upper Lagarto	11	177.6	181.1	-3.5
8018401	Victoria	5928573	18759740	Lissie	2	21.9	23.4	-1.4
7946803	Refugio	5781419	18617118	Willis	3	38.6	45.7	-7.0
7904104	DeWitt	5689760	18862901	Lower Lagarto	14	285.3	295.3	-10.0
8019802	Calhoun	5985411	18745336	Lissie	2	0.4	6.2	-5.8
8017905	Victoria	5915917	18750785	Upper Goliad	5	24.2	24.4	-0.2
7913808	Goliad	5743910	18789363	Upper Lagarto	11	154.3	160.1	-5.9
7915905	Victoria	5834431	18789559	Willis	3	78.2	80.0	-1.8
7932602	Victoria	5881589	18713122	Willis	3	29.6	30.1	-0.5
6649701	Lavaca	5887970	18936519	Upper Lagarto	11	122.1	125.5	-3.4
8026501	Calhoun	5946726	18715821	Lissie	2	6.2	8.8	-2.6
8018402	Victoria	5932192	18760855	Lissie	2	22.9	23.1	-0.2
7905502	DeWitt	5744219	18852493	Upper Lagarto	11	209.4	210.7	-1.3
7915901	Victoria	5834225	18794105	Lissie	2	81.0	81.7	-0.7
8005502	Jackson	6063314	18865917	Beaumont	1	20.3	24.1	-3.8
7913806	Goliad	5742411	18788822	Upper Lagarto	11	155.7	160.1	-4.4
6625203	Lavaca	5892575	19099469	Lower Lagarto	14	244.8	259.5	-14.7
7931502	Goliad	5817680	18716912	Willis	3	67.5	70.6	-3.1
7914202	Goliad	5774292	18823767	Lower Goliad	9	146.1	148.4	-2.3
7913804	Goliad	5741489	18790217	Upper Lagarto	11	156.7	160.1	-3.4
7922201	Goliad	5779065	18773406	Lower Goliad	9	117.7	121.6	-3.9
8019503	Calhoun	5978894	18761232	Lissie	2	7.3	9.5	-2.1
7913512	Goliad	5743028	18812001	Upper Lagarto	11	175.1	176.2	-1.1
7915903	Victoria	5834886	18789165	Willis	3	81.5	80.0	1.5
7931901	Refugio	5840658	18703644	Upper Goliad	5	51.6	51.9	-0.3
7913809	Goliad	5742383	18790035	Lower Goliad	9	157.4	159.5	-2.1
7904103	DeWitt	5689760	18862901	Lower Lagarto	14	289.8	295.3	-5.5
7906306	DeWitt	5795316	18875269	Lower Goliad	9	156.0	152.4	3.6
7937901	Goliad	5754314	18660356	Lissie	2	67.4	69.0	-1.6
6748203	Lavaca	5854075	19001658	Middle Lagarto	13	202.9	207.7	-4.7
7904202	DeWitt	5694268	18867754	Lower Lagarto	14	293.0	296.9	-4.0

State Well Number	County	GAM Coordinates		Formation	Model Layer	Hydraulic Head		Residual
		Easting (ft)	Westing (ft)			Observed	Simulated	
8019506	Calhoun	5984925	18764198	Lissie	2	6.3	5.6	0.7
8012502	Jackson	6025015	18813097	Beaumont	1	8.0	7.1	0.9
7928304	Goliad	5719470	18728573	Lower Goliad	9	130.2	131.8	-1.5
8006101	Jackson	6082002	18883426	Lissie	2	27.7	26.0	1.7
6763605	DeWitt	5829890	18896883	Willis	3	148.4	138.6	9.9
7913612	Goliad	5754950	18807627	Lower Goliad	9	165.6	161.7	3.9
8004601	Jackson	6037802	18867025	Lissie	2	35.0	30.4	4.6
7913609	Goliad	5755762	18810882	Lower Goliad	9	164.7	160.4	4.3
7938301	Goliad	5796292	18684420	Lissie	2	68.7	65.5	3.2
7922210	Goliad	5783452	18779581	Upper Goliad	5	122.2	119.0	3.2
7938202	Goliad	5784026	18682705	Lissie	2	72.2	68.8	3.4
8005102	Jackson	6042054	18878493	Lissie	2	39.0	33.6	5.4
7928303	Goliad	5719191	18726090	Lower Goliad	9	131.5	130.2	1.3
7939104	Goliad	5805190	18692428	Lissie	2	69.2	64.6	4.6
6641703	Lavaca	5878641	18972448	Lower Goliad	9	157.5	155.0	2.4
6625103	Lavaca	5885664	19096831	Middle Lagarto	13	265.8	271.7	-5.9
7928302	Goliad	5721490	18726849	Lower Goliad	9	131.8	129.2	2.6
7905908	Goliad	5756473	18833458	Upper Lagarto	11	191.6	182.4	9.2
7906703	DeWitt	5772183	18844960	Upper Lagarto	11	175.0	166.0	9.1
7908903	Victoria	5872330	18835372	Lissie	2	89.7	78.5	11.2
6643704	Lavaca	5967239	18980534	Lissie	2	111.9	105.6	6.3
6746606	DeWitt	5792479	18982761	Lower Lagarto	14	276.9	275.9	1.0
6762704	DeWitt	5759719	18880072	Middle Lagarto	13	221.5	211.3	10.2
8004908	Jackson	6029964	18848058	Beaumont	1	33.5	23.6	9.9
6739306	Lavaca	5826828	19053044	Oakville	15	359.1	353.3	5.8
6746605	DeWitt	5786843	18988997	Oakville	15	284.5	276.0	8.5
6761402	DeWitt	5730692	18896595	Lower Lagarto	14	283.9	279.7	4.2
6641203	Lavaca	5890037	19014342	Lower Goliad	9	186.8	180.4	6.4
6634201	Lavaca	5933718	19049932	Lower Goliad	9	174.6	165.8	8.8
6634202	Lavaca	5931835	19049188	Lower Goliad	9	176.0	165.8	10.2
7913223	Goliad	5744685	18817198	Lower Goliad	9	192.3	175.0	17.3
6739518	Lavaca	5821434	19040164	Oakville	15	350.2	337.9	12.3

State Well Number	County	GAM Coordinates		Formation	Model Layer	Hydraulic Head		Residual
		Easting (ft)	Westing (ft)			Observed	Simulated	
7913508	Goliad	5739530	18813437	Upper Lagarto	11	194.3	176.2	18.1
6634207	Lavaca	5938749	19054819	Lower Goliad	9	177.7	163.5	14.2
7905406	DeWitt	5720292	18858621	Middle Lagarto	13	265.8	247.6	18.2
6740301	Lavaca	5872545	19054023	Middle Lagarto	13	270.9	261.2	9.7
7913227	Goliad	5736877	18820558	Upper Lagarto	11	216.6	192.8	23.7
6635901	Lavaca	5981361	19025694	Lower Goliad	9	141.6	117.9	23.7
7913811	Goliad	5740607	18789893	Upper Lagarto	11	185.8	160.1	25.6
7913807	Goliad	5743393	18788643	Lower Goliad	9	187.4	159.5	27.9
7913810	Goliad	5742988	18790757	Lower Goliad	9	188.3	159.5	28.8
7913224	Goliad	5742448	18817854	Lower Goliad	9	214.4	181.7	32.6
7913803	Goliad	5740710	18789289	Lower Goliad	9	191.2	159.5	31.7

4.4 Applications of the Victoria County Groundwater Flow Model to Predict Drawdown from Pumping

The VCGFM was used to predict drawdowns from a single pumping well at the five locations shown in **Figure 4-52**. At each of the five locations, the pumping occurred from a single model layer that contained brackish groundwater with a TDS concentration between 2,000 and 3,000 mg/L. **Table 4-7** lists the model layer, formation, and the thickness of the formation that is pumped by a well at each of the five locations.

Table 4-7 Locations where pumping brackish water was simulated to estimate drawdown impacts

Well ID	Formation	GAM Coordinates		Model Layer	Model Layer Thickness	Transmissivity (ft^2/day)
		Easting (ft)	Westing (ft)			
1	Lower Goliad	5949635	18783891	8	199	749
2	Lower Goliad	5908260	18787186	9	199	424
3	Lower Goliad	5893425	18803081	10	181	363
4	Upper Lagarto	5853689	18742153	11	245	193
5	Middle Lagarto	5888657	18885201	13	447	316

At each of the five locations, two sets of pumping scenarios were modeled. One scenario involved pumping at 1,000 gpm for 30 years. The other scenario involve pumping at 250 gpm for 30 years. **Figure 4-53** shows the simulated drawdown cones associated with pumping at location 1 (Upper Goliad). For each of the two pumping scenarios, drawdown plots are provided for the model layer being pumped, the first model layer above the pumped model layer that contains fresh water the pumping

location, and drawdown plots for a layer in between the "pumped" and the "fresh-water" model layers. Drawdown plots consist of contours of drawdowns at 5, 10, 25, and 50 ft. If no drawdown plots are provided, then the maximum predicted drawdown was less than 5 ft. The contours for the simulated drawdowns for well locations 1 through 5 are provided in Figures 4-53 through 4-57, respectively. **Table 4-8** provides the simulated drawdown to the nearest foot for the pumped model layer and the "fresh-water" model layer.

Table 4-8 Simulated drawdown after 30 years of pumping at 1,000 gpm and 250 gpm for five well locations shown in 4-52

Well ID	Formation Pumped by Well	Drawdown in the grid cell containing the pumping well				Drawdown in the grid cell above the pumping well in a model containing fresh water			
		Model Layer	Depth(ft) Midpoint	1000 gpm	250 gpm	Model Layer	Depth(ft) Midpoint	1000 gpm	250 gpm
1	Lower Goliad	8	1606	140	35	6	1164	7.7	1.9
2	Lower Goliad	9	1629	237	59	7	1241	10.3	2.6
3	Lower Goliad	10	1681	282	71	7	1140	8.0	2.0
4	Upper Lagarto	11	1709	485	121	8	1231	11.9	3.0
5	Middle Lagarto	13	1621	347	87	10	909	12.0	3.0

At each pumping location, there is a linear relationship between the pumping rate and the simulated drawdown. This relationship is expected because all of the pumping is occurring in the confined portions of the aquifer. In a confined aquifer, the groundwater flow rate is linearly dependent on the hydraulic gradient. For purposes of planning and permitting, the linear relationship between pumping and drawdown can be used to estimate drawdown for pumping rates in the range of 200 to 1,000 gpm.

Table 4-7 shows that, for a given pumping rate, the drawdown that occurs in a grid cell containing a well varies by more than a factor of 4. For the pumping rate of 1,000 gpm, the drawdown ranges from 80 to 369 ft. The primary reason for the difference in drawdown amounts are difference in the transmissivity of the model layer at the pumping location. As a general rule, the spatial differences in transmissivity across a formation is primarily controlled by the thicknesses and extent of the sand beds. The highest transmissivity values are expected to occur there the sands are the thickest and where sands have the least amounts of interbedded fines/clays

For all five of the pumping locations, the closest grid cell containing fresh water is at least two layers above the model layer containing the pumping well. For all cases, the maximum drawdown in the fresh water is at least 10 times less than the maximum drawdown in the pumped brackish zone. The primary reason for drawdown to diminish more rapidly with vertical distance than with horizontal distance is that vertical hydraulic conductivity is typically much smaller than the horizontal hydraulic conductivity.

As a general rule, the spatial differences in vertical hydraulic conductivity across a formation is primarily controlled by the thicknesses and extent of the clay beds. The lowest vertical hydraulic conductivity values are expected to occur where clays are the thickest and contain the least amount of sands and fractures.

To provide additional information that may be useful for developing District rules for managing pumping brackish groundwater, the central Gulf Coast GAM (Chowdhury and others, 2004) was used to simulate the drawdown impacts caused by pumping at 1,000 and 250 gpm. **Table 4-9** provides the simulated drawdowns using the central Gulf Coast GAM for the same five locations.

Table 4-9 Simulated drawdown based on using the Central Gulf Coast GAM

Well ID	Predicted Drawdown In Pumped Layer			Predicted Drawdown In Overlying Freshwater Layer		
	Formation	1000 gpm	250 gpm	Aquifer	1000 gpm	250 gpm
1	Evangeline	29	7.3	Chicot	3.0	0.75
2	Evangeline	30	7.6	Chicot	0.67	0.18
3	Evangeline	29	7.3	Chicot	1.4	0.36
4	Evangeline	31	7.8	Chicot	0.6	0.14
5	Evangeline	30	7.5	Chicot	0.3	0.06

Compared to the VCGFM, the central Gulf Coast GAM simulated drawdowns are considerable smaller and has a smaller range of values. For the case of a well pumping 1,000 gpm, whereas the GAM predicts drawdowns at the pumping well that range between 29 to 31 ft, the VCGFM predicts drawdowns that range between 80 and 369 ft. The smaller drawdown value predicted by the GAM is primarily attributed to the thicker grid cells. As a general rule, predictions from a model with model layers with thickness that are close to the well screen intervals will provide a more accurate simulation of drawdowns than from models with model layers that are three to four times thicker than the well screen interval of the pumped well. The similarity in the predicted drawdown in the GAM model is primarily caused by the assumption that the aquifers in the vicinity of Victoria County have fairly homogeneous hydraulic conductivity values. Since the central Gulf Coast GAM was developed, a considerable amount of work has been funded by the TWDB to map and to characterize the lithology of the formations that comprise the Gulf Coast Aquifer System (Young and others, 2010, 2012a, 2016).

4.5 Senstivity Analysis on Simulated Drawdown

A sensitivity analysis was performed on the VCGCD to determine the potential impact of changes in predicted water levels and drawdowns to changes in the GHBCs. The sensitivity analysis focused on value of the hydraulic conductance for the GHBCs. The hydraulic conductance is the primary model parameter that was adjusted during model calibration. For our analysis, only the hydraulic conductance values of most importance are those associated with the GHBCs controlling the recharge rate. These GHBCs are located in grid cells representing the outcrop of the Gulf Coast Aquifer System. The changes that were made to these GHBCs was to change the hydraulic conductance by a factor of 10.

4.5.1 Simulated water levels for steady-state conditions

Figure 4-58 shows the simulated versus observed hydraulic heads for 150 wells after the hydraulic conductance for the general head boundaries for recharge was multiplied by 0.1. The figures shows that the model general under predicts the observed water levels. The lower values for the simulated water levels is attributed to the decrease in the average recharge rate of 0.066 to 0.025 inches/year, which is a reduction of approximately 62%. The reduced recharge rate caused the root mean square error to increase from 12 to 32 ft.

Figure 4-59 shows the simulated versus observed hydraulic heads for 150 wells after the hydraulic conductance for the general head boundaries for recharge was multiplied by 10. The figures shows that the model general over predicted the observed water levels. The lower values for the simulated water levels is attributed to the increase in the average recharge rate of 0.066 to 0.15 inches/year, which is an increase of approximately 120%. The increased recharge rate caused the root mean square error to increase from 12 to 32 ft.

4.5.2 Simulated drawdown for pumping conditions

For the two steady-state models that were created in Section 4.5.2, the pumping of 1,000 gpm for 30 years was simulated at the five locations listed in Table 4-10. **Table 4-10** compares the simulated drawdown after 30 years among these two models and the calibrated model. The comparison shows that, for all five locations, the three simulated drawdown values differ by less than 0.3%. At each location, the model with GHBCs with lower hydraulic conductances has the greatest drawdown and the model with higher hydraulic conductances has the least drawdown.

The simulated drawdowns have negligible sensitivity to changes in the hydraulic conductance used by the GHBCs. The primary reason for the insensitivity of the simulated drawdowns to recharge rates is that the pumping wells are located far away from the GHBCs and almost all of the pumped water originates from aquifer storage. For the drawdown have a notable sensitivity to the recharge rate, the pumping wells would need to be located at a much shallower elevation and/or the duration of pumping would need to be much longer than 30 years.

Table 4-10 Simulated drawdown associated with pumping brackish water at a rate of 1,000 gpm at five locations for the calibrated model and two models where the GHBCs providing recharge have been adjusted by either increasing or decreasing the hydraulic conductance by a factor of 10.

Well ID	Formation	Model Layer	Drawdown in the grid cell containing the well pumping at 1000 gpm		
			Multiplier of GHBCs' Hydraulic Conductance		
			1	10	0.1
1	Lower Goliad	8	139.931	139.861	139.939
2	Lower Goliad	9	236.579	236.460	236.594
3	Lower Goliad	10	282.346	282.156	282.371
4	Upper Lagarto	11	485.216	485.006	485.243
5	Middle Lagarto	13	347.049	346.094	347.187

Table 4-11 shows simulated drawdown as a function of radial distance for pumping 1,000 gpm at the five well locations. For all five locations, the simulated decrease in drawdown with distance is similar when the drawdown is expressed as a percentage of simulated drawdown in the grid cell containing the

well. At a radial distances of 0.5 miles, the simulated drawdowns range between 31% and 38% of the simulated drawdown at location of the pumping well. At a radial distances of 1 mile, the simulated drawdowns range between 16% and 22% of the simulated drawdown at location of the pumping well. At a radial distances of 3 miles, the simulated drawdowns range between 3% and 8% of the simulated drawdown at location of the pumping well.

Table 4-11 Simulated drawdowns as a function of radial distance for a pumping rate 1,000 gpm after 30 years

Well ID	Formation	Simulated drawdown at different radial distances in the formation that is pumped*								
		Model Layer	0.0 miles	0.25 miles	0.5 miles	0.75 miles	1 mile	1.5 miles	2 miles	3 miles
1	Lower Goliad	7	140	79	54	40	32	22	16	11
2	Lower Goliad	8	237	127	81	58	44	28	20	12
3	Lower Goliad	9	282	153	98	70	53	34	24	14
4	Upper Lagarto	10	485	247	152	104	76	46	31	14
5	Middle Lagarto	12	347	197	133	98	76	50	36	21

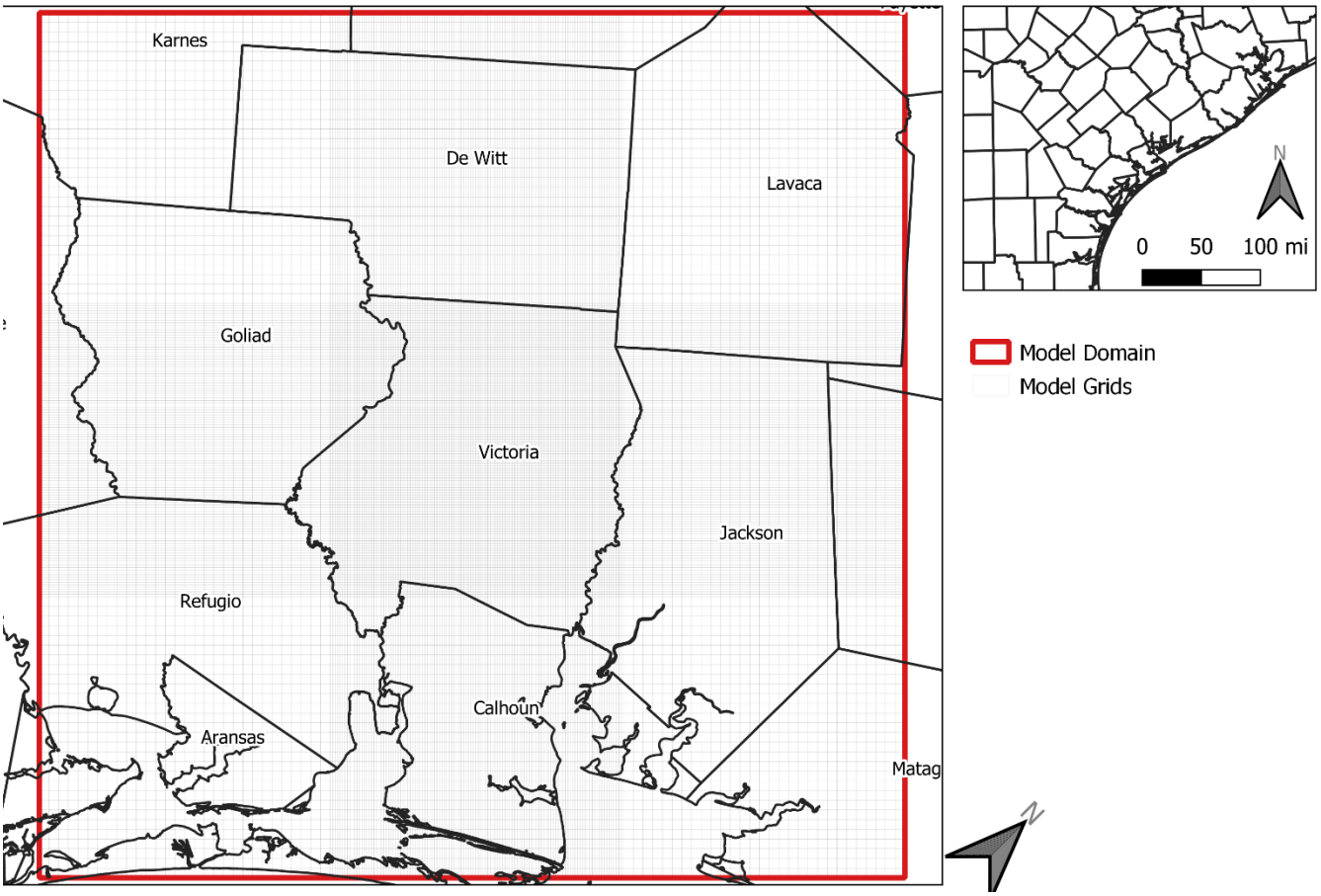

Figure 4-1 Aerial view of the numerical grid for the groundwater flow model

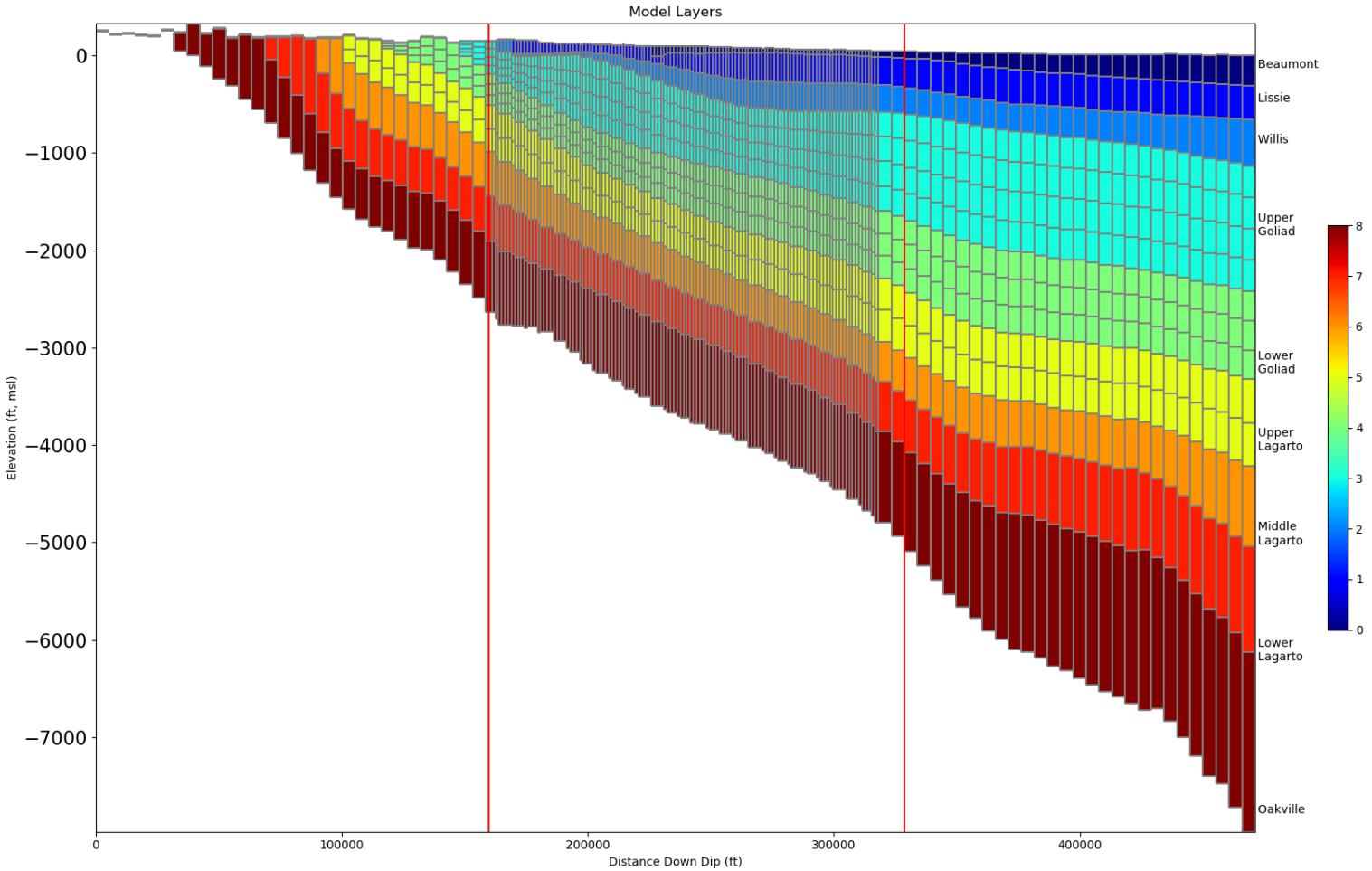

Figure 4-2 Northwest-southeast vertical cross-section showing the 15 model layers that comprise the numerical grid of the groundwater flow model along an axis that extends from up dip to down dip and crosses through the proposed well location. The red lines mark the boundaries for Victoria County.

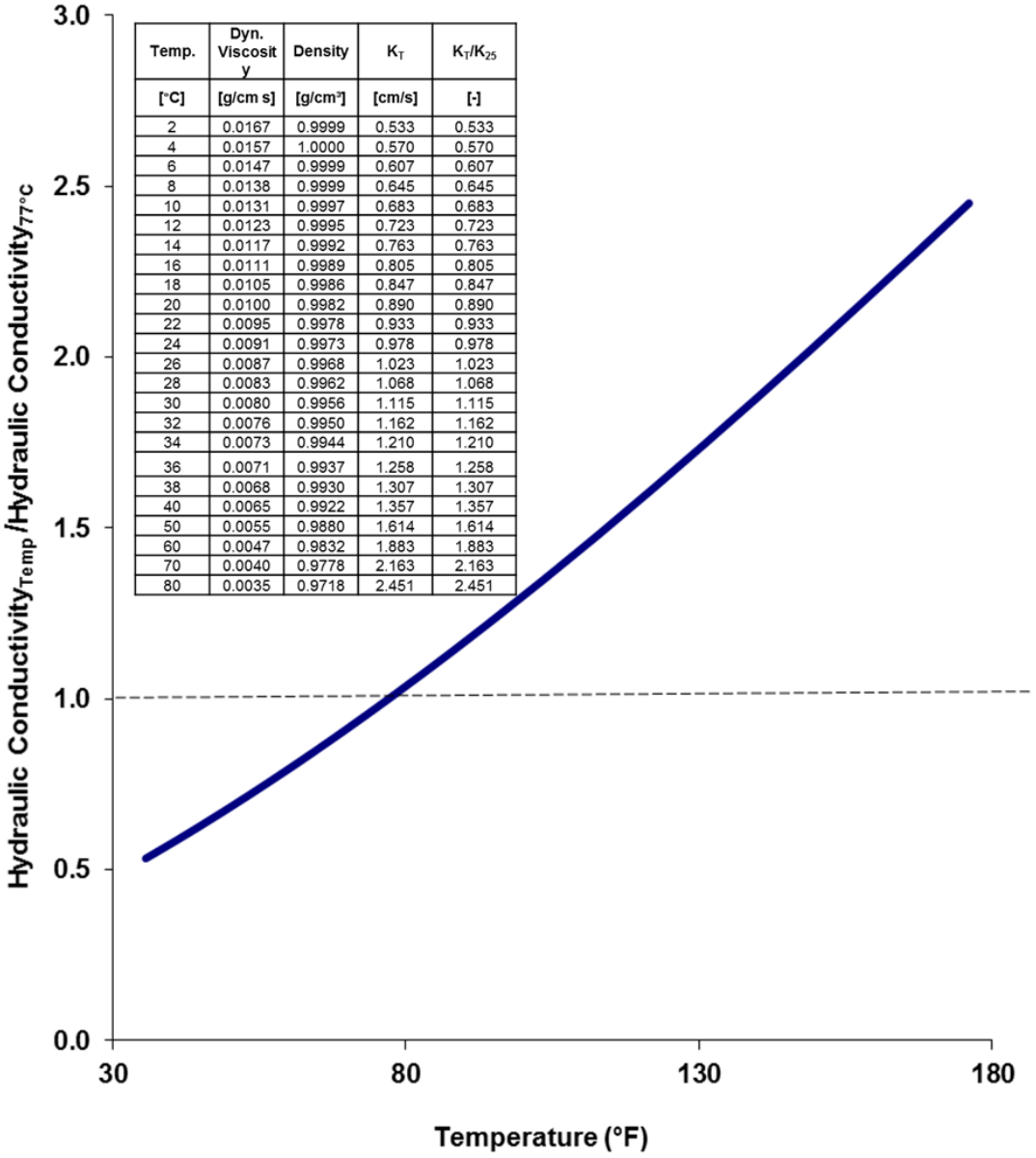

Temp.	Dyn. Viscosity	Density	K_T	K_T/K_{25}
[°C]	[g/cm s]	[g/cm³]	[cm/s]	[-]
2	0.0167	0.9999	0.533	0.533
4	0.0157	1.0000	0.570	0.570
6	0.0147	0.9999	0.607	0.607
8	0.0138	0.9999	0.645	0.645
10	0.0131	0.9997	0.683	0.683
12	0.0123	0.9995	0.723	0.723
14	0.0117	0.9992	0.763	0.763
16	0.0111	0.9989	0.805	0.805
18	0.0105	0.9986	0.847	0.847
20	0.0100	0.9982	0.890	0.890
22	0.0095	0.9978	0.933	0.933
24	0.0091	0.9973	0.978	0.978
26	0.0087	0.9968	1.023	1.023
28	0.0083	0.9962	1.068	1.068
30	0.0080	0.9956	1.115	1.115
32	0.0076	0.9950	1.162	1.162
34	0.0073	0.9944	1.210	1.210
36	0.0071	0.9937	1.258	1.258
38	0.0068	0.9930	1.307	1.307
40	0.0065	0.9922	1.357	1.357
50	0.0055	0.9880	1.614	1.614
60	0.0047	0.9832	1.883	1.883
70	0.0040	0.9778	2.163	2.163
80	0.0035	0.9718	2.451	2.451

Figure 4-3 Relative change in hydraulic conductivity values caused by the temperature dependence of the density and viscosity of water (data from http://www.viscopedia.com/viscosity-tables/substances/water/)

Note: °F=degrees Fahrenheit; Hydraulic Conductivity$_{Temp}$=hydraulic conductivity corrected for temperature; Hydraulic Conductivity$_{77°C}$=hydraulic conductivity at 77 degrees Celsius

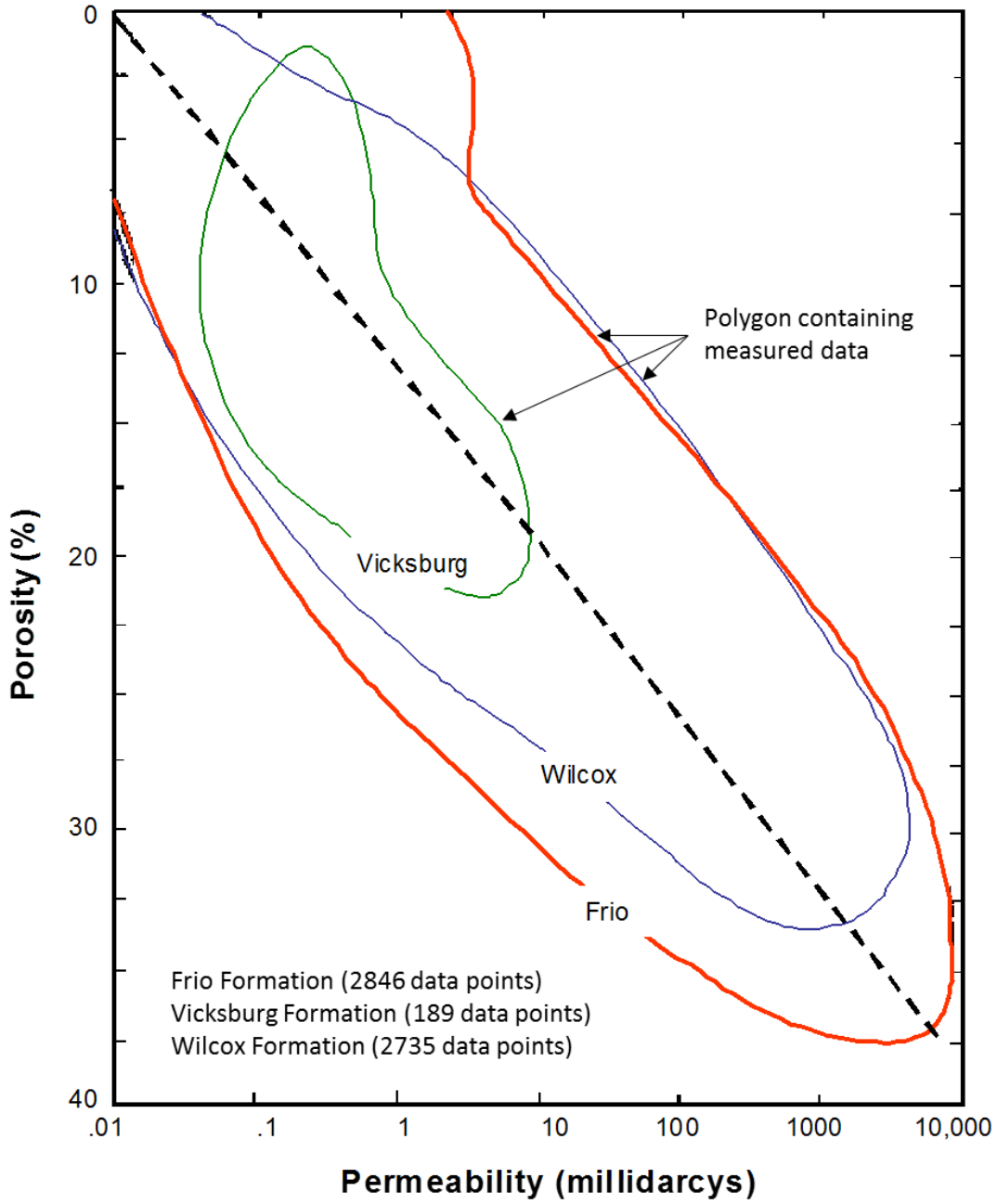

Figure 4-4 Observed relationship between porosity in percent and permeability in millidarcys measured in laboratory cores for geological formations in Texas (modified from Loucks and others, 1986)

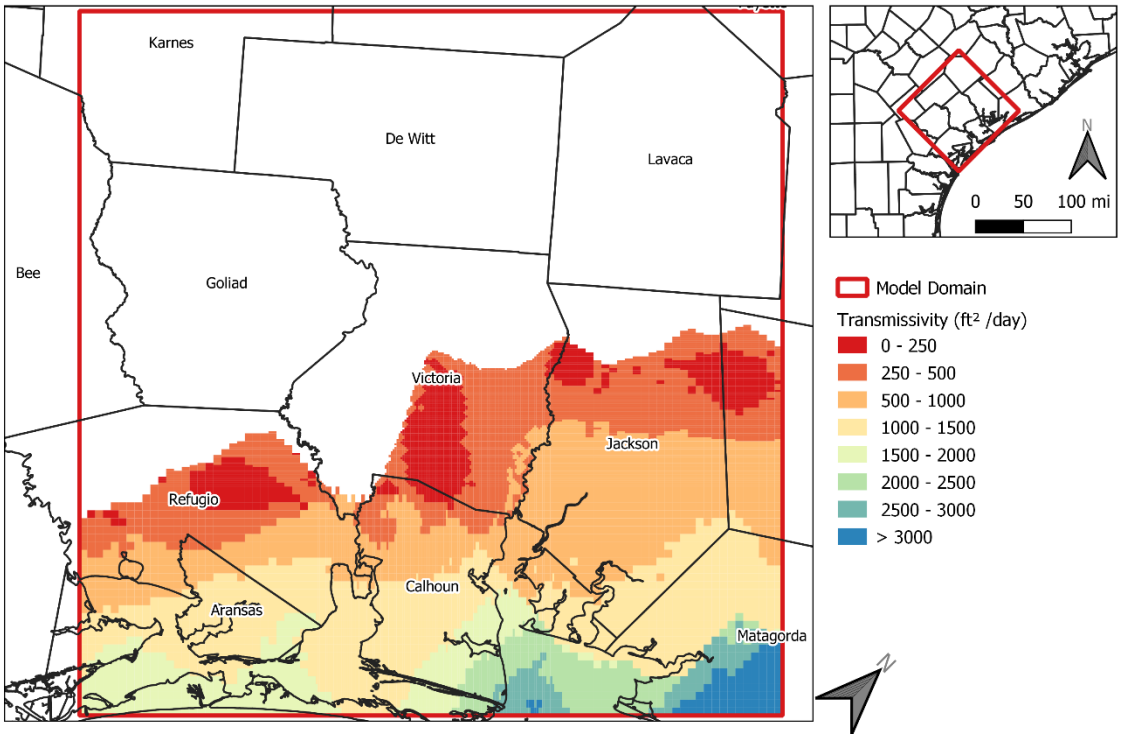

Figure 4-5 Transmissivity (ft^2/day) of model layer 1 (Beaumont Formation)

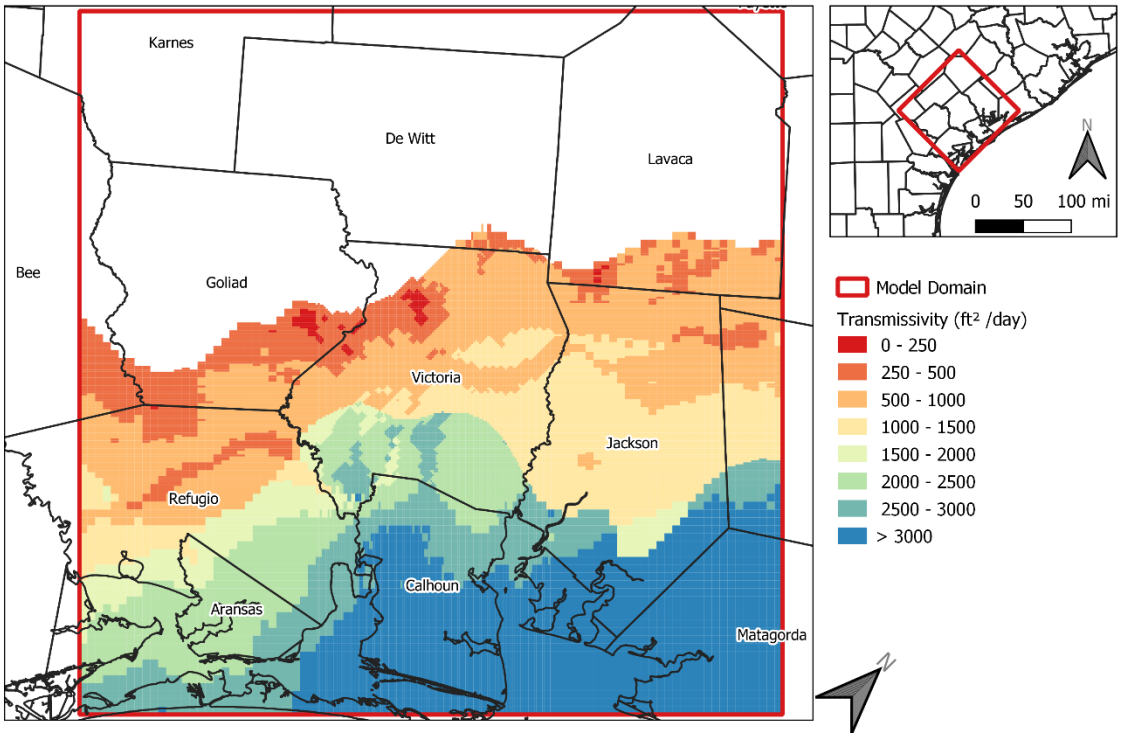

Figure 4-6 Transmissivity (ft^2/day) of model layer 2 (Lissie Formation)

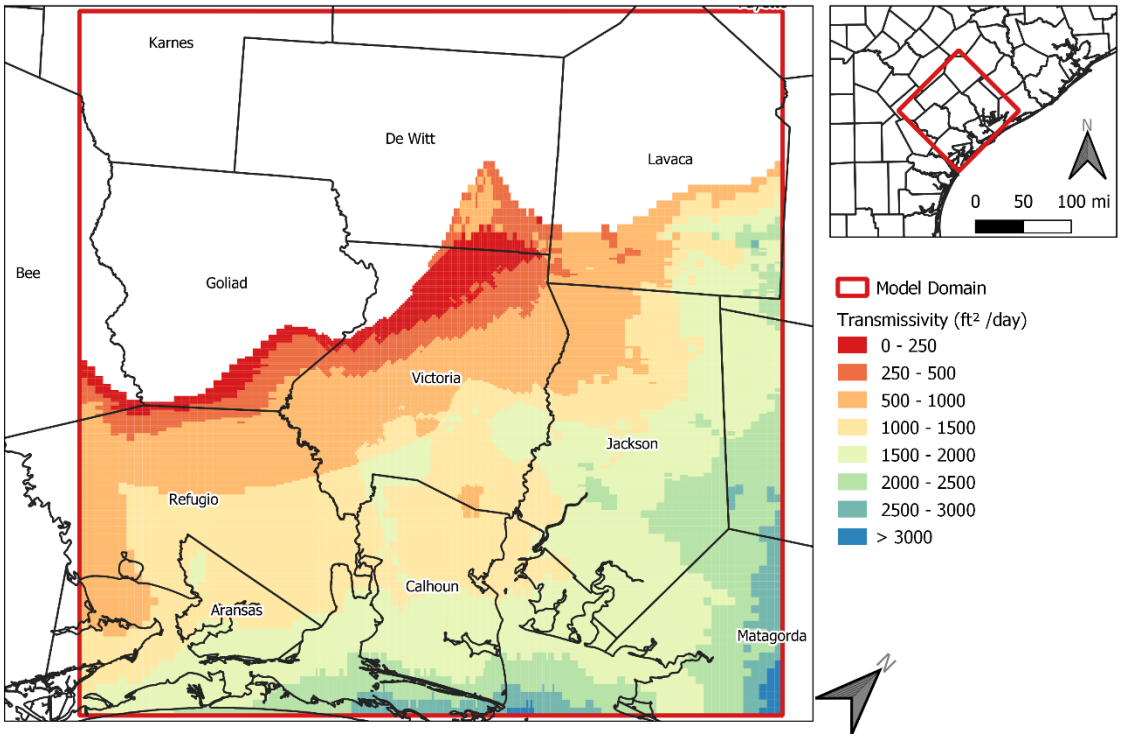

Figure 4-7 Transmissivity (ft^2/day) of model layer 3 (Willis Formation)

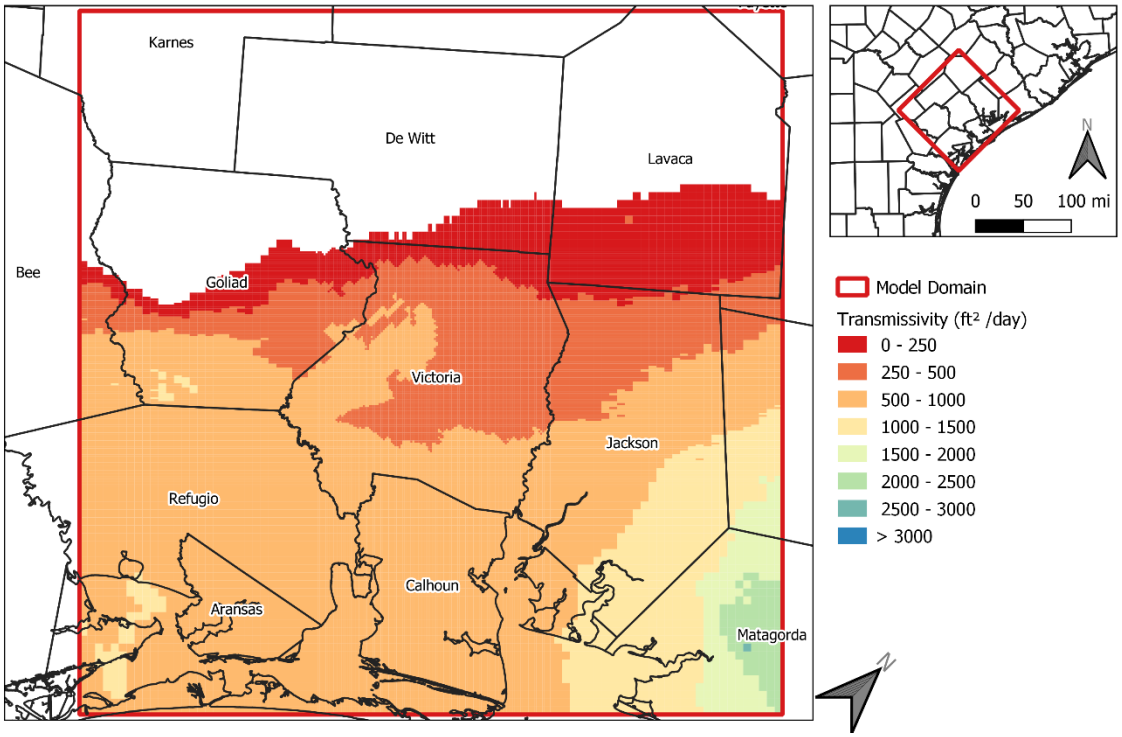

Figure 4-8 Transmissivity (ft^2/day) of model layer 4 (uppermost quartile of the Upper Goliad Formation)

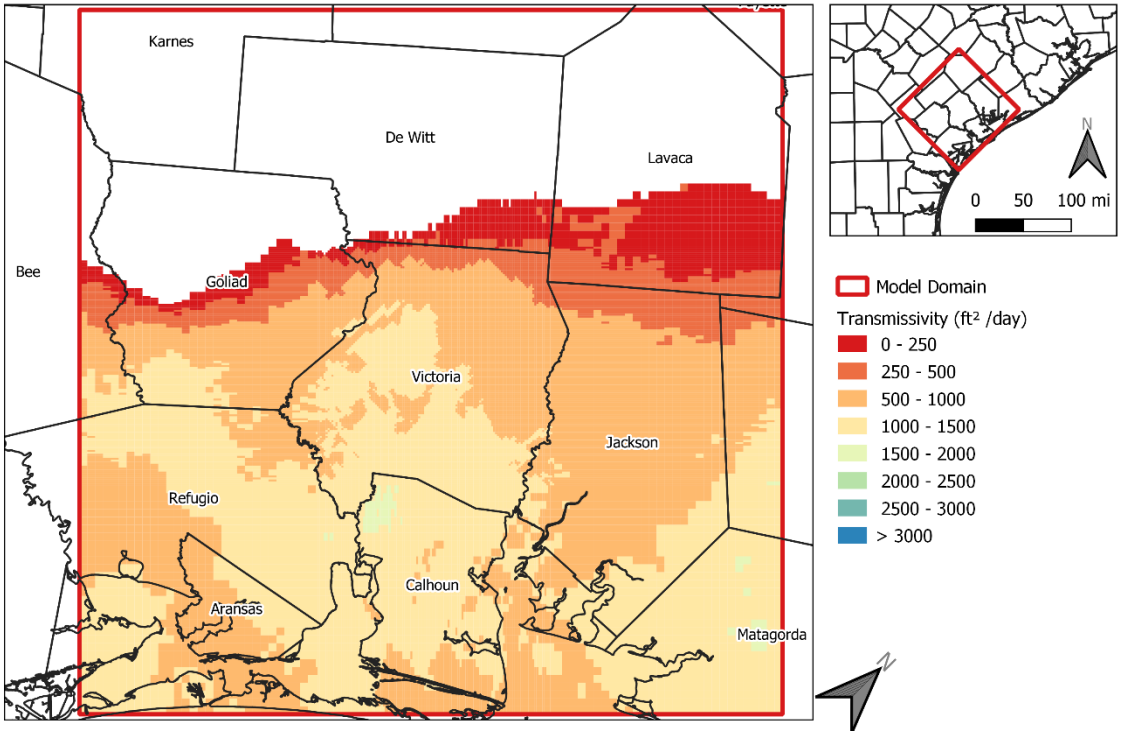

Figure 4-9 Transmissivity (ft^2/day) of model layer 5 (upper quartile of the Upper Goliad formation)

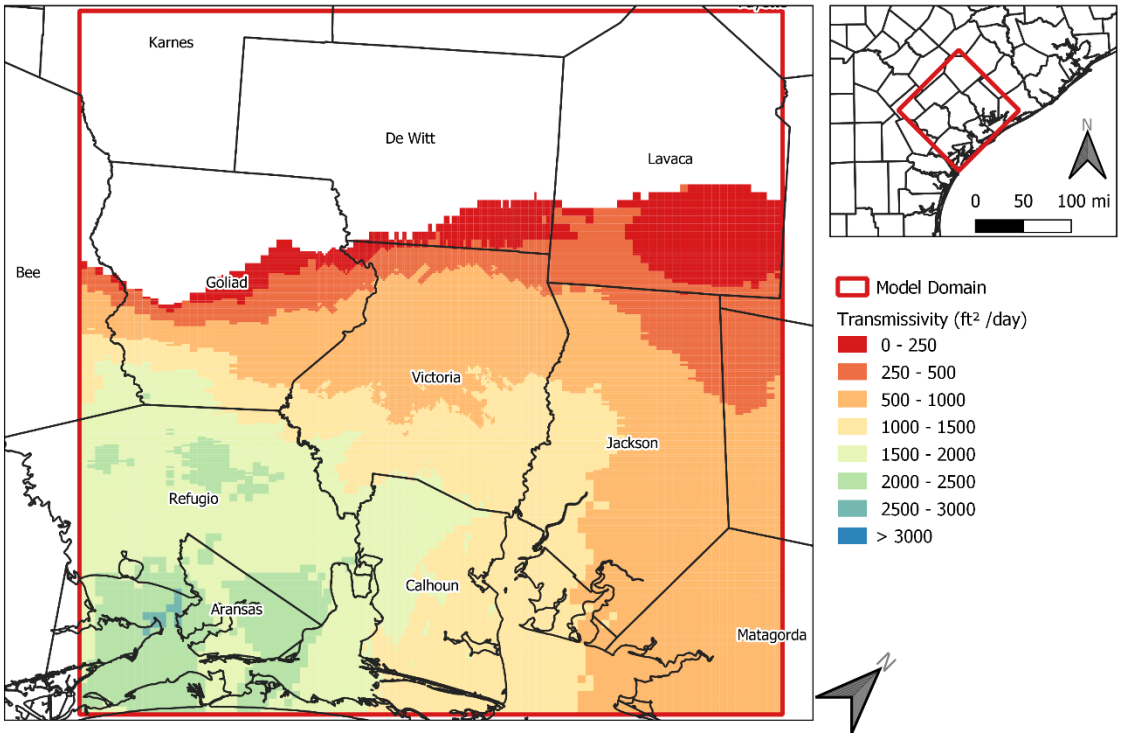

Figure 4-10 Transmissivity (ft^2/day) of model layer 6 (lower quartile of the Upper Goliad formation)

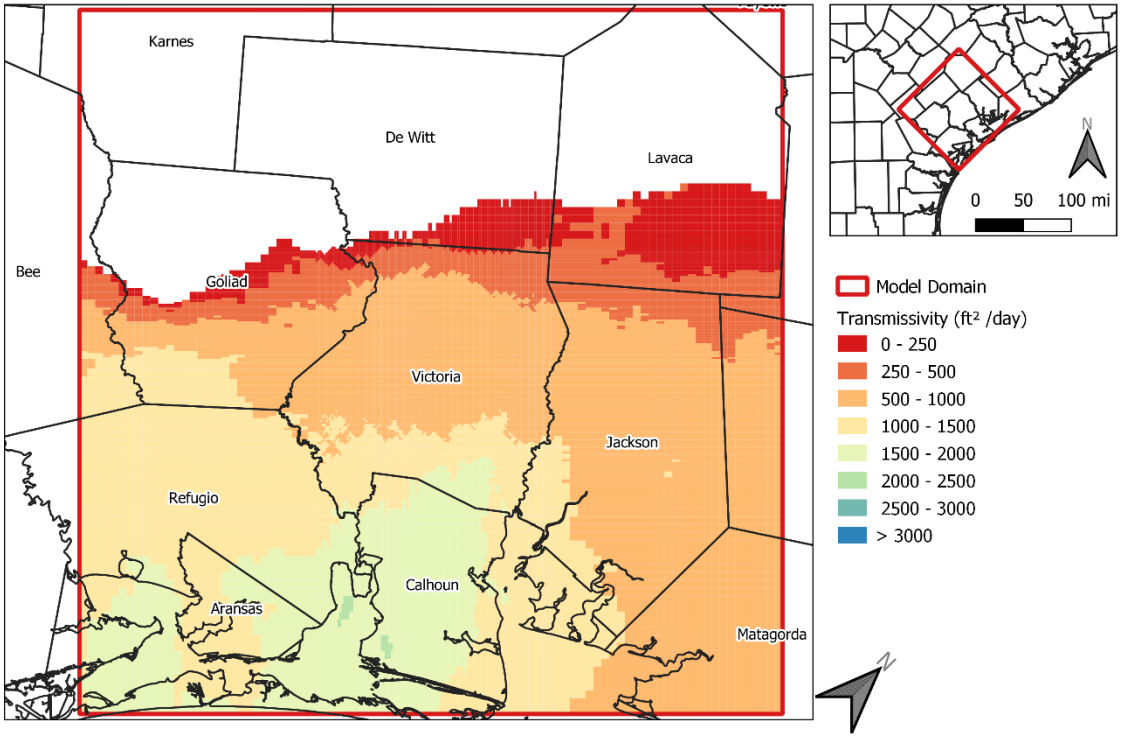

Figure 4-11 Transmissivity (ft^2/day) of model layer 7 (lowermost quartile of the Upper Goliad formation)

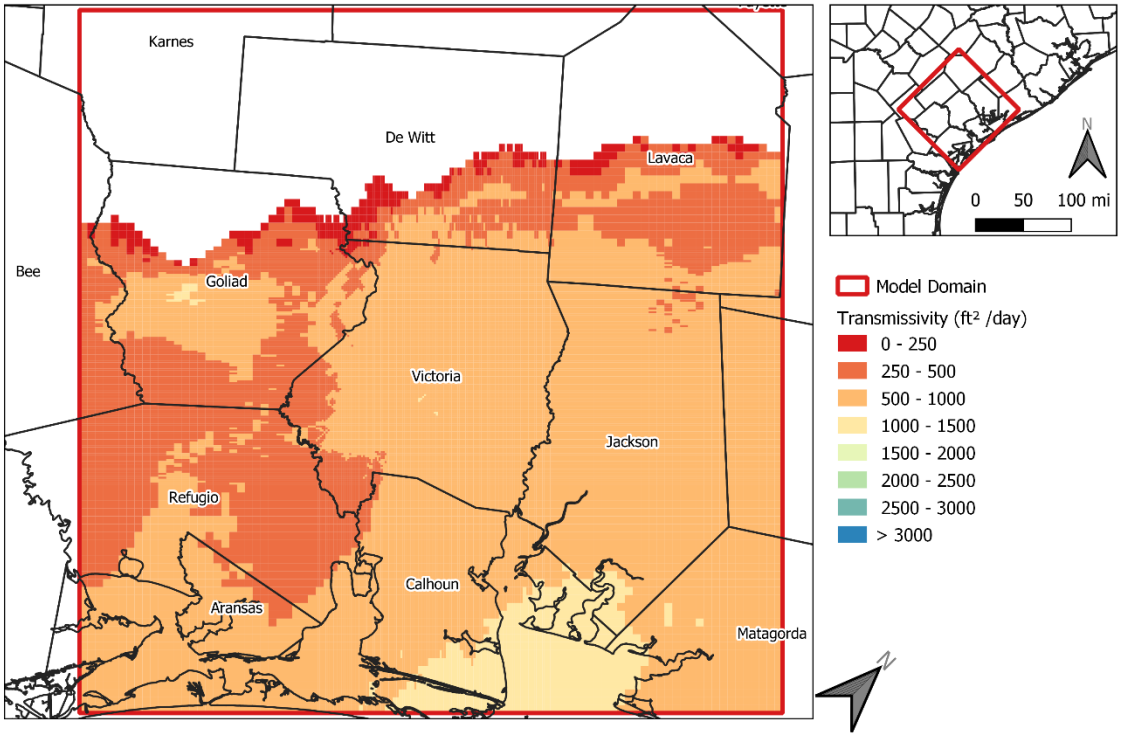

Figure 4-12 Transmissivity (ft^2/day) of model layer 8 (upper thrid of the Lower Goliad formation)

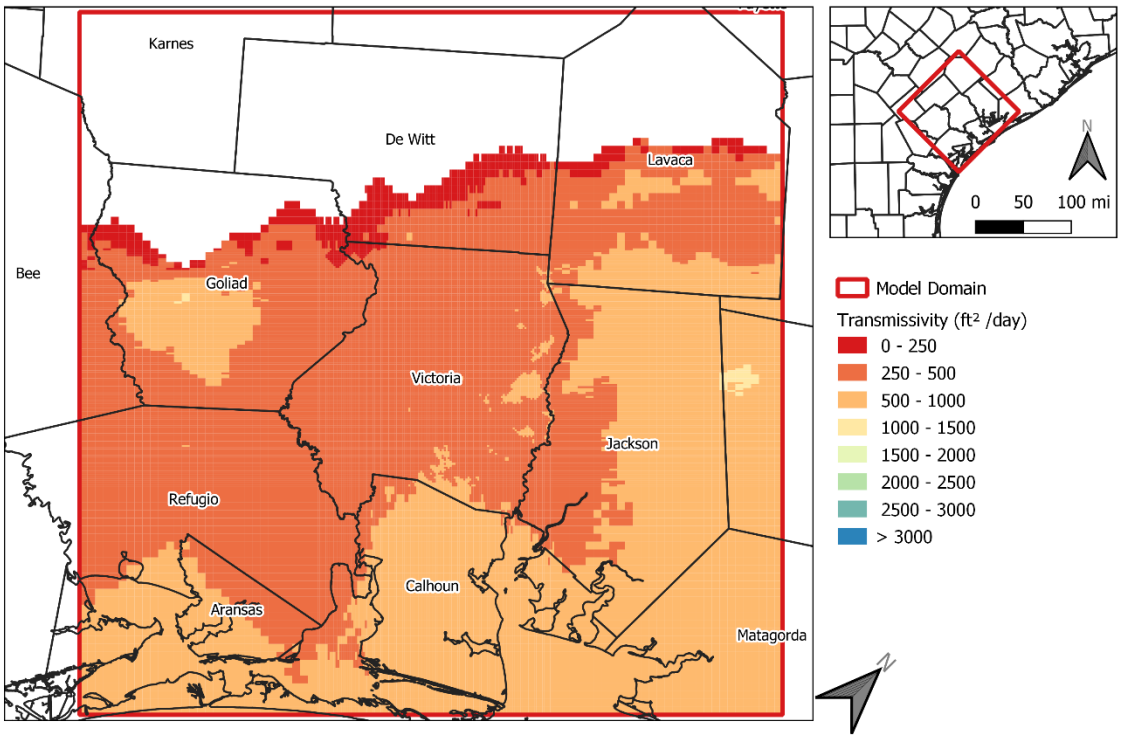

Figure 4-13 Transmissivity (ft^2/day) of model layer 9 (middle third of the Lower Goliad formation)

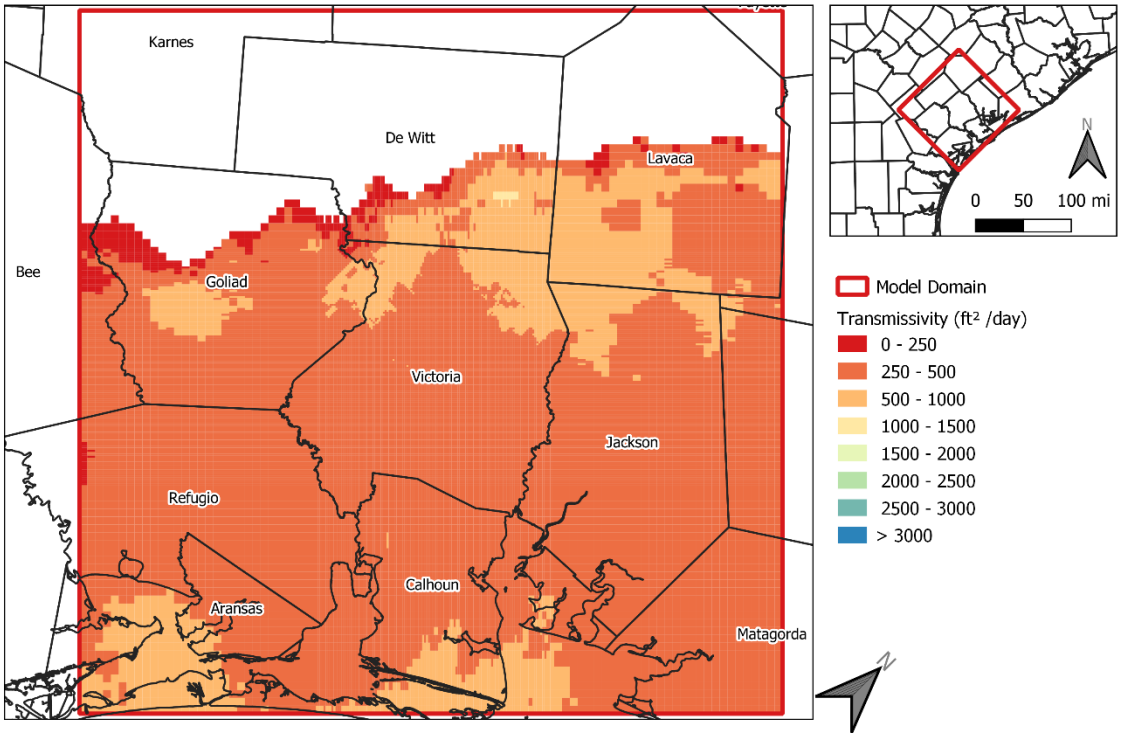

Figure 4-14 Transmissivity (ft^2/day) of model layer 10 (lower third of the Lower Goliad formation)

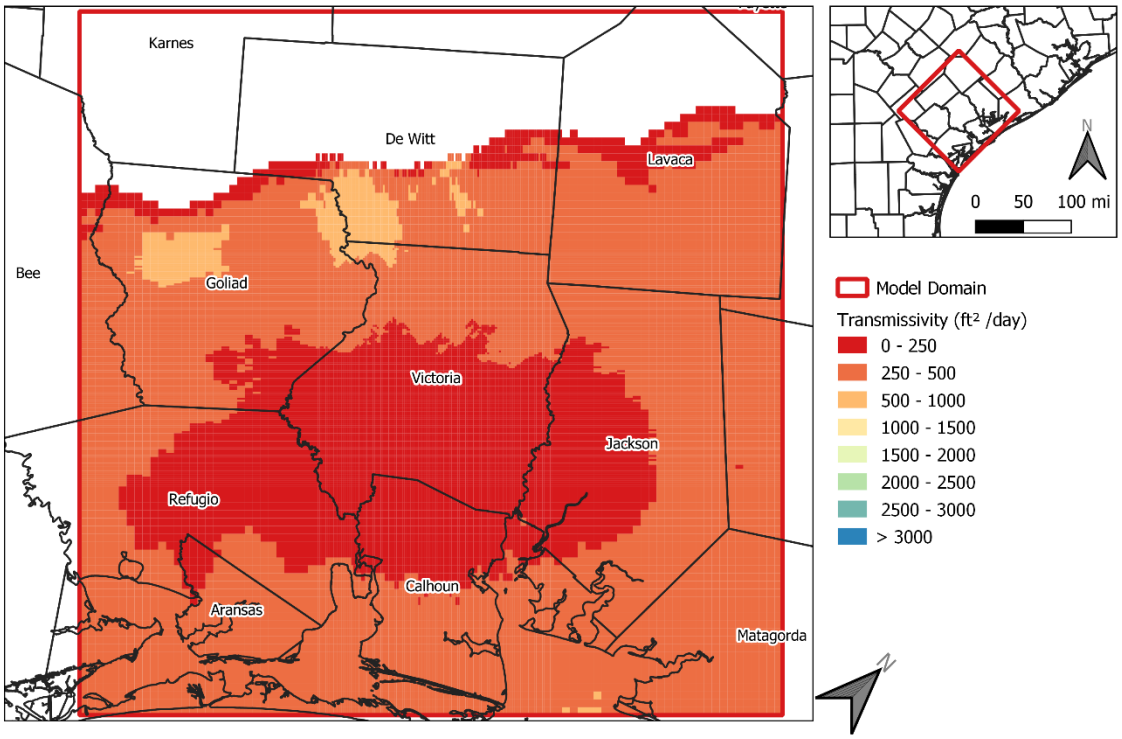

Figure 4-15 Transmissivity (ft^2/day) of model layer 11 (upper half of the Upper Lagarto formation)

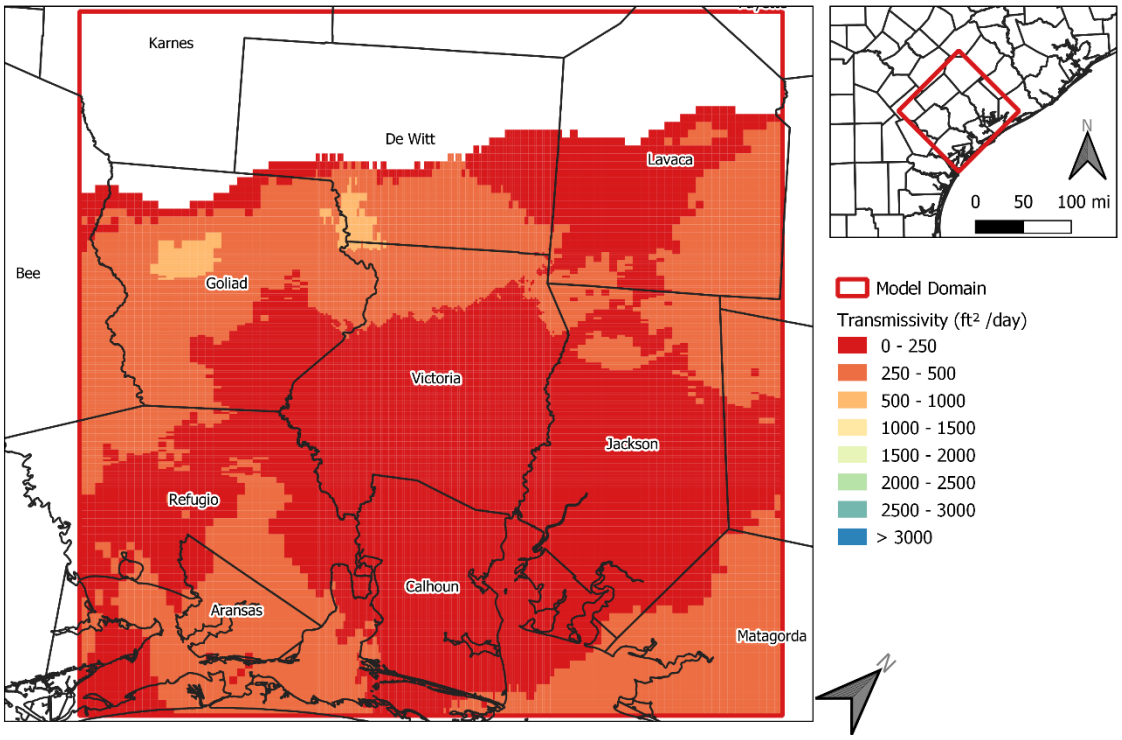

Figure 4-16 Transmissivity (ft^2/day) of model layer 12 (lower half of the Upper Lagarto formation)

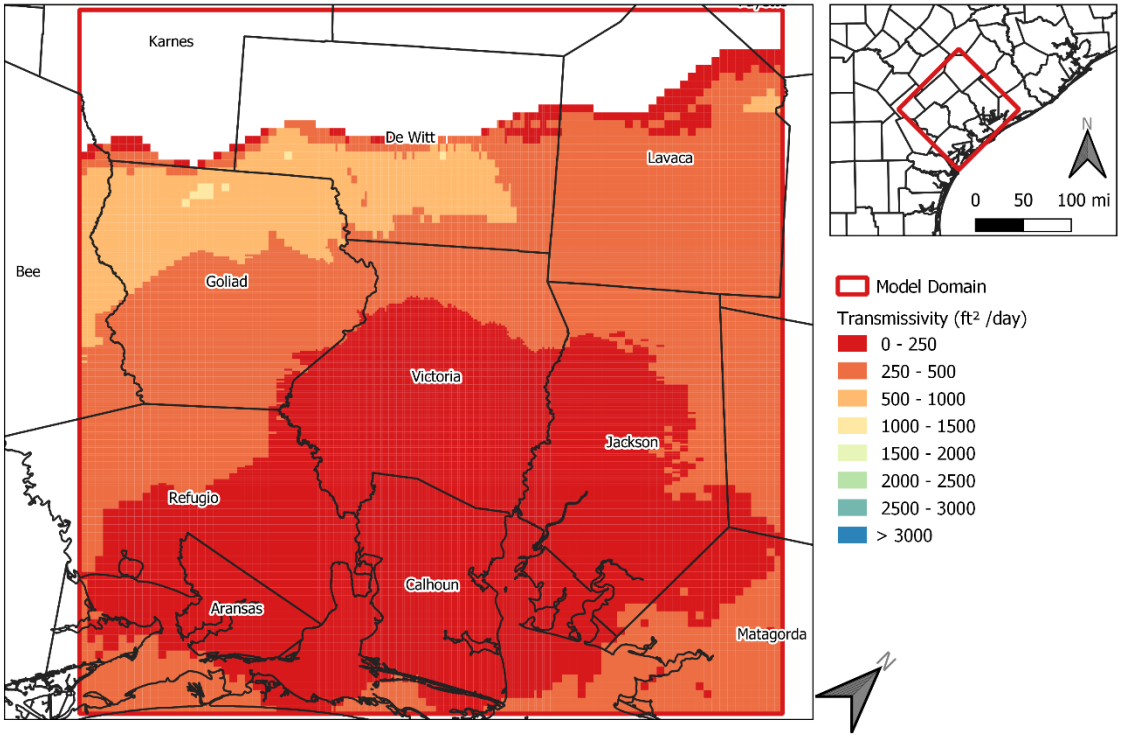

Figure 4-17 Transmissivity (ft^2/day) of model layer 13 (Middle Lagarto formation)

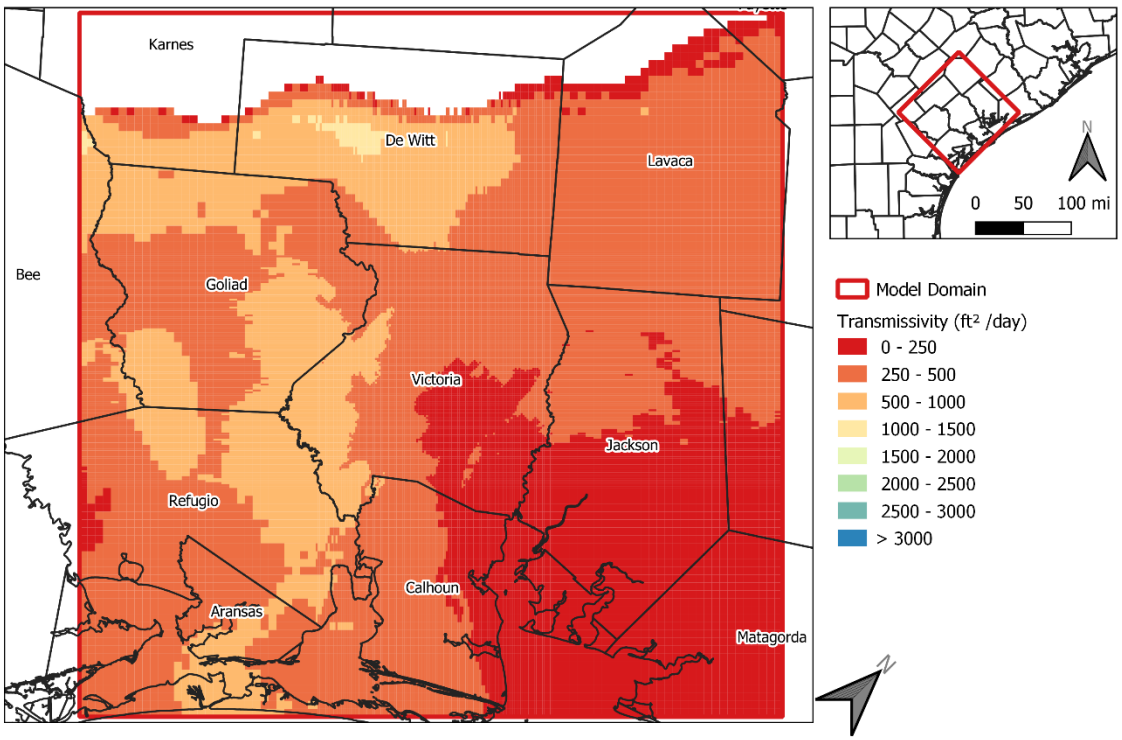

Figure 4-18 Transmissivity (ft^2/day) of model layer 14 (Lower Lagarto formation)

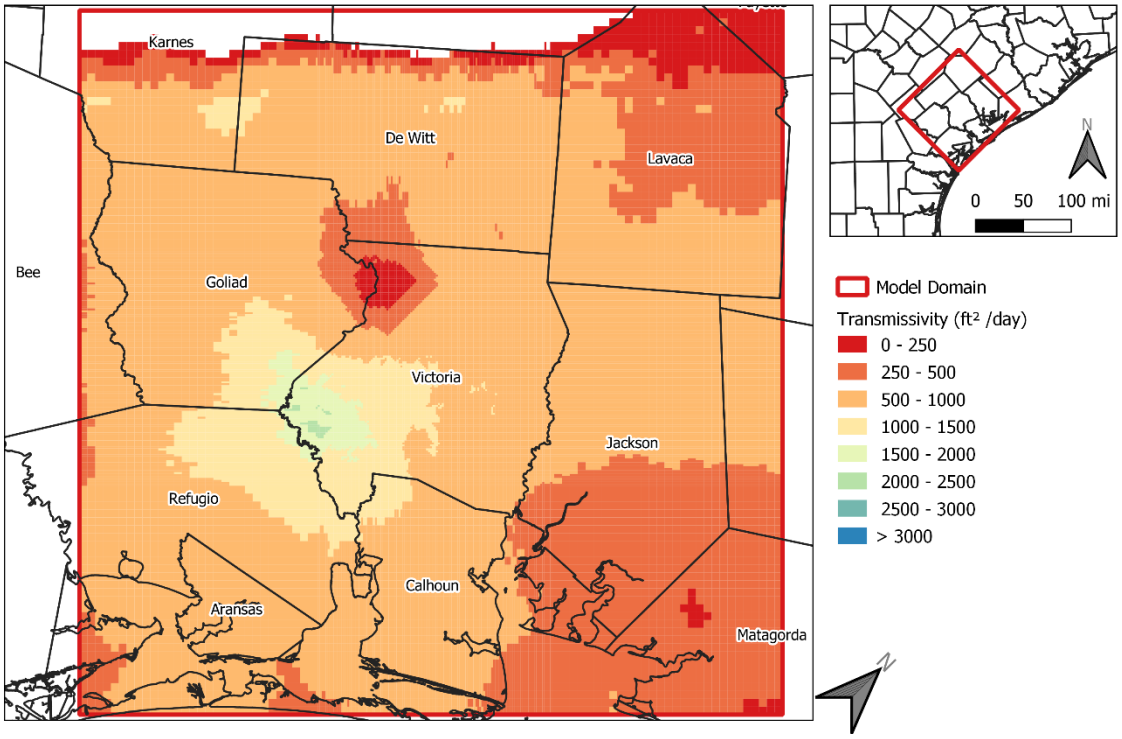

Figure 4-19 Transmissivity (ft^2/day) of model layer 15 (Oakville formation)

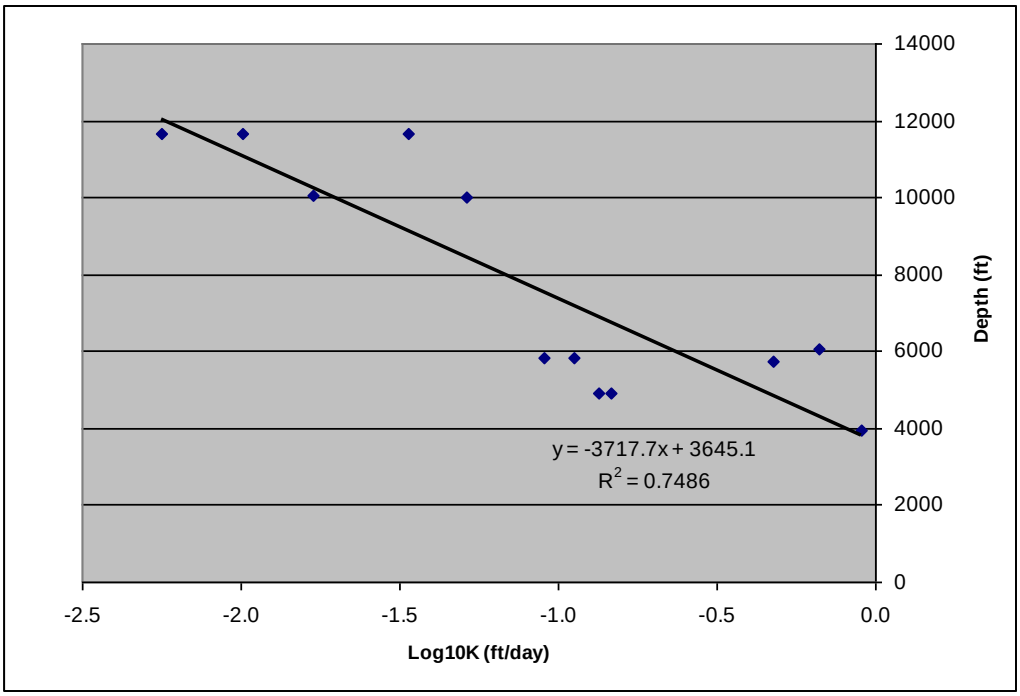

Figure 4-20 Hydraulic conductivity of pliocene clays as a function of depth of burial (Neglia, 2004)

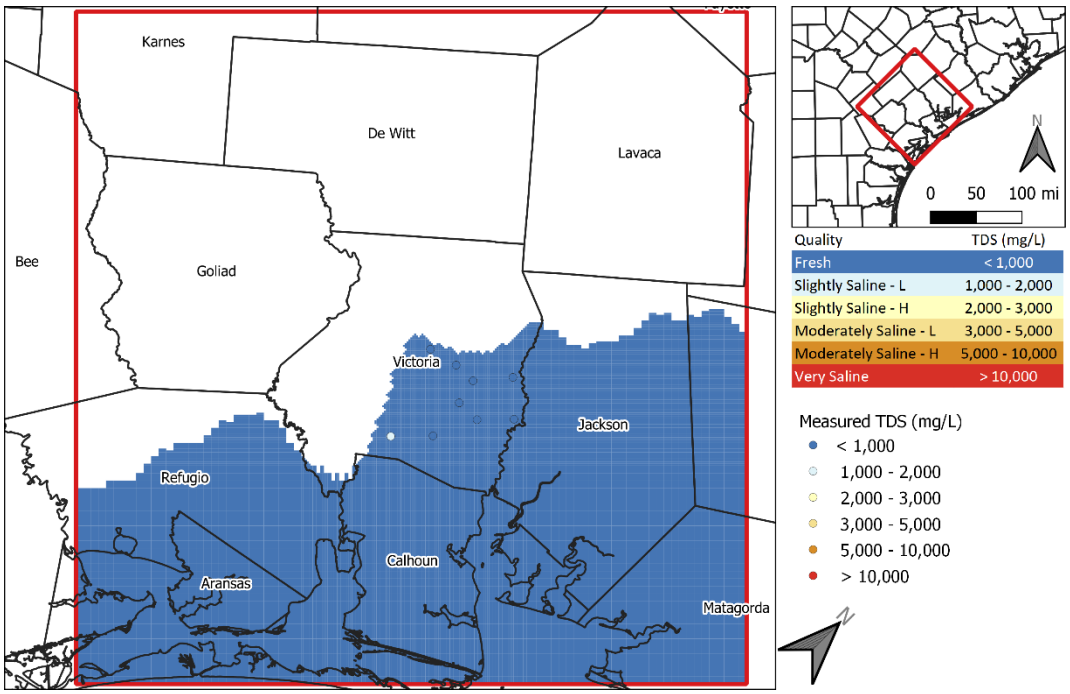

Figure 4-21 TDS concentrations (1) determined from the analysis of geophysical logs for groundwater in model layer 1 (Beaumont Formation) and (2) measured in wells screened across model layer 1

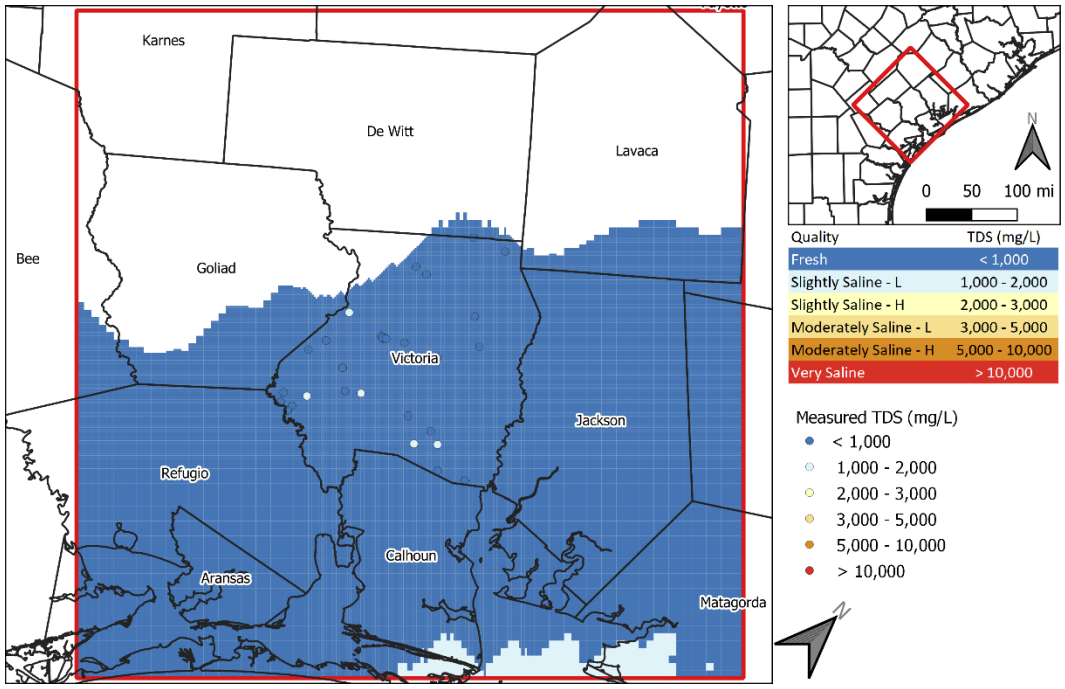

Figure 4-22 TDS concentrations (1) determined from the analysis of geophysical logs for groundwater in model layer 2 (Lissie Formation) and (2) measured in wells screened across model layer 2

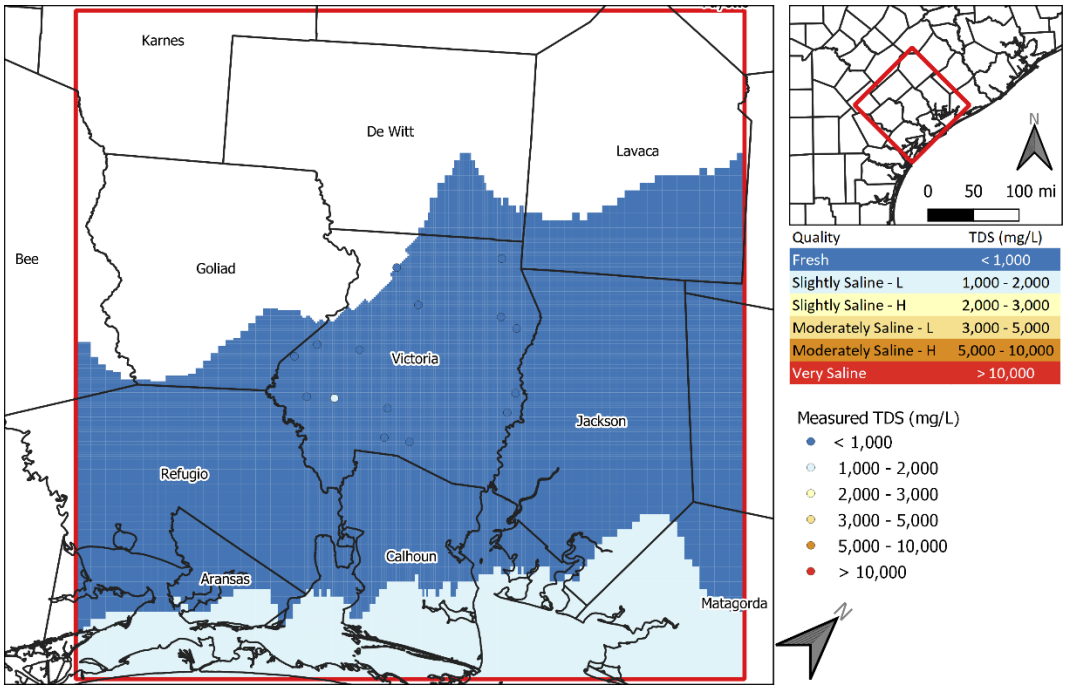

Figure 4-23 TDS concentrations (1) determined from the analysis of geophysical logs for groundwater in model layer 3 (Willis Formation) and (2) measured in wells screened across model layer 3

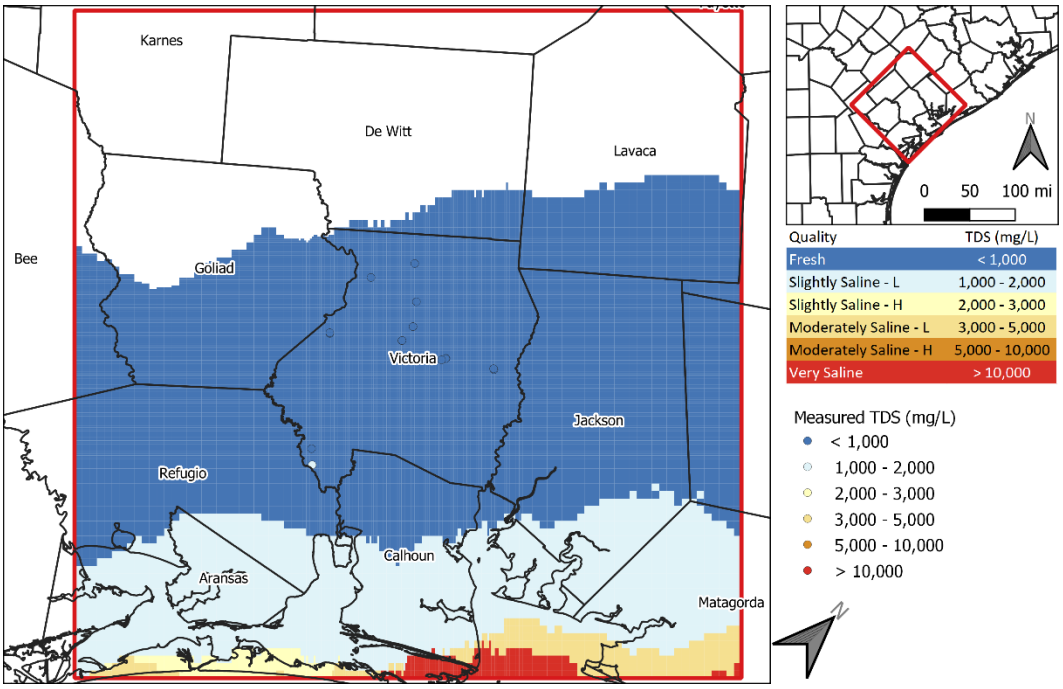

Figure 4-24 TDS concentrations (1) determined from the analysis of geophysical logs for groundwater in model layer 4 (Upper Goliad Formation) and (2) measured in wells screened across model layer 4

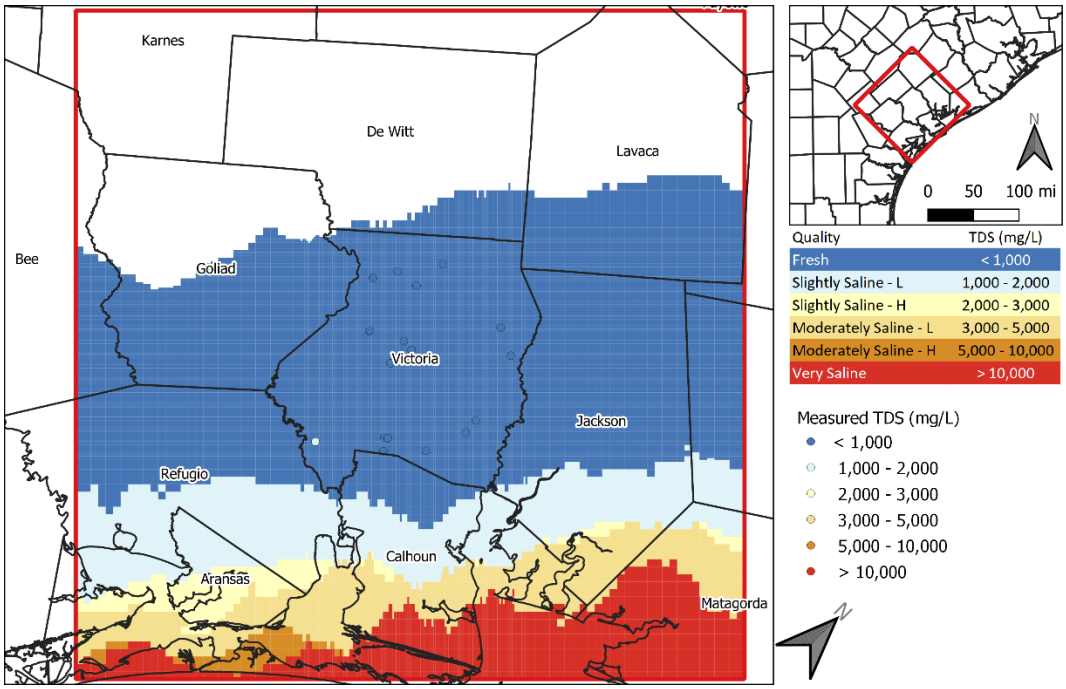

Figure 4-25 TDS concentrations (1) determined from the analysis of geophysical logs for groundwater in model layer 5 (Upper Goliad Formation) and (2) measured in wells screened across model layer 5

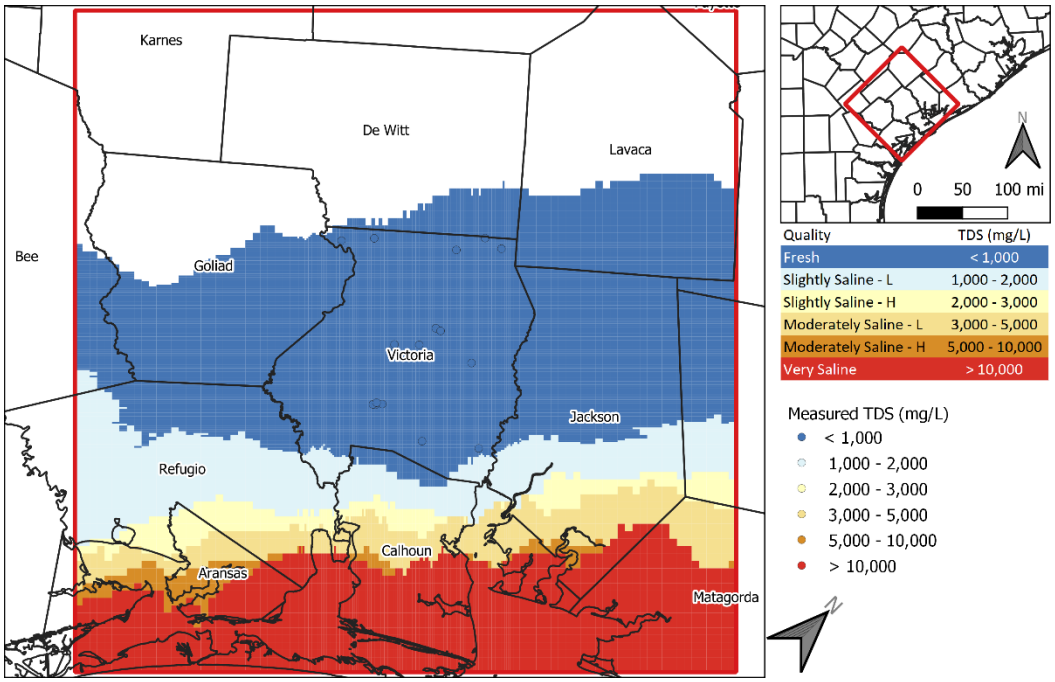

Figure 4-26 TDS concentrations (1) determined from the analysis of geophysical logs for groundwater in model layer 6 (Upper Goliad Formation) and (2) measured in wells screened across model layer 6

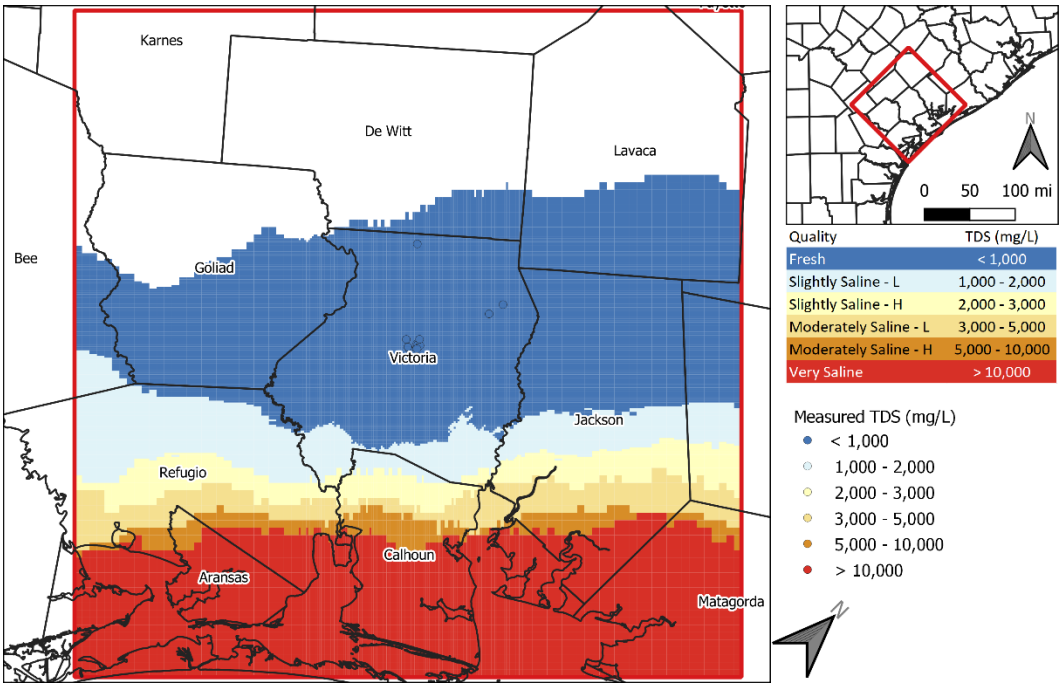

Figure 4-27 TDS concentrations (1) determined from the analysis of geophysical logs for groundwater in model layer 7 (Upper Goliad Formation) and (2) measured in wells screened across model layer 7

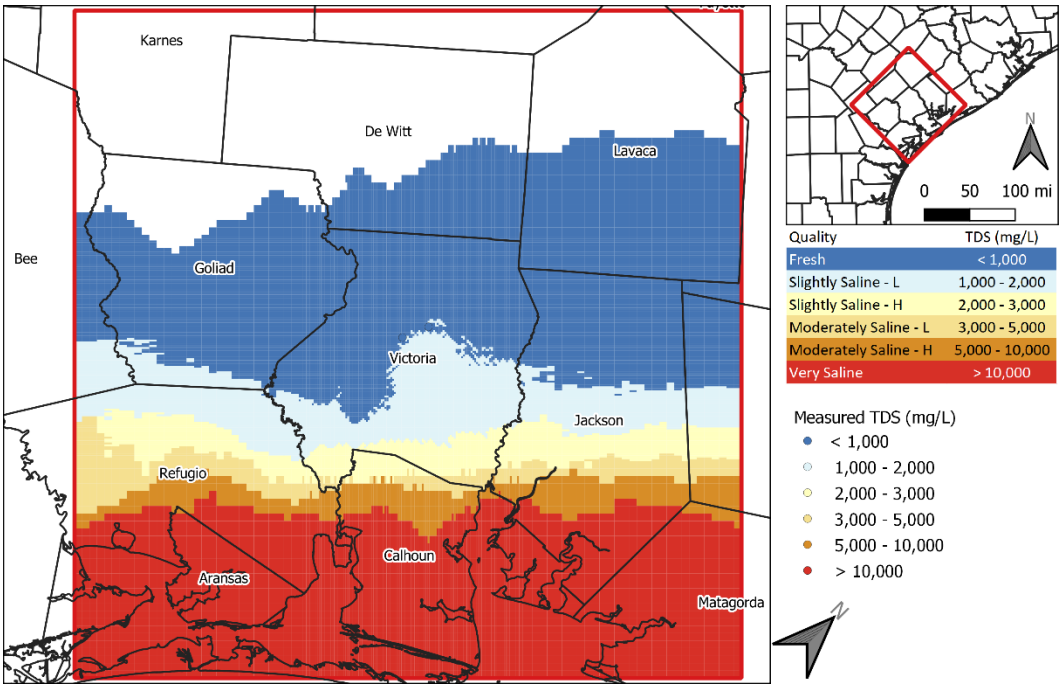

Figure 4-28 TDS concentrations (1) determined from the analysis of geophysical logs for groundwater in model layer 8 (Lower Goliad Formation) and (2) measured in wells screened across model layer 8

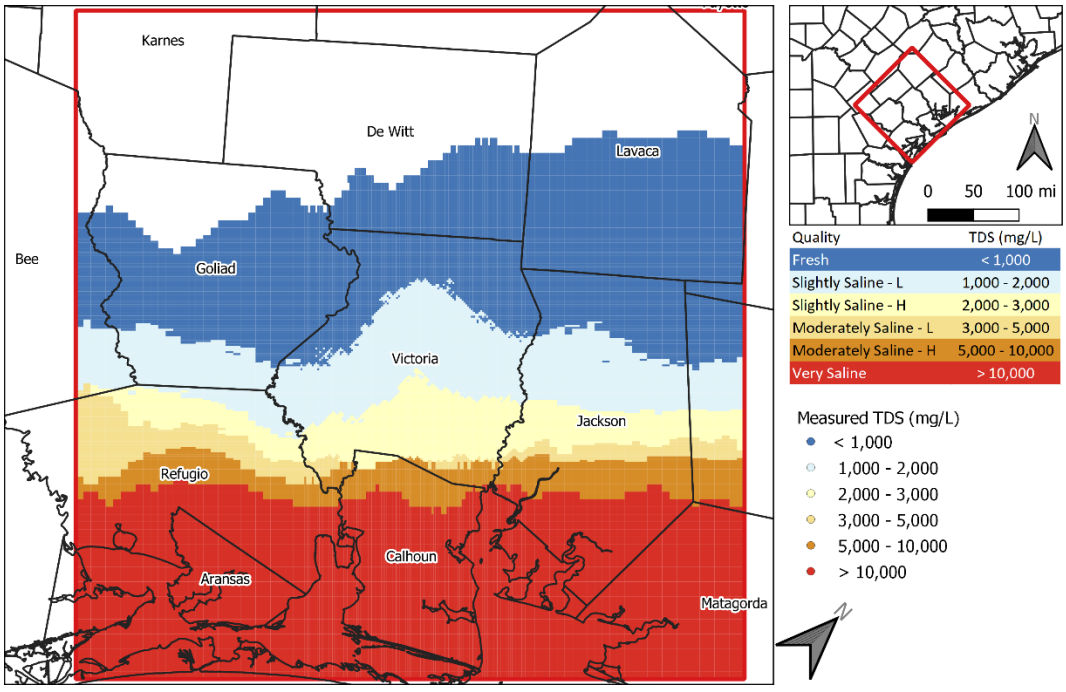

Figure 4-29 TDS concentrations (1) determined from the analysis of geophysical logs for groundwater in model layer 9 (Lower Goliad Formation) and (2) measured in wells screened across model layer 9

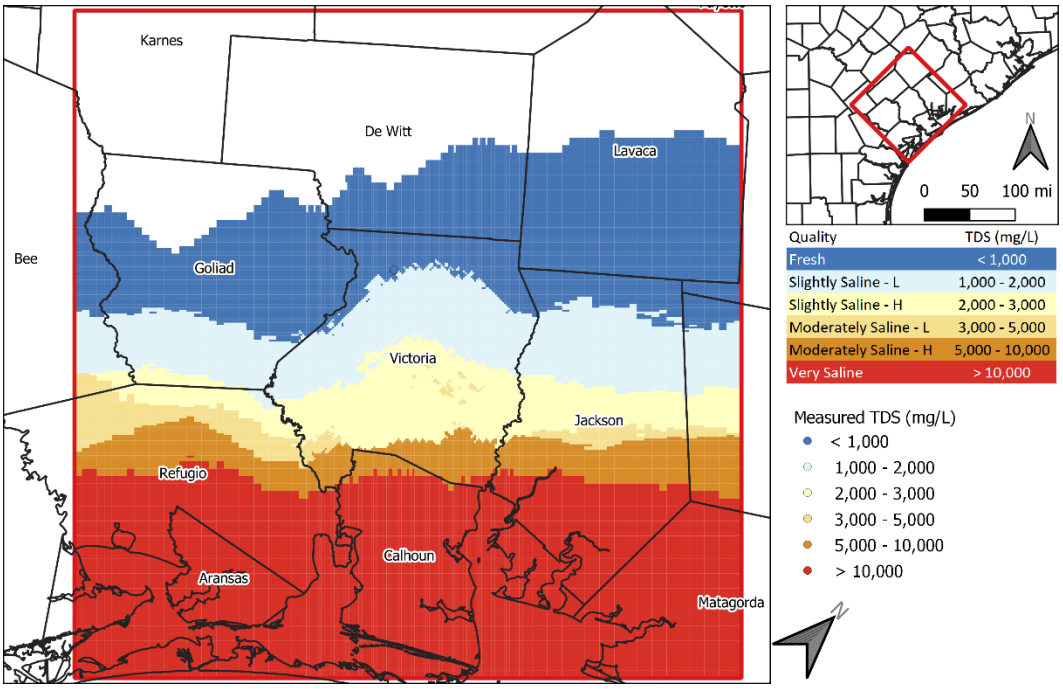

Figure 4-30 TDS concentrations (1) determined from the analysis of geophysical logs for groundwater in model layer 10 (Lower Goliad Formation) and (2) measured in wells screened across model layer 10

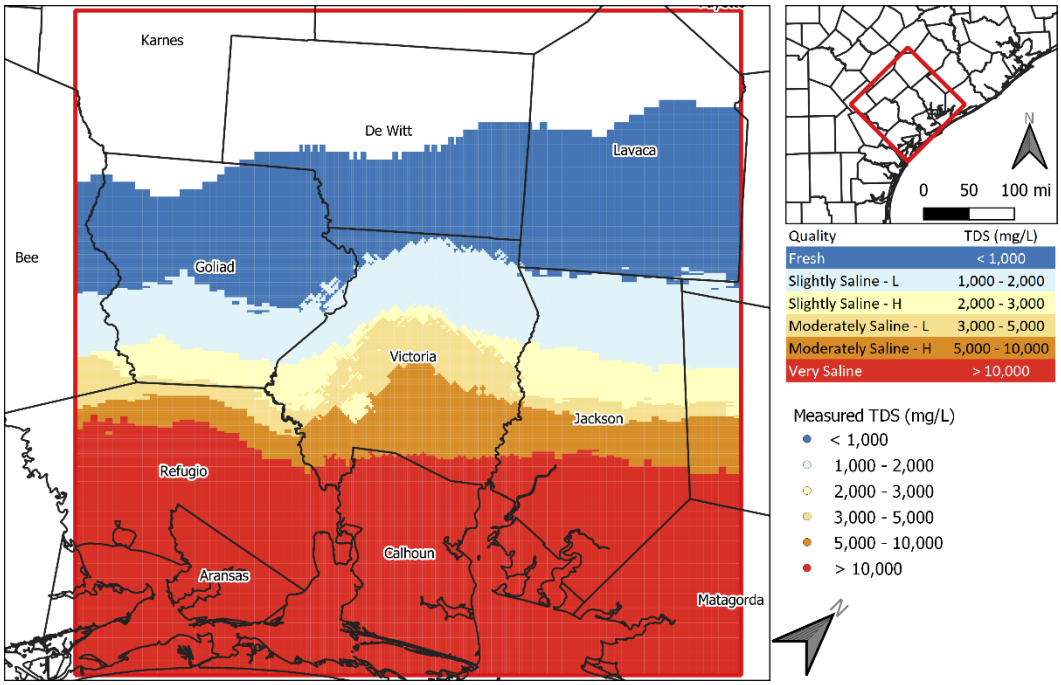

Figure 4-31 TDS concentrations (1) determined from the analysis of geophysical logs for groundwater in model layer 11 (Upper Lagarto Formation) and (2) measured in wells screened across model layer 11

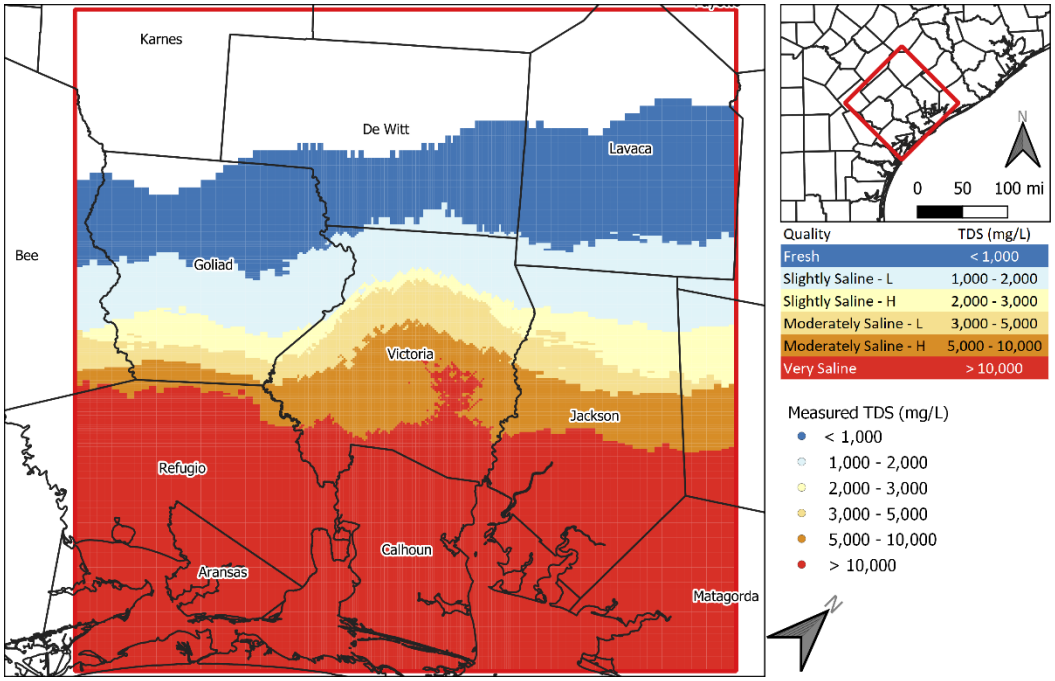

Figure 4-32 TDS concentrations (1) determined from the analysis of geophysical logs for groundwater in model layer 12 (Upper Lagarto Formation) and (2) measured in wells screened across model layer 12

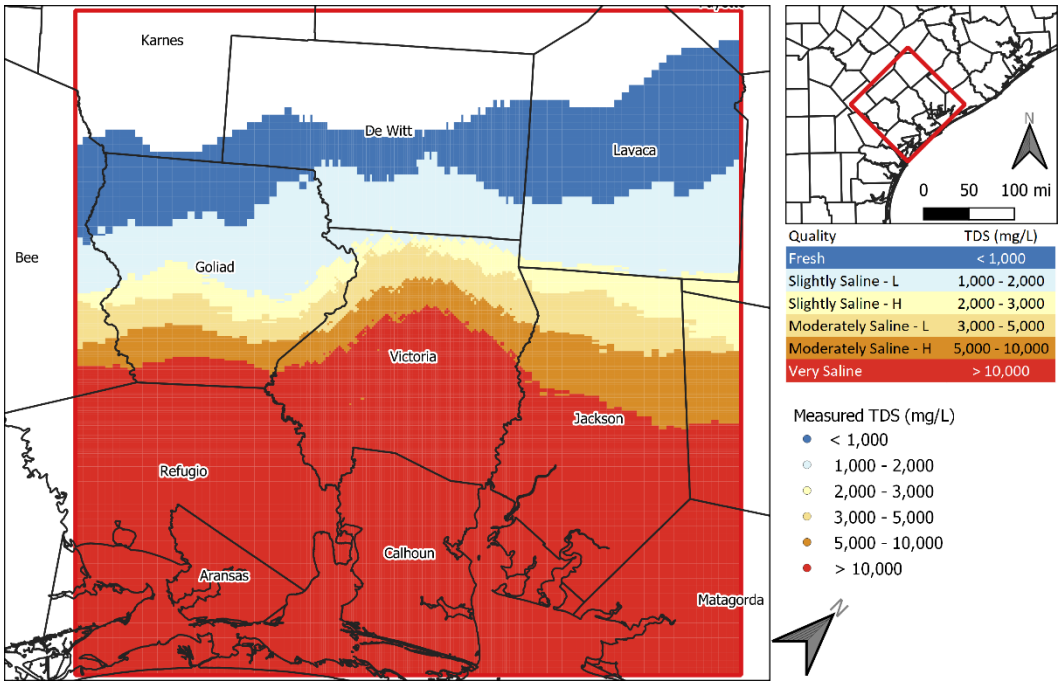

Figure 4-33 TDS concentrations (1) determined from the analysis of geophysical logs for groundwater in model layer 13 (Middle Lagarto Formation) and (2) measured in wells screened across model layer 13

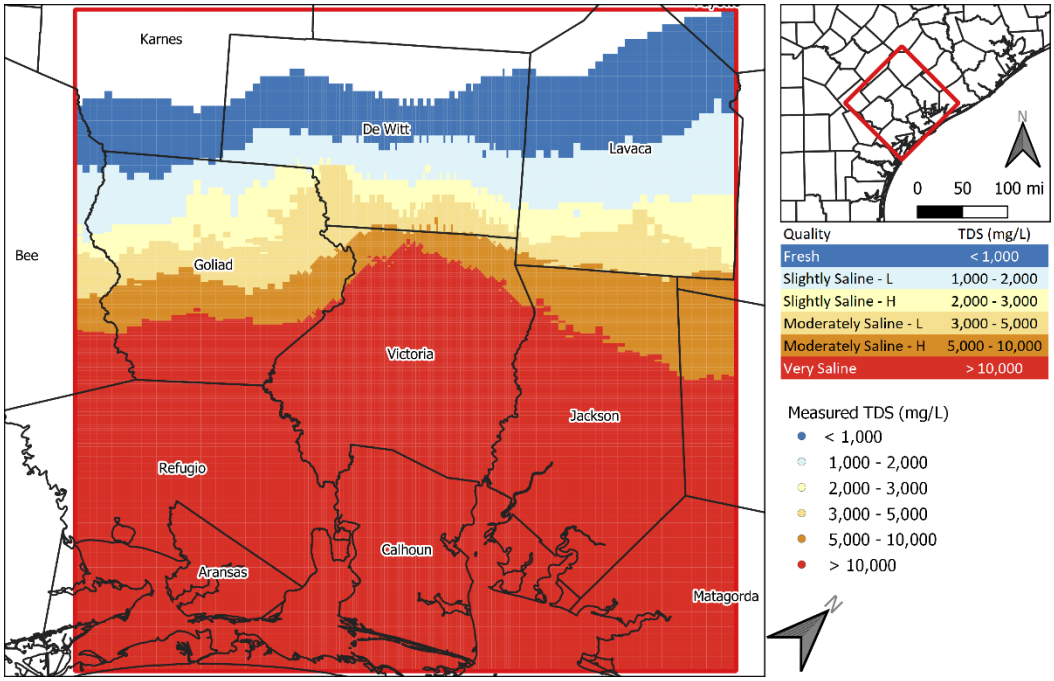

Figure 4-34 TDS concentrations (1) determined from the analysis of geophysical logs for groundwater in model layer 14 (Lower Lagarto Formation) and (2) measured in wells screened across model layer 14

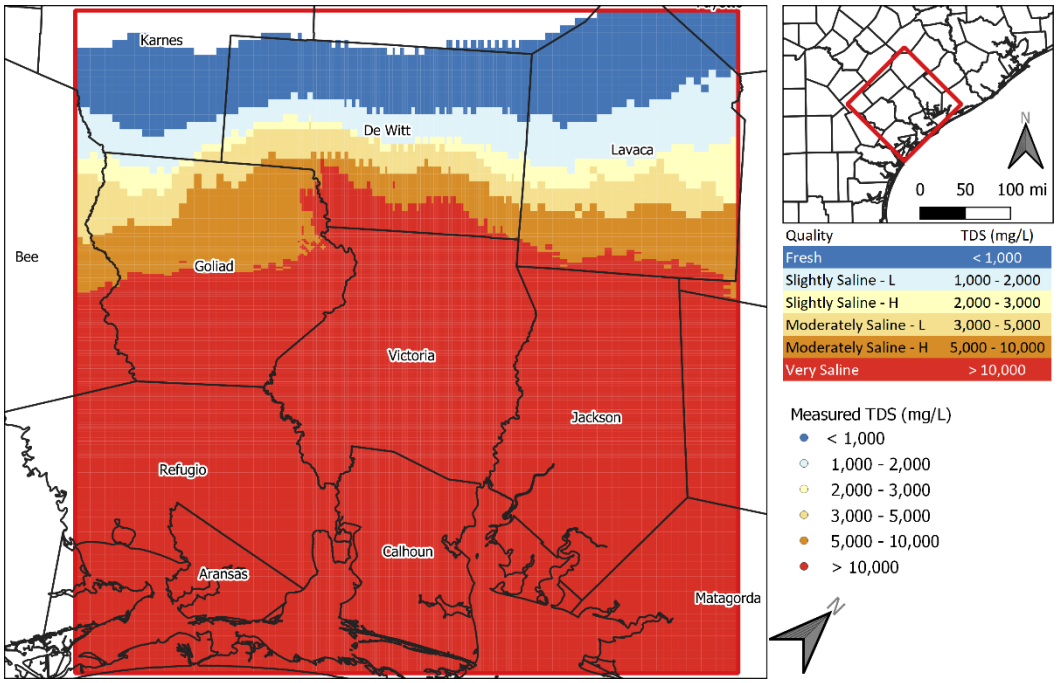

Figure 4-35 TDS concentrations (1) determined from the analysis of geophysical logs for groundwater in model layer 17 (Oakville Formation) and (2) measured in wells screened across model layer 15

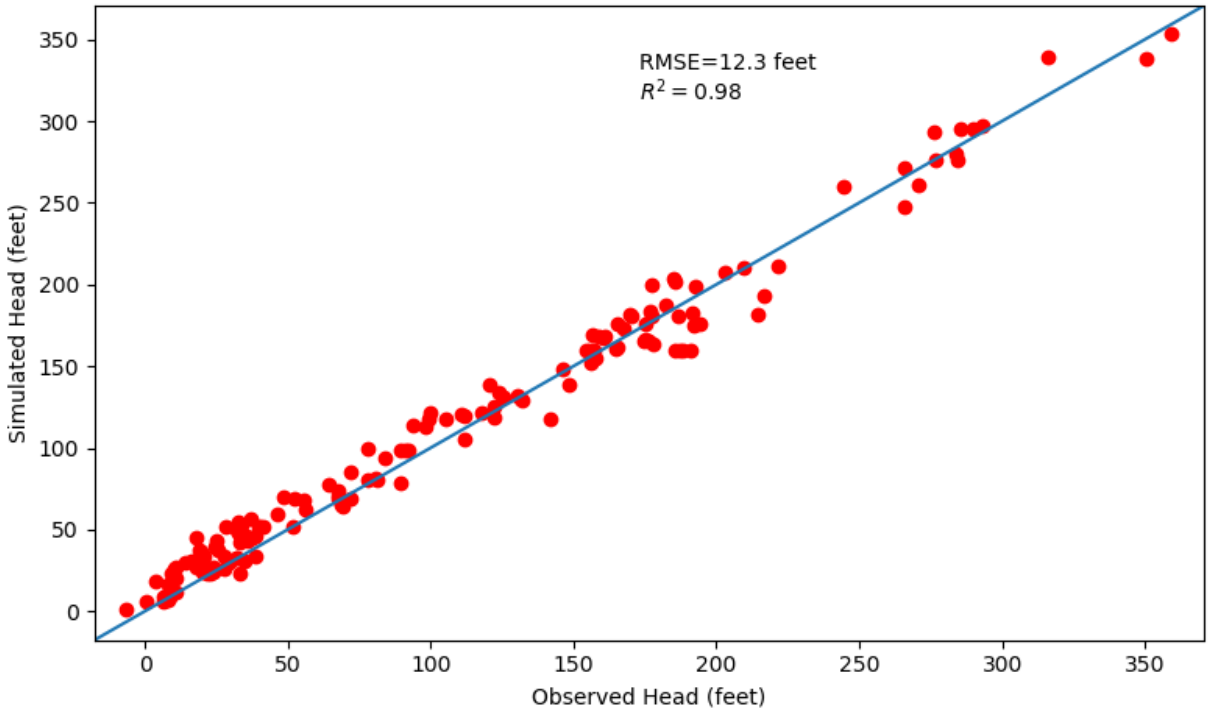

Figure 4-36 Comparison of simulated verus observed hydraulic heads for 150 wells in the model domain

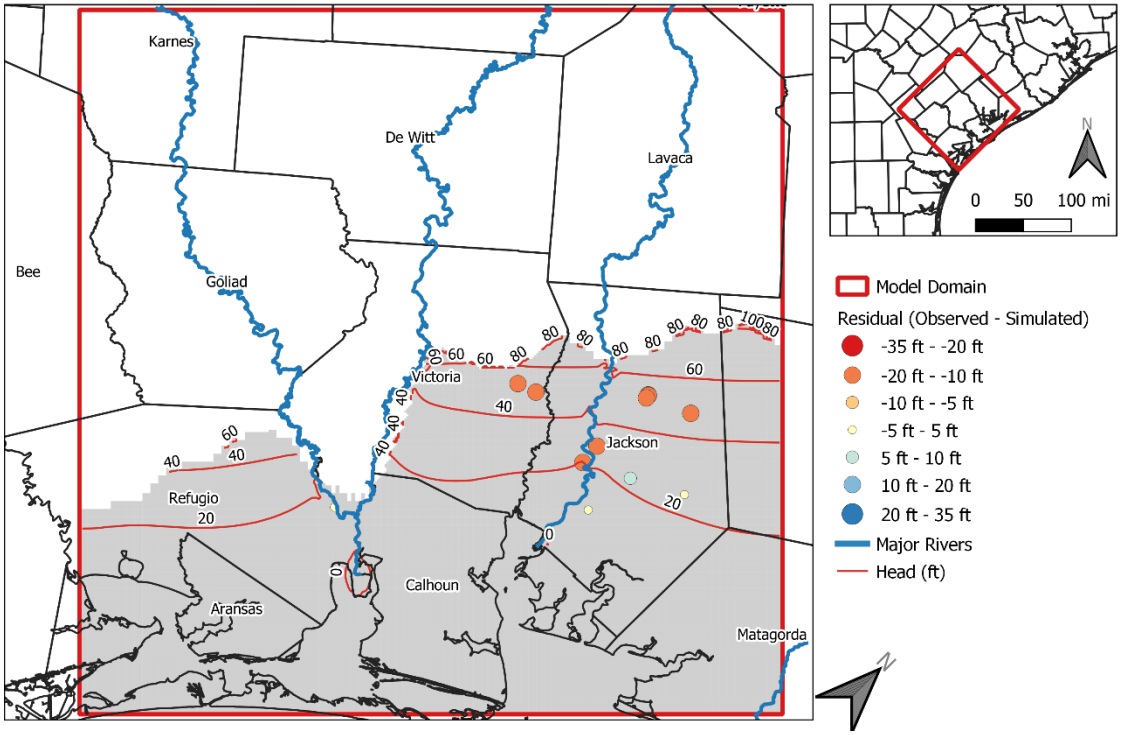

Figure 4-37 Simulated water levels and calculated difference between observed and simulated hydraulic heads for Model Layer 1

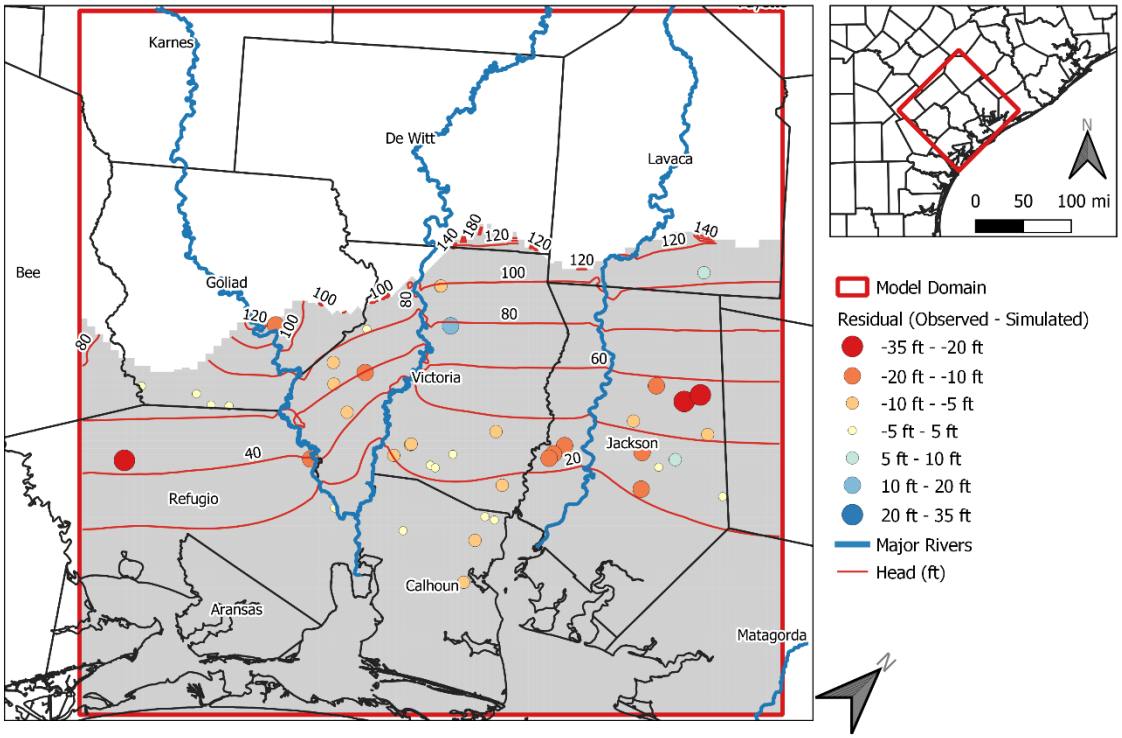

Figure 4-38 Simulated water levels and calculated difference between observed and simulated hydraulic heads for Model Layer 2

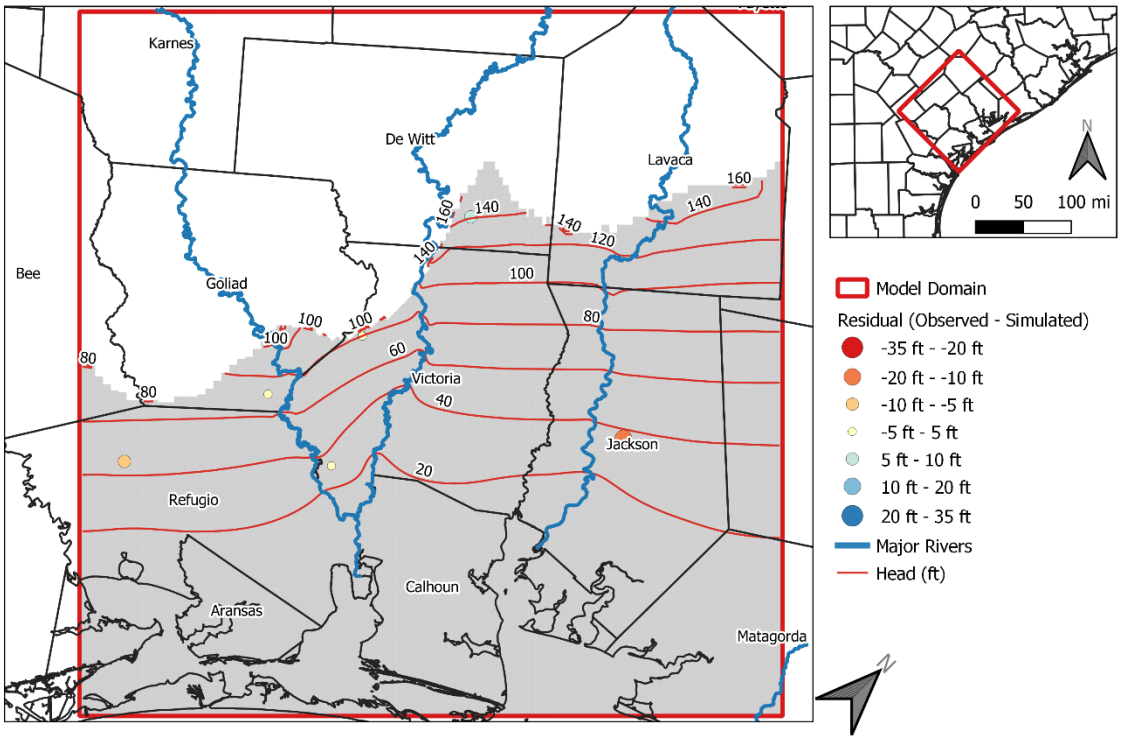

Figure 4-39 Simulated water levels and calculated difference between observed and simulated hydraulic heads for Model Layer 3

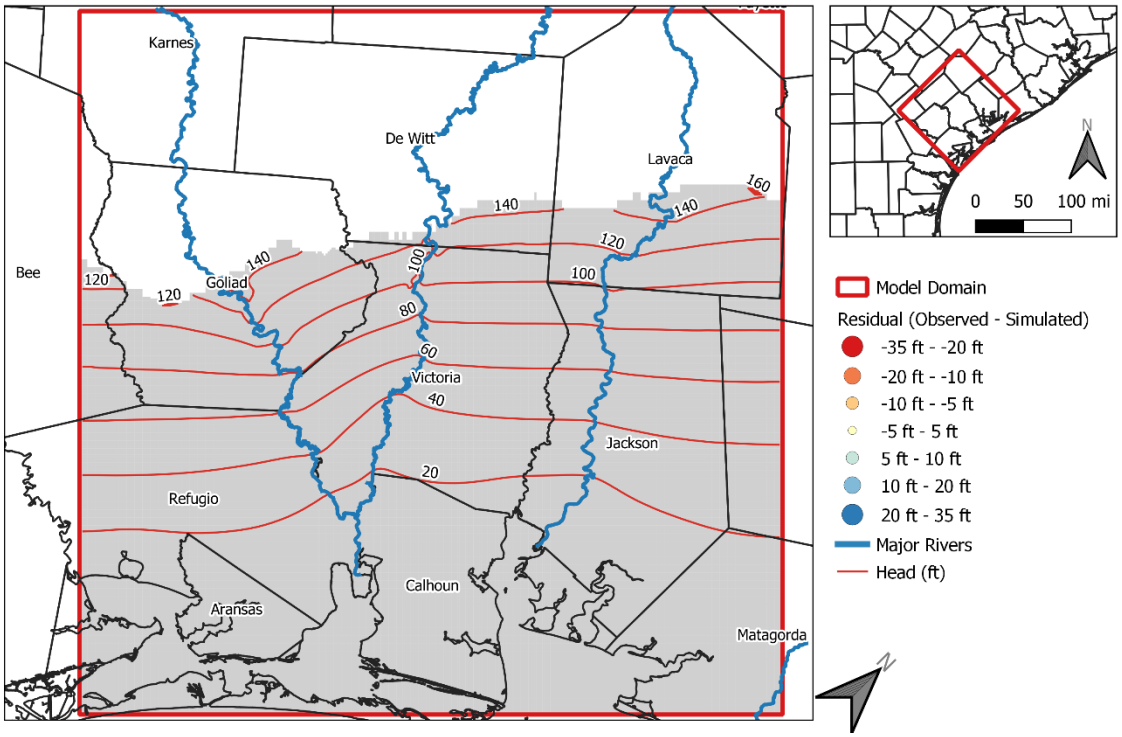

Figure 4-40 Simulated water levels and calculated difference between observed and simulated hydraulic heads for Model Layer 4

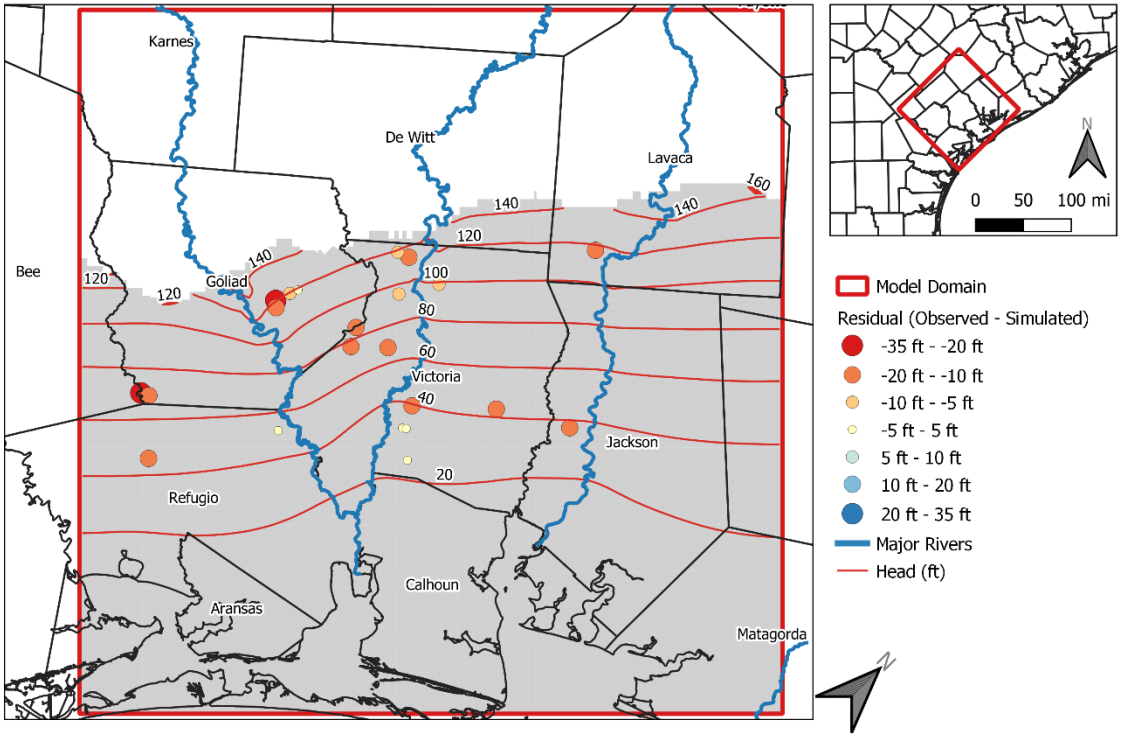

Figure 4-41 Simulated water levels and calculated difference between observed and simulated hydraulic heads for Model Layer 5

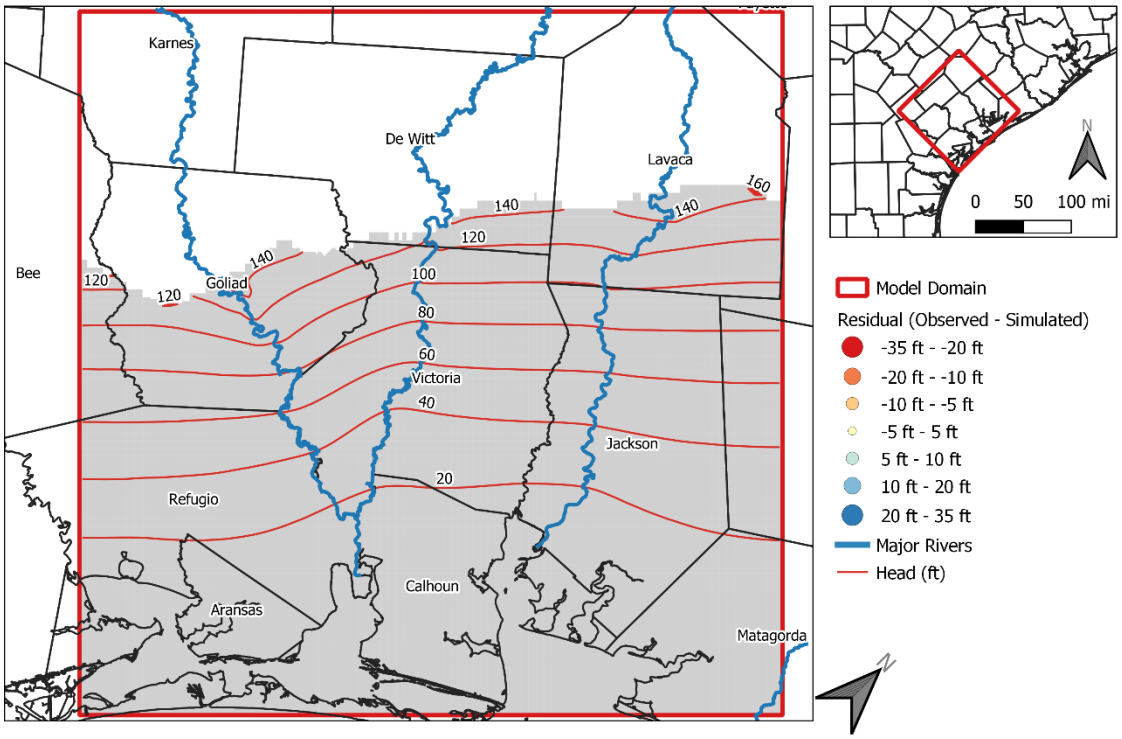

Figure 4-42 Simulated water levels and calculated difference between observed and simulated hydraulic heads for Model Layer 6

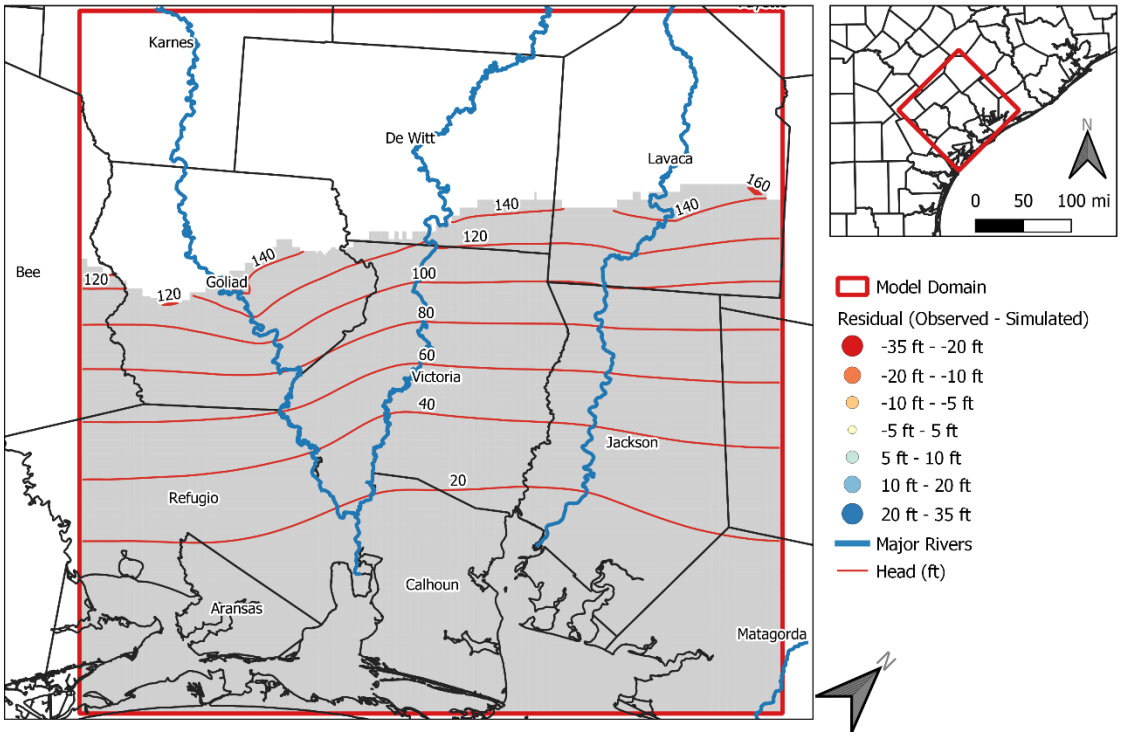

Figure 4-43 Simulated water levels and calculated difference between observed and simulated hydraulic heads for Model Layer 7

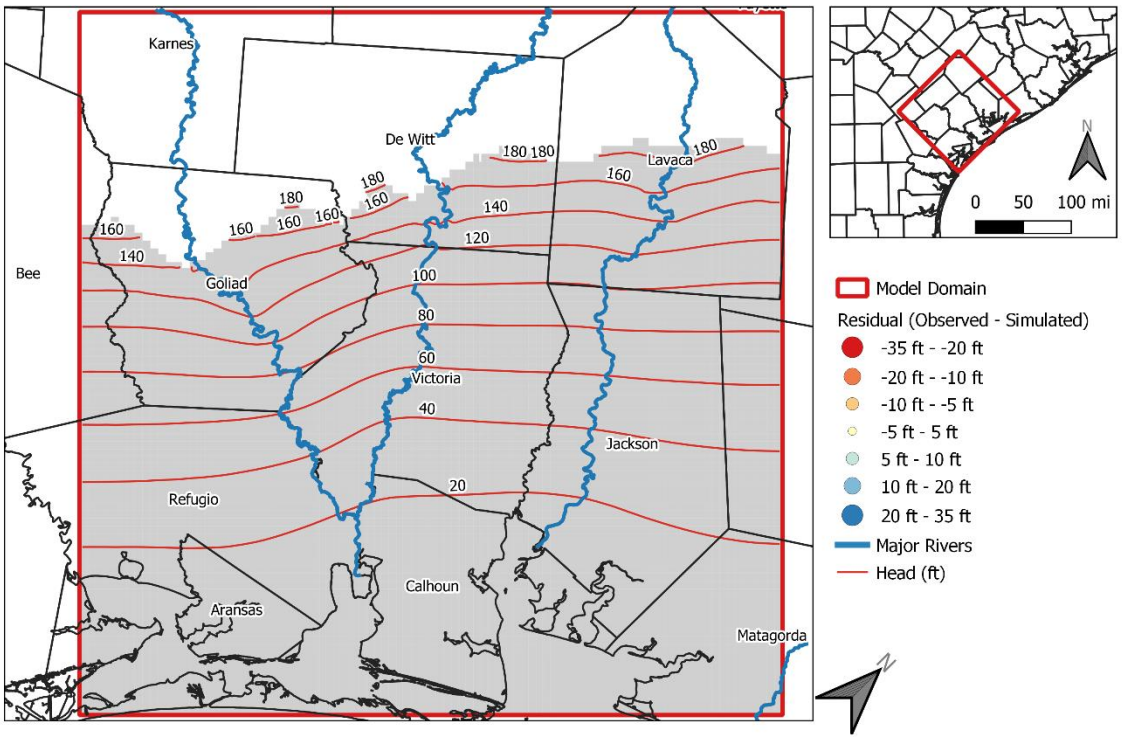

Figure 4-44 Simulated water levels and calculated difference between observed and simulated hydraulic heads for Model Layer 8

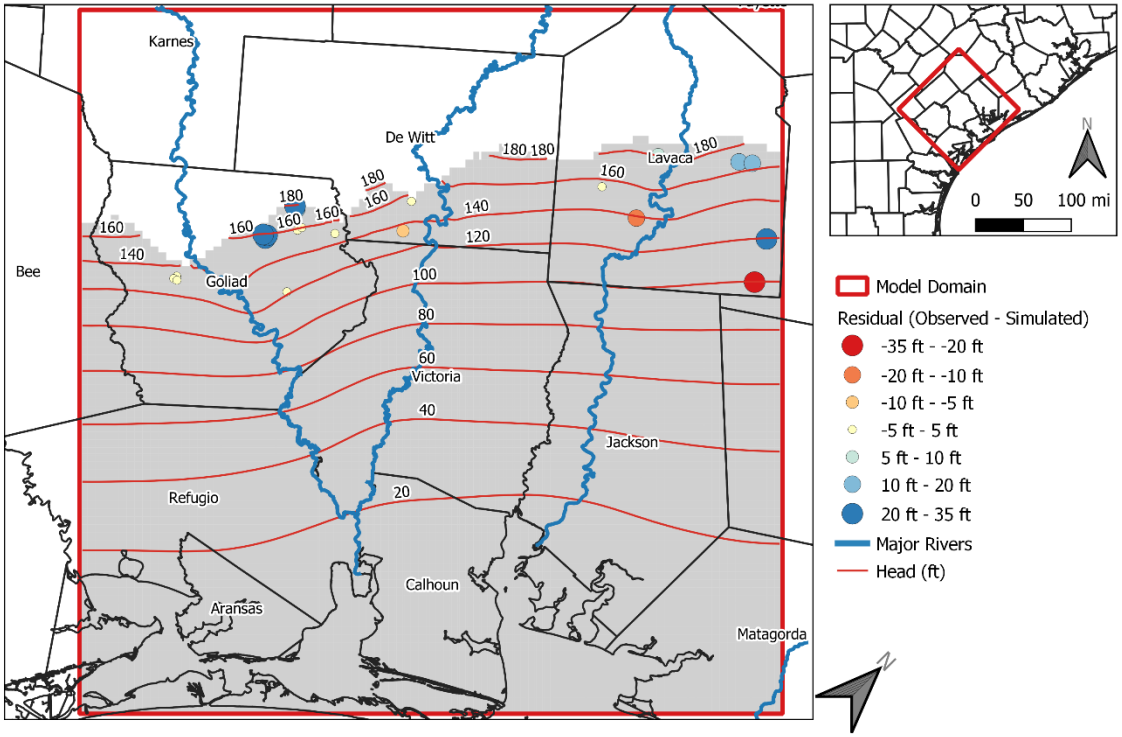

Figure 4-45 Simulated water levels and calculated difference between observed and simulated hydraulic heads for Model Layer 9

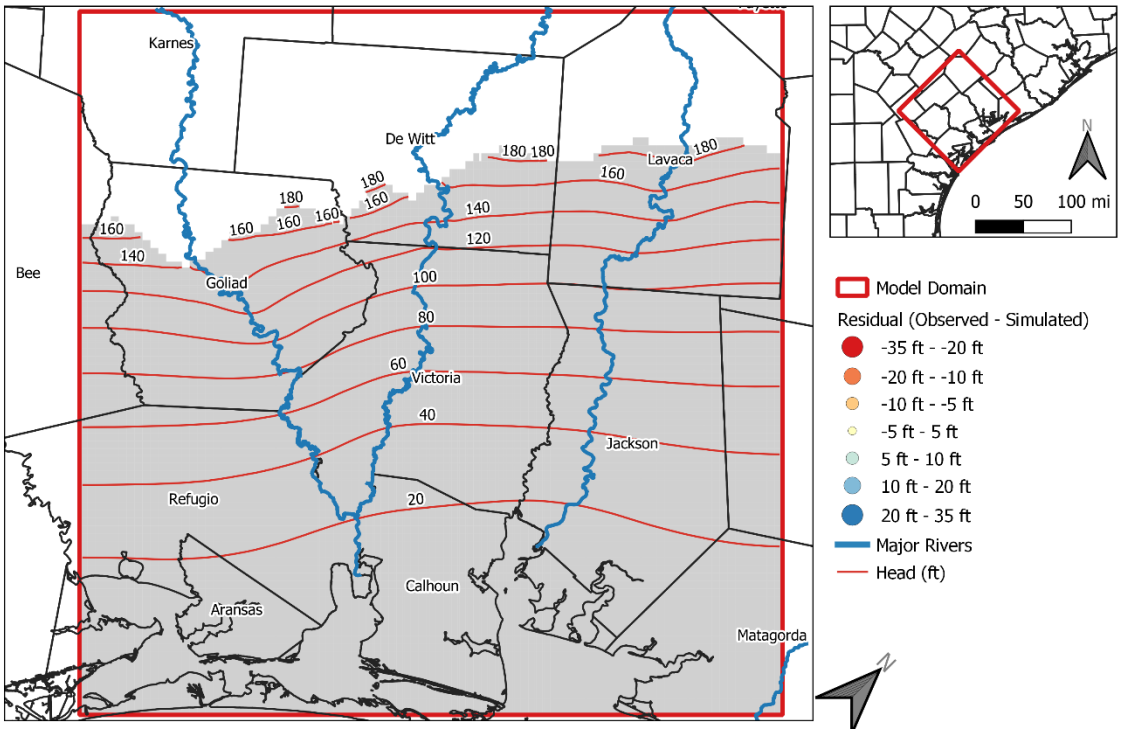

Figure 4-46 Simulated water levels and calculated difference between observed and simulated hydraulic heads for Model Layer 10

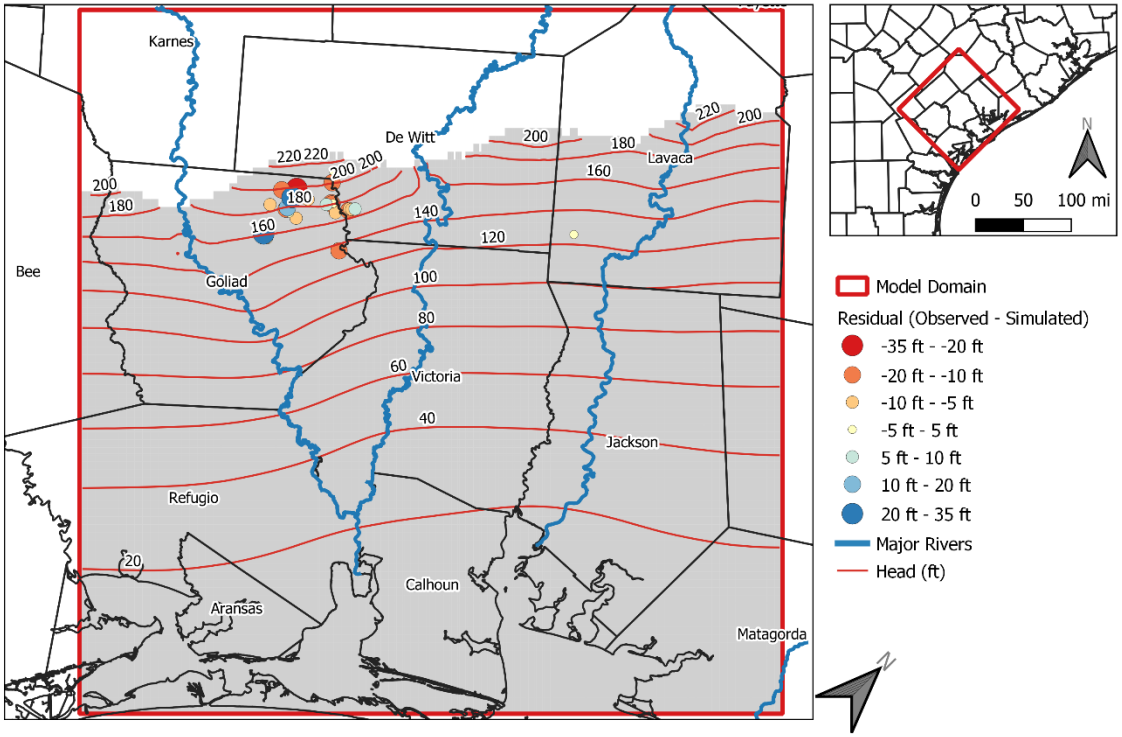

Figure 4-47 Simulated water levels and calculated difference between observed and simulated hydraulic heads for Model Layer 11

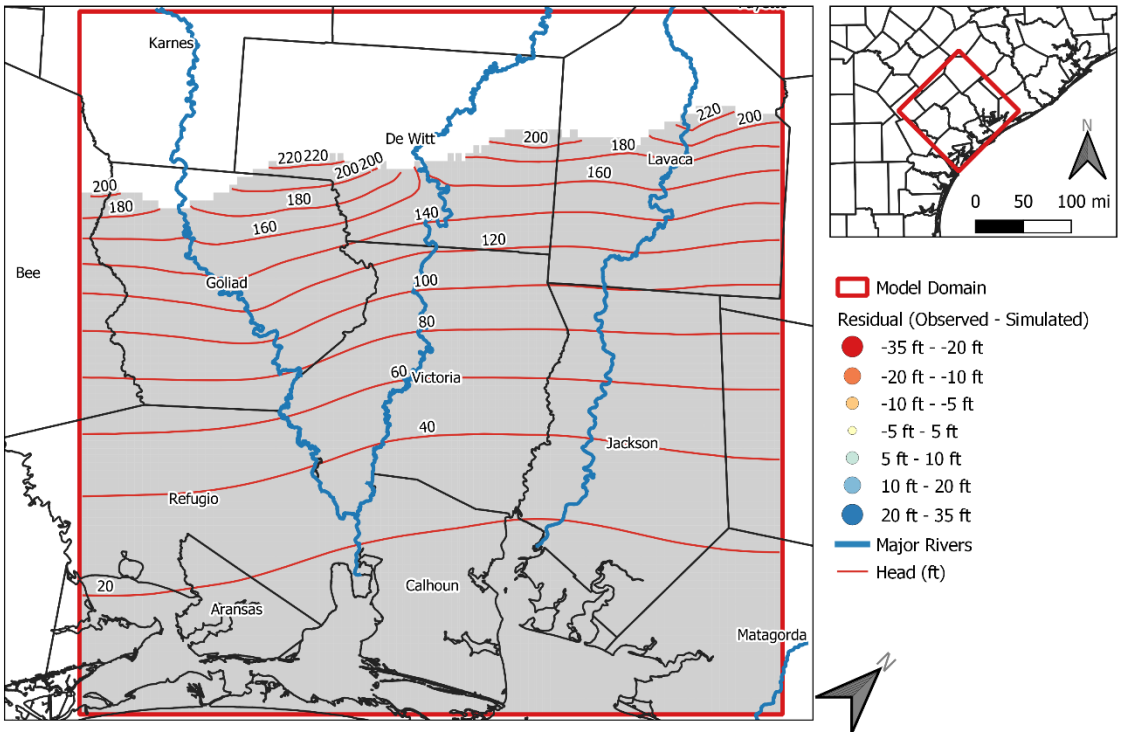

Figure 4-48 Simulated water levels and calculated difference between observed and simulated hydraulic heads for Model Layer 12

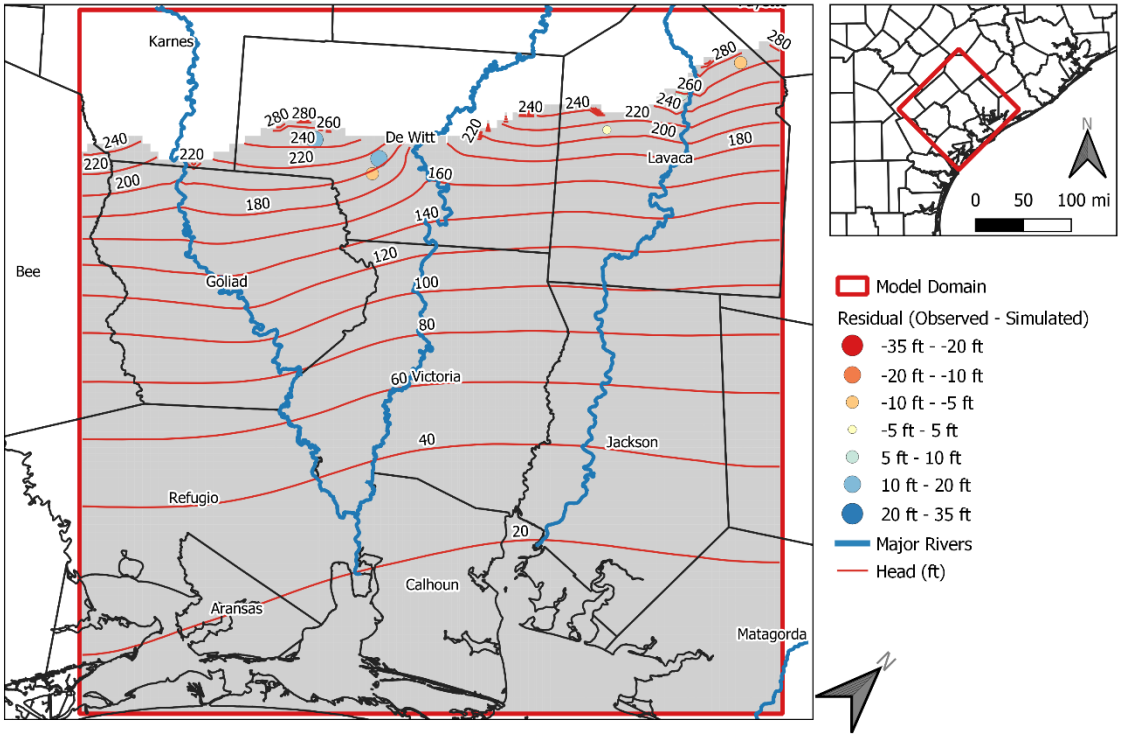

Figure 4-49 Simulated water levels and calculated difference between observed and simulated hydraulic heads for Model Layer 13

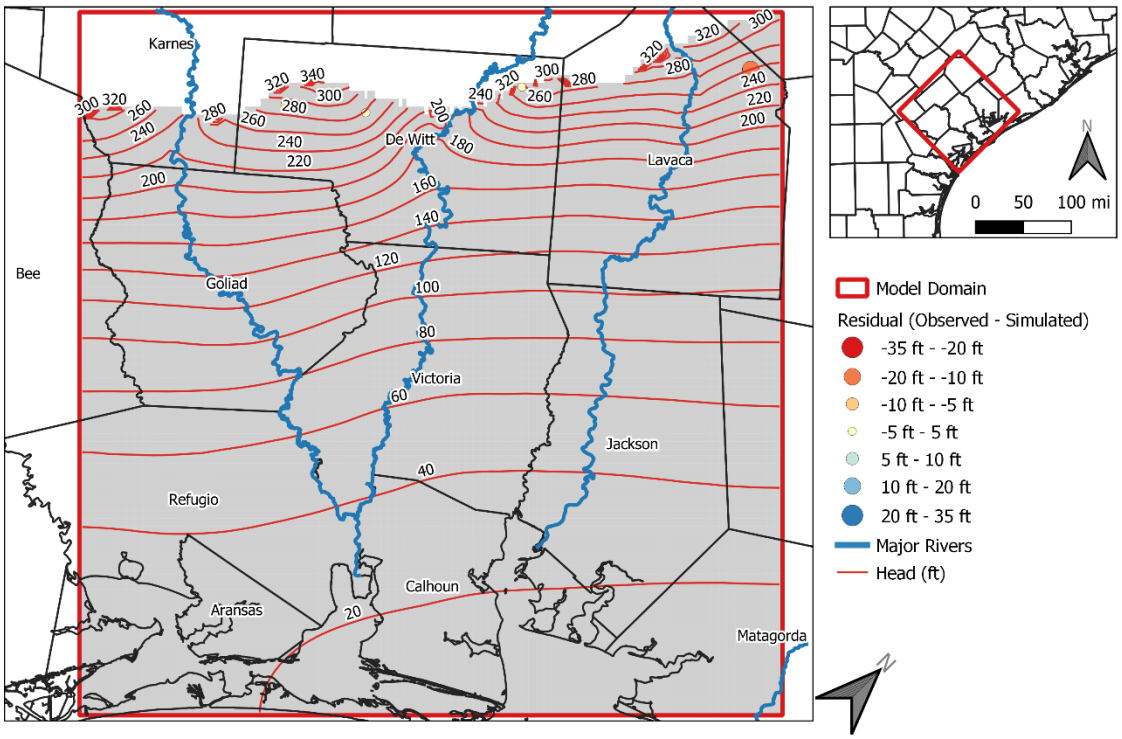

Figure 4-50 Simulated water levels and calculated difference between observed and simulated hydraulic heads for Model Layer 14

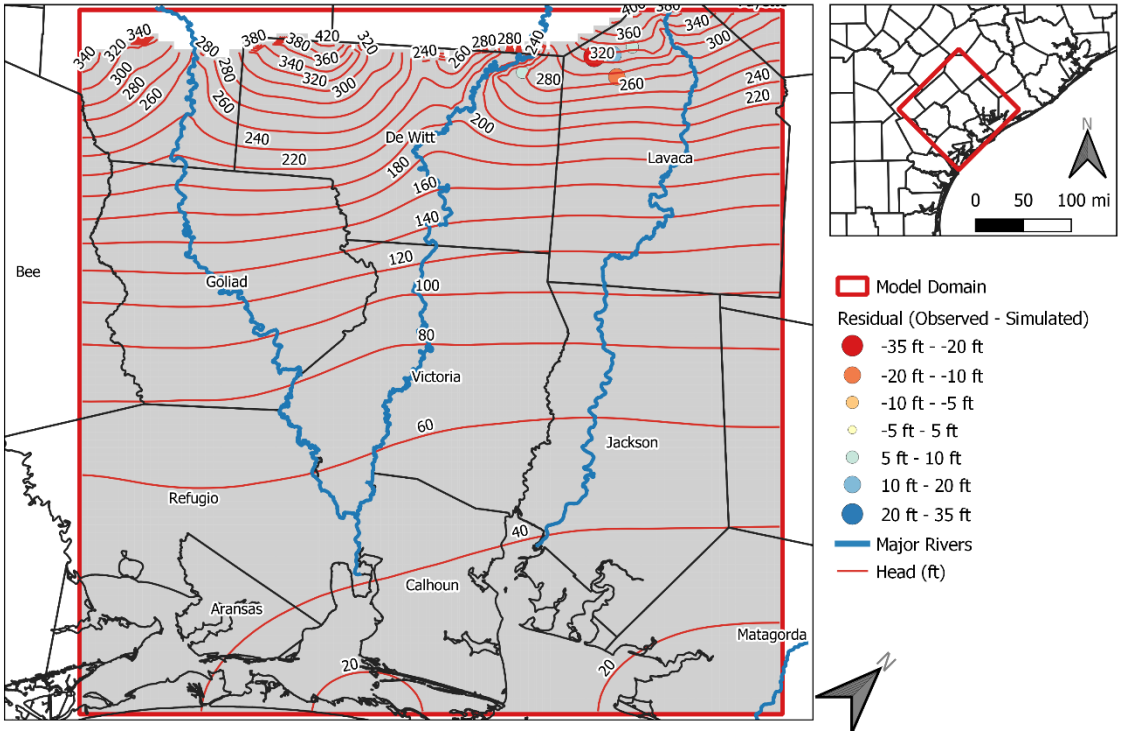

Figure 4-51 Simulated water levels and calculated difference between observed and simulated hydraulic heads for Model Layer 15

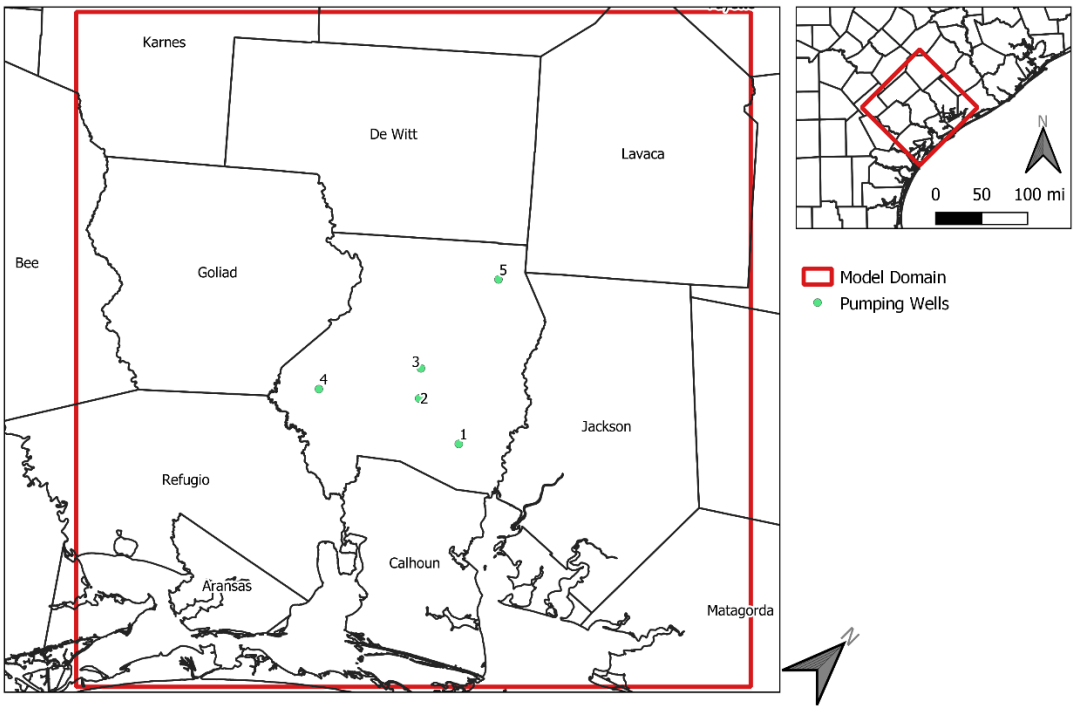

Figure 4-52 Locations where groundwater models were used to estimate drawdowns caused by pumping brackish groundwater

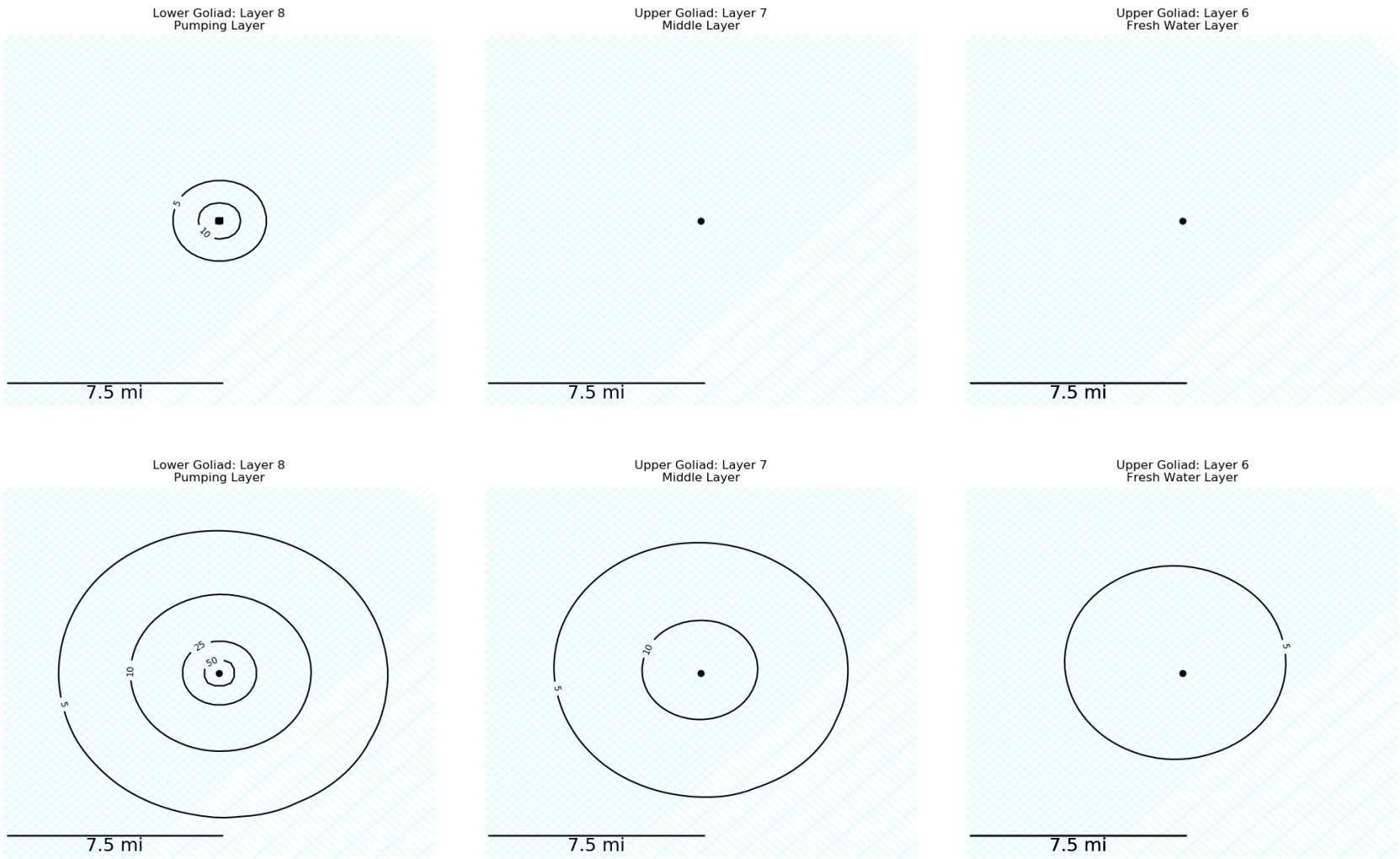

Figure 4-53 Simulated drawdowns caused by pumping at :Location #1 for 30 years at a rate of: 250 gpm (top) and 1000 gpm (bottom)

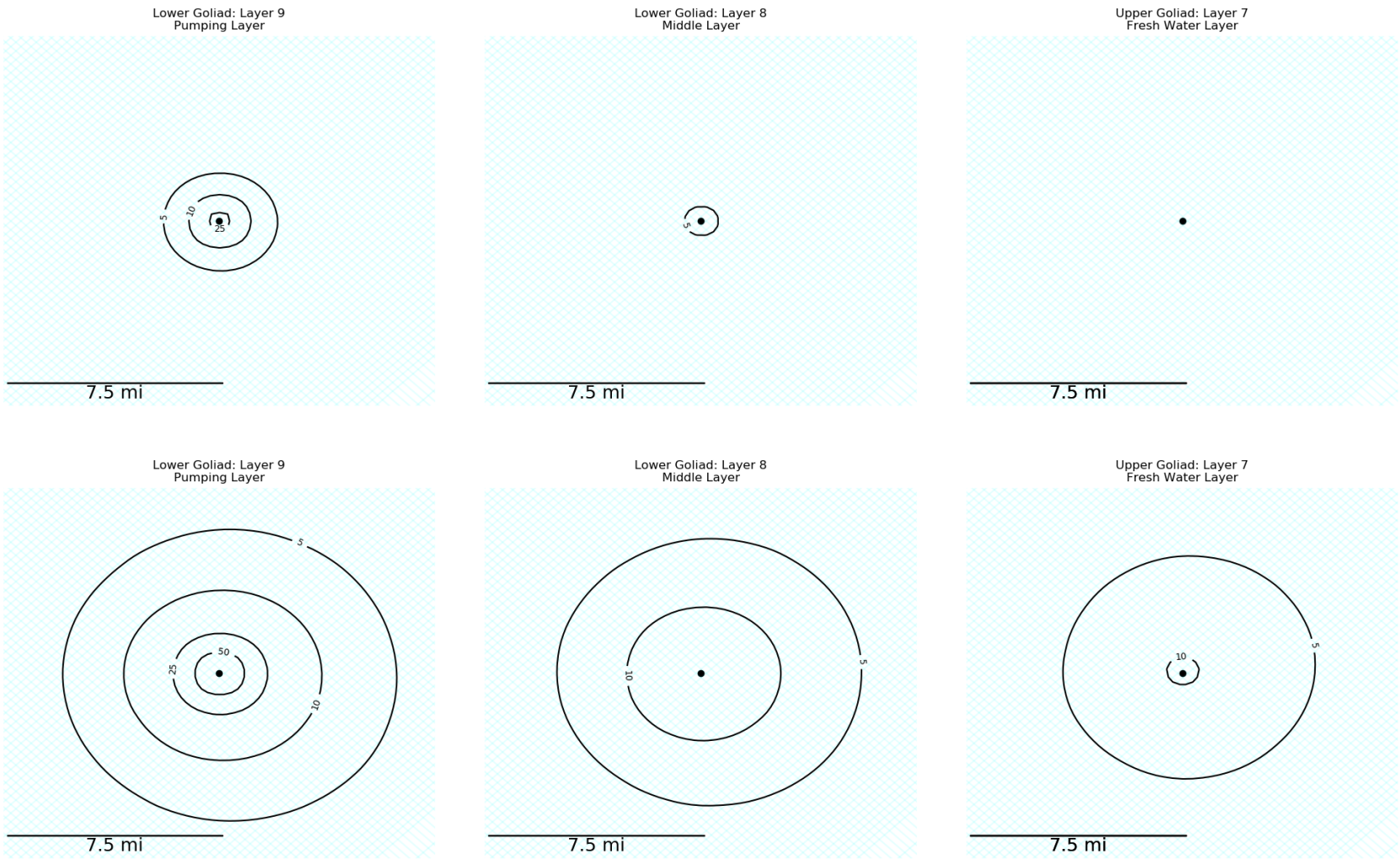

Figure 4-54 Simulated drawdowns caused by pumping at :Location #2 for 30 years at a rate of:250 gpm (top) and 1000 gpm (bottom)

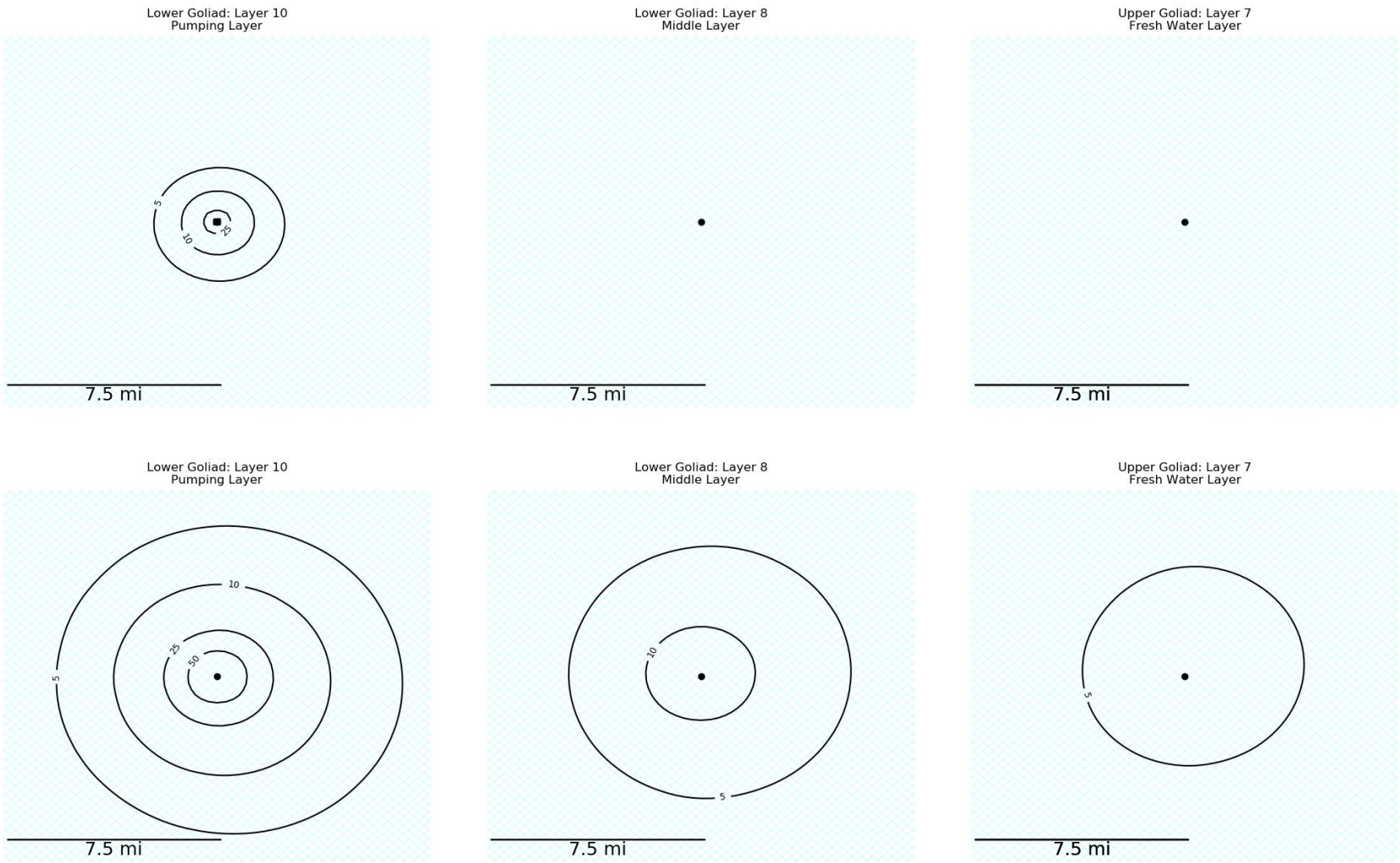

Figure 4-55 Simulated drawdowns caused by pumping at :Location #3 for 30 years at a rate of 250 gpm (top) and 1000 gpm (bottom)

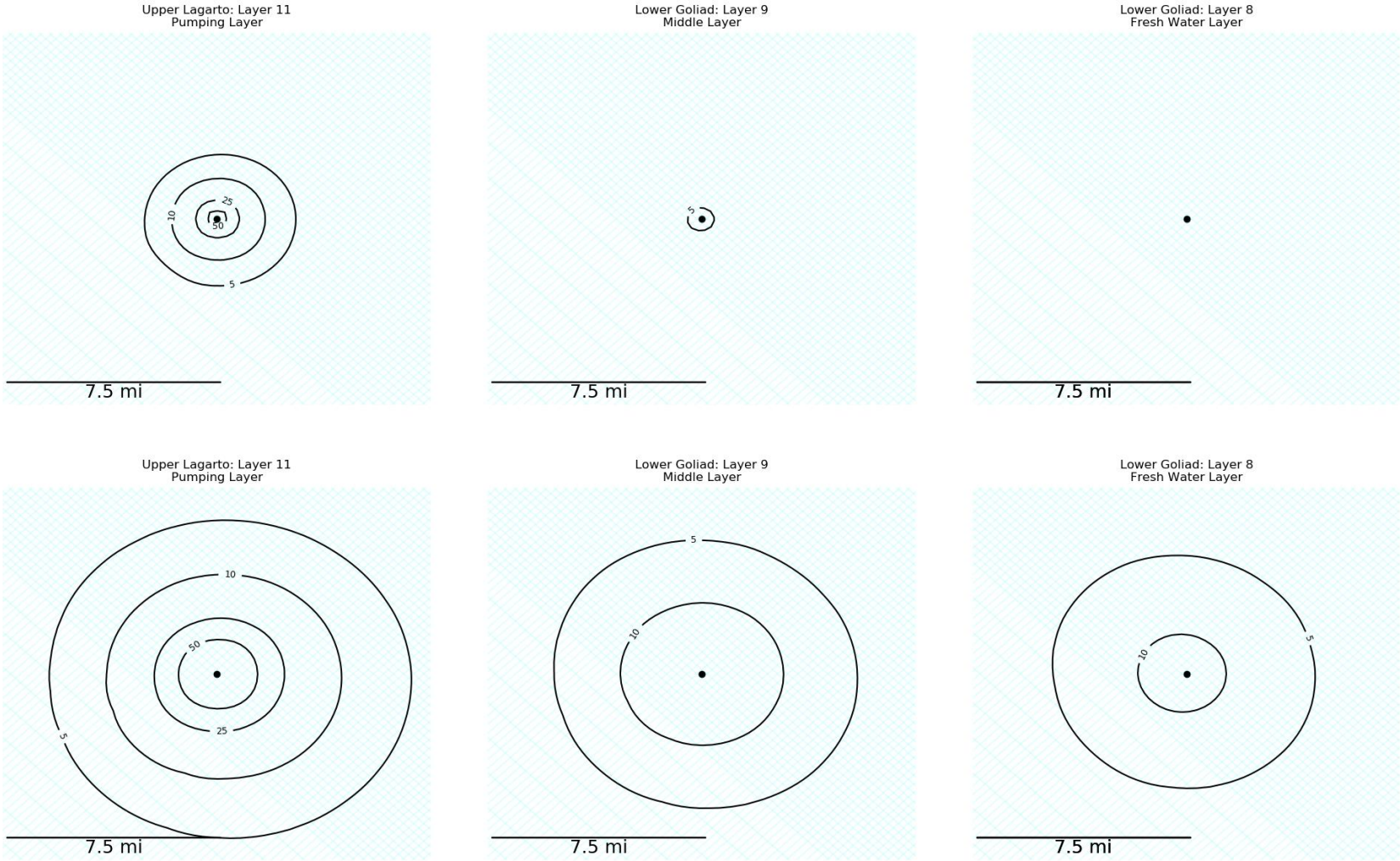

Figure 4-56 Simulated drawdowns caused by pumping at :Location #4 for 30 years at a rate of 250 gpm (top) and 1000 gpm (bottom)

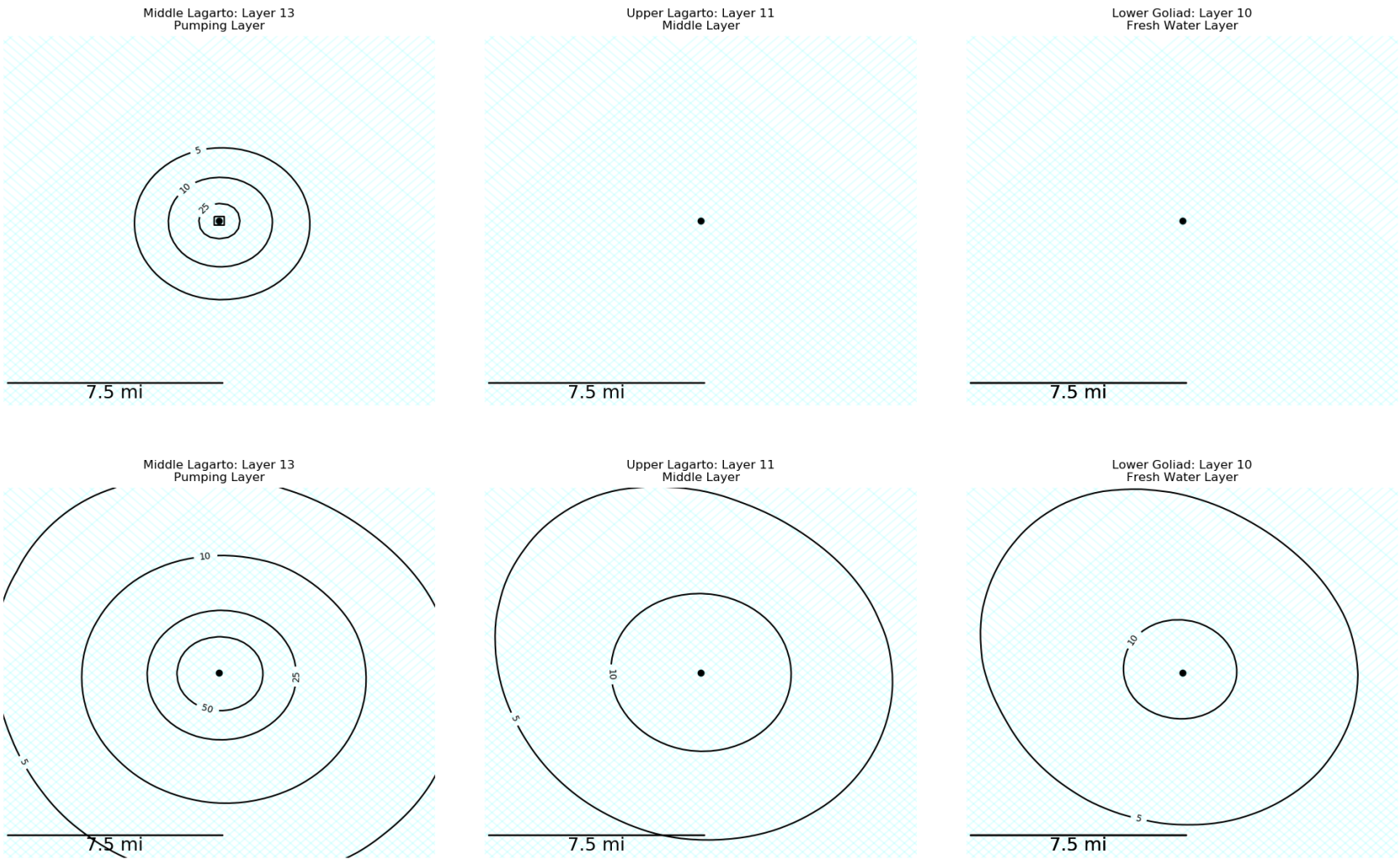

Figure 4-57 Simulated drawdowns caused by pumping at :Location #5 for 30 years at a rate of : 250 gpm (top) and 1000 gpm (bottom)

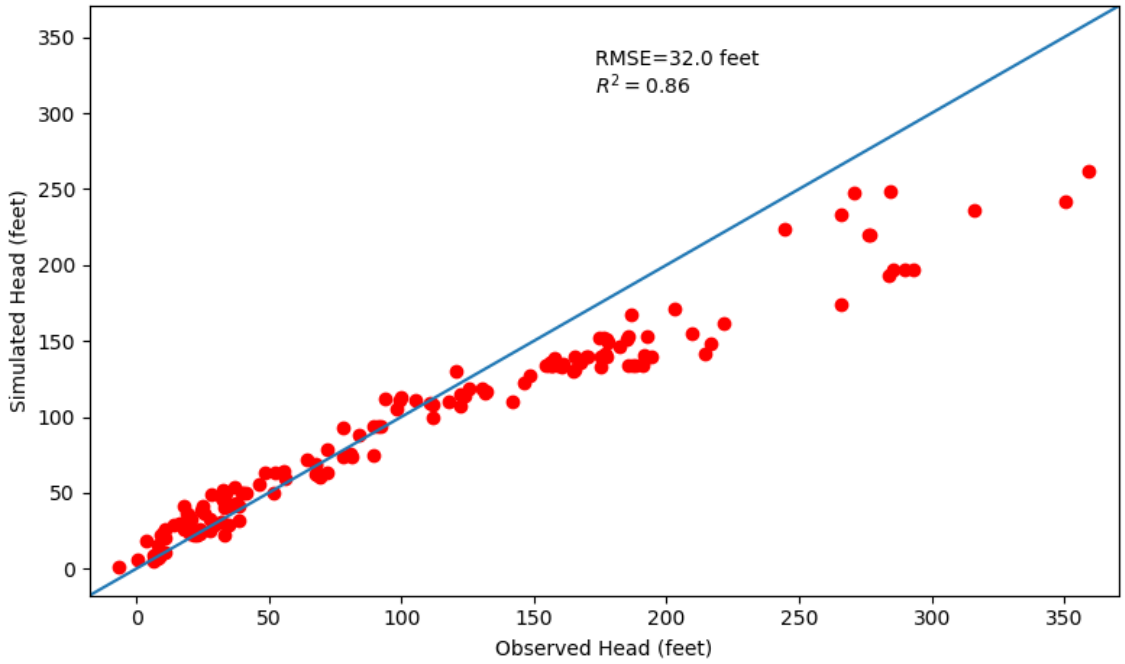

Figure 4-58 Comparison of simulated versus observed hydraulic heads for 150 wells in the model domain after the hydraulic conductance for the general head boundaries for recharge was multiplied by 0.1

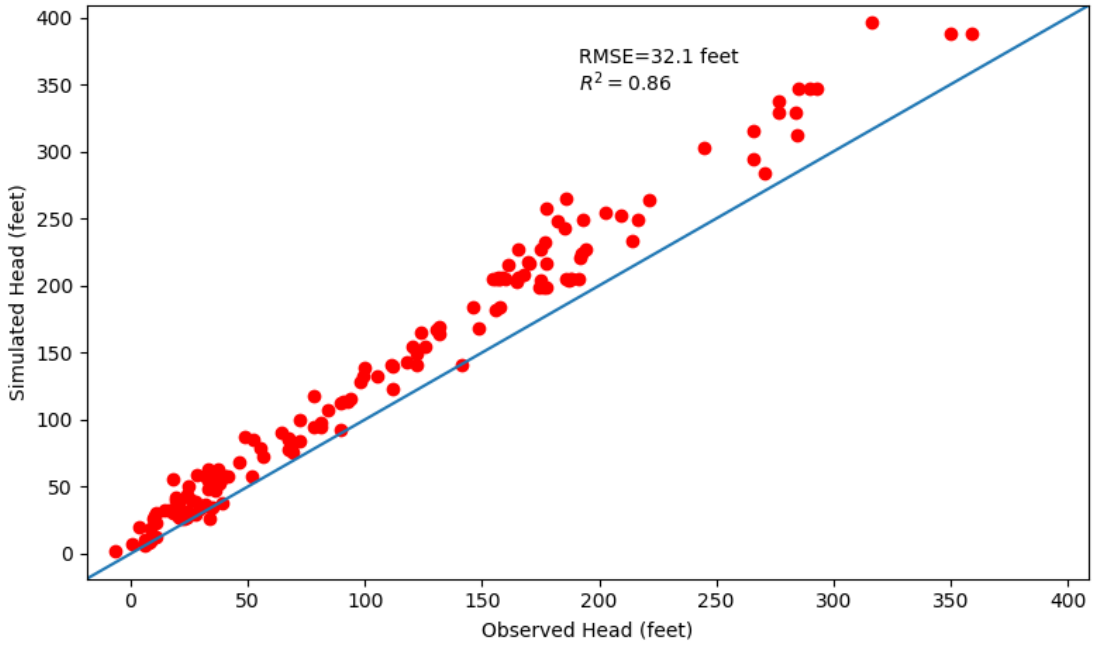

Figure 4-59 Comparison of simulated verus observed hydraulic heads for 150 wells in the model domain after the hydraulic conductance for the general head boundaries for recharge was multiplied by 10

This page intentionally left blank.

5.0 REFERENCES

Anderson, M.P., and Woessner, W.W., 1992, *Applied Groundwater Modeling*: Academic Press, San Diego, CA, 381 p.

Chowdhury, A.H, S. Wade, R.E. Mace, and C. Ridgeway. 2004. Groundwater Availability Model of the Central Coast Aquifer System: Numerical Simulations through 1999.

Cooper, H.H., and Jacob, C.E., 1946, A generalized graphical method for evaluating formation constants and summarizing well-field history: Transactions of the American Geophysical Union, v. 217, p. 626-634.

Deeds, N., Kelley, V., Fryar, D., Jones, T., Whellan, A. J., and Dean, K. E., 2003, Groundwater availability model for the Southern Carrizo-Wilcox Aquifer: prepared for the TWDB.

Deeds, N.E., Yam. T., Singh, A., Jones, T., Kelley, V., Knox, P., and Young, S., 2010, Groundwater availability model for the Yegua-Jackson Aquifer: prepared for the TWDB.

Doherty, J., 2018, Model-Independent parameter estimation user manual Part I: PEST, SENSAN, and global optimisers: 7th Edition: Brisbane, Australia, Watermark Numerical Computing.

Dutton, A.R., Harden, R.W., Nicot, J.P., and O'Rourke, D., 2003, Groundwater availability model for the central part of the Carrizo-Wilcox Aquifer in Texas: The University of Texas at Austin, Bureau of Economic Geology, prepared for the TWDB

Estepp, J., 1998, Evaluation of ground-water quality using geophysical logs: Texas Natural Resource Conservation Commission, unpublished Report, 516 p.

Freeze, R.A., and Cherry, J.A., 1979, Groundwater: Englewood Cliffs, N.J. Prentice Hall, 604 pp

Gabrysch, R.K., and C.W. Bonnet. 1974. Land-Surface Subsidence in the Area of Burnett, Scott, and Crystal Bays Near Baytown, Texas, U.S. Geological Survey Water-Resources Investigations Report 74-21.

Gabrysch, R.K., and C.W. Bonnet. 1975. Land-surface subsidence in the Houston-Galveston region, Texas: Texas Water Development Board Report 188, 19 p.

Gabrysch, R.K., and C.W. Bonnet. 1976a. Land-surface subsidence in the area of Moses Lake near Texas City, Texas: U.S. Geological Survey Water-Resources Investigation 76-32, 42 p.

Gabrysch, R.K., and C.W. Bonnet. 1976b. Land-surface subsidence at Seabrook, Texas: U.S. Geological Survey Water Resources Investigation 76-31, 53 p.

Galloway, W.E., Ganey-Curry, P.E., Li, X., and Buffler, R.T., 2000, Cenozoic depositional history of the Gulf of Mexico basin: American Association of Petroleum Geologists Bulletin, vol. 84, p. 1743–1774.

Hamlin, S., B.R. Scanlon, R. Reedy, S.C. Young, and M. Jigmond. 2016. Fresh, Brackish, and Saline Groundwater in the Carrizo-Wilcox Aquifer in Groundwater Management Area 13 -- Location, Quantification, Producibility, and Impacts

Hamlin and de la Rocha, L., 2015, Using electric logs to estimate groundwater salinity and map brackish groundwater resources in the Carrizo-Wilcox Aquifer in South Texas: GCAGS Journal v.4 (2015), p. 109-131.

Hutchison, W.R., Hill, M.E, Anaya, R., Hassan, M., Oliver, W., Jigmond, M., Wade, S., and Aschenbach, E., 2011, Groundwater Management Area 16 groundwater flow model, unnumbered report: Texas Water Development Board.

Kasmarek, M.C. 2012. Hydrogeology and Simulation of Groundwater Flow and Land-Surface Subsidence in the Northern Part of the Gulf Coast Aquifer System, Texas, 1891-2009: U.S. Geological Survey Scientific investigations Report 2012-5154, 55 p.

Kelley, V., Deeds, N., Young, S., Pinkard, J., 2018. Subsidence Risk Assessment and Regulatory Considerations for the Brackish Jasper Aquifer. Prepared for Harris-Galveston and Fort Bend Subsidence Districts. Prepared by INTERA, Austin, TX

Kelley, V.A., Deeds, N.E., Fryar, D.G., and Nicot, J-P, 2004, Groundwater availability models for the Queen City and Sparta aquifers: prepared for the TWDB.

Kelley, V.A., Ewing, J., Jones, T.A., Young, S.C., Deeds, N., and Hamlin, eds, S., 2014, FINAL REPORT Updated groundwater availability model of the Northern Trinity and Woodbine aquifers: prepared by INTERA for North Texas GCD, Northern Trinity GCD, Prairielands GCD, and Upper Trinity GCD, August 2014.

Loucks, R.G., Dodge, M.M., and Galloway, W.E., 1984, Regional controls on diagenesis and reservoir quality in lower Tertiary sandstones along the Texas Gulf Coast, *in* Clastic Diagenesis, eds McDonald, D.A., and Surdam, R.C.: American Association of Petroleum Geologists Memoir 37.

Loucks, R.G., Dodge, M. M., and Galloway, W.E., 1986, Controls on porosity and permeability of hydrocarbon reservoirs in Lower Tertiary sandstones along the Texas Gulf Coast: The University of Texas at Austin, Bureau of Economic Geology Report of Investigations No. 149, 78 p.

Mace, R. E. 2001, Estimating transmissivity using specific-capacity data: The University of Texas at Austin, Bureau of Economic Geology, Geological Circular No. 01-2, 44 p.

Magara, K., 1978, Compaction and fluid migration – Practical petroleum geology: Elsevier Scientific Publishing Company, New York. 350 pages.

Maidment, D.R. 1992. Handbook of hydrology: McGraw-Hill, Inc.

Meyer, J., Croskrey, A., Wise, M., and Kalaswad, S., 2014. Brackish Groundwater in the Gulf Caost Aquifer, Lower Rio Grande Valeey, Texas. Texas Water Development Board, Austin, TX, Report 383.

Myers, B.N. 1969. Compilations of Results of Aquifer Tests in Texas. Report 98. Texas Water Development Board, Austin, TX. 530 p.

Neglia, S. 1979, Migration of fluids in sedimentary basins: in AAPG Bulletin, v. 63, p. 573-597, The American Association of Petroleum Geologists.

Nelson, P.H., 1994, Permeability-porosity relationships in sedimentary rocks. Society of Petrophysicists and Well-Log Analysts.

Niswonger, R.G., S. Panday, and M. Ibaraki. 2011. MODFLOW-NWT, A Newton formulation for MODFLOW-2005: U.S. Geological Survey Techniques and Methods 6-A37, 44 p.

Prudic, D.E. 1991. Estimates of hydraulic conductivity from aquifer test analyses and specific capacity data, Gulf Coast regional aquifer systems, south-central United States: U.S. Geological Survey Water Resources Investigation Report 90-4121, 38 p.

Shestakov, V., 2002, "Development of relationship between specific storage and depth of sandy and clay formations", Environmental Geology, Volume 42, Numbers 2-3 / June, 2002. pp. 127-130

Stanton, J.S., D.W. Anning, C.J. Brown, R.B. Moore, V.L. McGuire, S.L. Qi, A.C. Harris, K.F. Dennehy, P.B. McMahon, J.R. Degnan, and J.K. Bohlke. 2017. Brackish groundwater in the United States: U.S. Geological Survey Professional Paper 1833, 185p., https://doi.org/10.3133/pp1833

Texas Administrative Code, 2016, https://texreg.sos.state.tx.us/public/readtac$ext.TacPage?sl=T&app=9&p_dir=F&p_rloc=166377&p_tloc=14748&p_ploc=1&pg=2&p_tac=&ti=30&pt=1&ch=307&rl=3.

Texas Water Development Board. 2016. Texas Aquifers Study: Groundwater Quantity, Quality and Contributions to Surface Water. Unnumbered report. TWDB. Austin, TX.

Wallace, R.H., Kraemeer, T. F., Taylor, R.E, and Wesselman, J B., 1972, Assessment of geopressured-geothermal resources in the Northern Gulf of Mexico Basin,

Winslow, A.G., and L.R. Kister. 1956. Saline-water resources of Texas: U.S. Geological Survey Water-Supply Paper 1365, 105 p.

Young, S.C., and V. Kelley, eds., N. Deeds, P. Knox, T. Budge, and E. Baker. 2006. A Site Conceptual Model to Support the Development of a Detailed Groundwater Model for Colorado, Wharton, and Matagorda Counties: Lower Colorado River Authority, Austin, Texas.

Young, S.C., Kelley, V., Budge, T., Deeds, N., and Knox, P. 2009. Development of the LCRB Groundwater Flow Model for the Chicot and Evangeline aquifers in Colorado, Wharton, and Matagorda counties: LSWP Report Prepared by the URS Corporation, prepared for the Lower Colorado River Authority, Austin, TX.

Young, S.C., Knox, P.R., Baker, E., Budge, T., Hamlin, S., Galloway, B., Kalbouss, R., and Deeds, N., 2010, Hydrostratigraphic of the Gulf Coast Aquifer from the Brazos River to the Rio Grande: Texas Water Development Board Report, 203 p.

Young, S., T. Ewing, S. Hamlin, E. Baker, and D. Lupton. 2012a. Final Report updating the hydrogeologic framework for the Northern Portion of the Gulf Coast Aquifer System. Prepared for the Texas Water Development Board, June 2012.

Young, S., 2012b. Letter Report to Mr. Tim Andruss, General Manager of Texana GCD dated May 25, 2015, “Deliverables Associated with Task 1 of Technical Support for Improving the Groundwater Availability Model for GMA 15, prepared by INTERA, Austin Texas

Young, S., 2012c. Letter Report to Mr. Tim Andruss, General Manager of Refugio County GCD dated May 25, 2015, “Deliverables Associated with Task 1 of Technical Support for Improving the Groundwater Availability Model for GMA 15, prepared by INTERA, Austin Texas

Young, S., 2012d. Letter Report to Mr. Tim Andruss, General Manager of Victoria County GCD dated May 25, 2015, “Deliverables Associated with Task 1 of Technical Support for Improving the Groundwater Availability Model for GMA 15, prepared by INTERA, Austin Texas

Young, S., 2012e. Letter Report to Mr. Neil Hudgins, General Manager of Coastal Plains GCD dated June 8, 2015, “Deliverables Associated with Task 1 of Technical Support for Improving the Groundwater Availability Model for GMA 15, prepared by INTERA, Austin Texas

Young, S., 2012f. Letter Report to Mr. Neil Hudgins, General Manager of Coastal Bend GCD dated June 8, 2015, “Deliverables Associated with Task 1 of Technical Support for Improving the Groundwater Availability Model for GMA 15, prepared by INTERA, Austin Texas

Young, S., 2012g. Letter Report to Ms. Charlotte Krause, General Manager of Pecan Valley GCD dated May 25, 2015, “Deliverables Associated with Task 1 of Technical Support for Improving the Groundwater Availability Model for GMA 15, prepared by INTERA, Austin Texas

Young, S., 2012h. Letter Report to Mr. Russell Labus, General Manager of Evergreen Underground WCD dated May 11, 2015, “Deliverables Associated with Task 1 of Technical Support for Improving the Groundwater Availability Model for GMA 15, prepared by INTERA, Austin Texas

Young, S.C., J. Pinkard, R. Bassett, and A. Chowdhury. 2013. Hydrogeochemical Evaluation of the Texas Gulf Coast Aquifer System and Implications for Developing Groundwater Availability Models, prepared for the Texas Water Development Board, unnumbered report.

Young, S.C., Pinkard, J., Bassett, R.L., and Chowdhury, A.H., 2014, Final hydrogeological evaluation of the Texas Gulf Coast Aquifer System and implications for developing groundwater availability models, prepared for the Texas Water Development Board, April 2014.

Young, S., Jigmond, M., De, eds., N., Blainey, J., Ewing, T., and Banjeri, 2016. Identification of Potential Brackish Groundwater Production Area – Gulf Coast Aquifer System, prepared for the TWDB, unpublished report, September 2016.

Appendix A

Transmissivity of the Formation that Comprise the Gulf Coast Aquifer System

Table A-1 Transmissivity (ft2/day) Ddsistribution by Percentile for Formations that Comprise the Gulf Coast Aquifer System

Formation	Percentile				
	10%	25%	50%	75%	90%
Beaumont	-	-	-	247	383
Lissie	372	638	937	2069	2428
Willis	90	365	738	1161	1484
Upper Goliad	1670	2712	3259	3887	4584
Lower Goliad	1223	1375	1502	1628	1704
Upper Lagarto	344	366	401	530	680
Middle Lagarto	118	139	186	254	340
Lower Lagarto	219	251	334	456	559
Oakville	515	608	796	1096	1466